Universidad de Zaragoza
Facultad de Ciencias
Departamento de Física Teórica

ESTUDIO EN EL RETÍCULO DE TRANSICIONES DÉBILES DE PRIMER ORDEN EN DIMENSIÓN 4.

Memoria de tesis doctoral

presentada por

Isabel M. Campos Plasencia

Zaragoza, Junio 1998.

ALFONSO TARANCON LAFITA, Profesor titular de Física Teórica de la Universidad de Zaragoza,

CERTIFICA

que la presente memoria, *"Estudio en el retículo de transiciones débiles de primer orden en dimensión 4"*, ha sido realizada en el Departamento de Física Teórica de la Universidad de Zaragoza bajo su dirección, y autoriza su presentación para que sea calificada como Tesis Doctoral.

Zaragoza, JUNIO 1998.

Fdo: Alfonso Tarancón Lafita.

Agradecimientos

Llegó la hora de los agradecimientos, y realmente no sabe una por donde empezar. A lo largo de estos años muchas personas me han prestado su ayuda a nivel científico y su apoyo a nivel personal, a todos ellos quiero dejar patente mi más profundo reconocimiento.

En primer lugar, gracias a Alfonso Tarancón, por querer asumir la responsabilidad de dirigir mi trabajo durante estos años, por todo lo que me ha enseñado, por las largas horas de explicaciones, y en especial por su esfuerzo en inculcarnos a todos una forma de trabajo en concordancia con el espíritu científico.

Gracias en general al resto de miembros de la colaboración RTN: Jose, Carlos, David, Héctor, Víctor, Juan Jesús, Antonio, Luis Antonio, Andrés y Jose Luis. Se espera del doctorando que destaque a las personas y no a las entidades pero realmente es muy difícil.

Sin embargo no sería justa si no menciono especialmente a Luis Antonio Fernández para darle las gracias por su generosidad a la hora de transmitir lo mucho que sabe, por su paciencia a la hora de contestar a mis muchas preguntas, y por sus valiosos consejos.

Gracias también a Jose Luis Alonso por tratar de contagiarnos a todos su interés y dinamismo a la hora de dedicarnos a la investigación científica, y por los ánimos que me ha dado siempre.

A Andrés Cruz, por la colaboración mantenida durante este tiempo, durante la cual me ha hecho llegar grandes dosis de sensatez.

Por supuesto el ambiente de trabajo creado por los miembros del departamento de Física Teórica ha ayudado a la feliz consecución de esta tesis. Quiero destacar especialmente a Isabel y a Pedro, sin los cuales, esto se nos vendría encima sin duda, y a mis sucesivos compañeros de despacho Peppe Bimonte, Arjan Van der Sijs y Jesús Salas.

Vamos ahora de paseo por Europa:

No tengo palabras para agradecer a Richard Kenway su hospitalidad, su encanto, su ayuda durante y después de mi estancia en Edimburgo.

Como ya no tengo más palabras, no se como decirle a Christian Lang que

le estoy muy agradecida por su amabilidad extrema, su simpatía, sus clases de Inglés, (y de Austríaco) y en general por la acogida en su departamento durante mi estancia en Graz, tan importante para mi formación tanto en el plano científico como en el humano, en resumen, gracias Christian.

Los comentarios (de todo tipo, remarco) de Jiri Jersák significaron mucho para mi en un momento difícil, y vinieron a despejar muy negros nubarrones. Gracias por esos días en Aachen y por las útiles discusiones que hemos mantenido desde entonces. Es una pena que no nos pongamos de acuerdo, pero todo llegará.

Por supuesto hay siempre que mirar hacia el futuro, y así he agradecer a István Montvay la magnífica oportunidad que me brinda para continuar mi formación a nivel post-doctoral.

Ya en el plano personal, no puedo olvidarme de los amigos que han estado siempre al otro lado de la pantalla, todos ellos por esos mundos de Dios: María Pilar y Juan Pablo, vaya mails hijos míos; Belén, Nuria y sólo falta Silvia, siempre en el otro lado del mundo, pero afortunadamente siempre tan cercana.

Y a Paula, y a Ana, por los buenos ratos que hemos pasado, y los que nos quedan por pasar, of course.

A esa panda que montamos en Edimburgo aquel glorioso verano del 95, y que siguen en mi vida desde entonces: Juan, María, Dora, gracias por ser tan majos; Maria Grazia, gracias por ser tan sensata siempre; por supuesto al inefable Tim, que no tiene arreglo (al menos que yo sepa) pero que también merece estar aquí.

Mis compañeros de piso han sido los que me han aguantado día a día, lo cual algunos días no era trivial. Estos pobres han soportado pacientemente todas mis veleidades, todas: Jano, Javier, Juan, Oscar, Alfonso y last but not least, *moquito*, el cócker más guapo del mundo.

Ya para el final el agradecimiento a quien más se lo merece, a mi familia, por proporcionarme la mejor educación posible, y por todo su apoyo. A mi madre, a mi hermano, y especialmente a mi padre, a cuya memoria está dedicado el trabajo de todos estos años.

Isabel, Junio 1998

Presentación

Desde que Feynman en 1948 introdujera la integral de camino en Teoría Cuántica de Campos (TCC), una gran parte de los físicos teóricos de partículas han trabajado usando este formalismo.

Las predicciones obtenidas estuvieron practicamente limitadas al regimen perturbativo (pequeñas fluctuaciones en torno al campo libre) en los primeros años, puesto que en este límite las integrales son Gaussianas y por tanto se pueden resolver por métodos analíticos.

No perturbativamente, una posible regularización se obtiene reemplazando el espacio-tiempo continuo por una red discreta (Wilson, 1974). Por supuesto la pregunta a responder es si las observaciones físicas que tenemos en el continuo se corresponden de alguna manera con la formulación de la teoría en la red. Si se puede probar que el límite continuo de una teoría de campos en la red existe, uno podría usar la definición de la teoría en la red como definición de la teoría en el continuo.

El trabajo pionero de Wilson desencadenó interés por atacar la solución de las integrales funcionales numericamente. El impresionante auge de la informática en la última década, con el consiguiente aumento de los recursos accesibles de potencia de calculo, ha favorecido sin duda el avance de este tipo de estudios, gracias a los cuales se ha obtenido conocimiento sobre los aspectos no pertubativos de TCC.

A lo largo de esta memoria se van a estudiar las propiedades de distintos modelos relevantes para la Física de Partículas mediante su formulación en una red espacio-temporal. Los análisis estarán basados en resultados que se obtienen con la ayuda de ordenadores. Para ello se van a usar ideas provenientes de la Mecánica Estadística Clásica. Así utilizaremos el concepto de transición de fase y de parámetro de orden, aplicándolos en diferentes contextos.

Cualquiera que esté interesado en el estudio numérico de fenómenos críticos debe considerar como fundamental el hecho de que las transiciones de fase ocurren sólo en el límite termodinámico. Cuando se hacen simulaciones numéricas se está forzado a trabajar con un número finito de

grados de libertad, por tanto no hay transiciones de fase. Sin embargo los efectos que se observan en redes de tamaño finito son precursores del verdadero comportamiento límite. La teoría de *Finite Size Scaling* dicta la forma concreta en que esto ocurre y por lo tanto, mediante el estudio de la evolución de los observables de interés con el tamaño de la red se pueden obtener predicciones sobre el comportamiento en el límite termodinámico. Las técnicas de tamaño finito son por lo tanto una herramienta fundamental en los análisis que se realizan a lo largo de esta memoria.

La estructura de la memoria es la siguiente. Se ha querido, por motivos de completitud, hacer una breve introducción al estudio de fenómenos críticos en la red en un capítulo preliminar. Trás este preliminar, en primer lugar se describe el modelo O(4) Anti-Ferromagnético. La motivación inicial de este trabajo fue la busqueda de puntos fijos no triviales en cuatro dimensiones en el sector Anti-Ferromagnético del Modelo Estándar.

El segundo capítulo corresponde al estudio de una transición que podríamos decir clásica en el marco de las simulaciones en la red de TCC, la transición de fase en el modelo SU(2)-Higgs a temperatura cero.

En el tercer capítulo se ha abordado un problema que durante los últimos años está sometido a una vigorosa discusión: la influencia de las condiciones de contorno en el orden de la transición de fase de la teoría U(1) compacta pura gauge.

Debido a la conexión existente entre Mecánica Estadística y TCC es - natural realizar incursiones en problemas puramente de Mecánica Estadística, dentro de la interacción con otros grupos de investigación. En mi caso esta incursión se hizo estudiando un problema podríamos decir que de *moda* como es la formulación de modelos adaptados a la descripción de procesos que envuelven un flujo de información. Este trabajo se describe en el capítulo final de esta memoria.

La estructura de cada capítulo consta de una introducción para motivar y presentar el trabajo realizado, seguida de una exposición del método utilizado y de los resultados obtenidos.

Finalmente se comentan las conclusiones obtenidas y se detalla la lista de publicaciones.

Chapter 1

Preliminares

1.1 Regularización no perturbativa en Teoría Cuántica de Campos

La Teoría Cuántica de Campos es el marco más adecuado para describir las interacciones fuerte y electrodébil. En el Modelo Estándar (SM) [1] la teoría unificada que describe estas interacciones está basada en el grupo gauge $SU(3) \otimes SU(2) \otimes U(1)_{\mathrm{Y}}$.

Uno de los posibles formalismos que permiten estudiar las propiedades de una TCC es el de la integral de camino. A esta formulación se llega a través de la generalización del concepto de integral de camino introducido por Feynmann para la Mecánica Cuántica, y su extensión a tiempos imaginarios (integral de camino Euclídea). En este contexto las funciones de Green Euclídeas o funciones de Schwinger a partir de las cuales se construye la TCC [2], se pueden escribir como los momentos de una determinada medida de probabilidad:

$$\mathcal{S}_{\mathrm{n}}(x_1, \ldots, x_n) = \int [d\Phi]\Phi(x_1)\cdots\Phi(x_n)e^{-S[\Phi]} \ , \tag{1.1}$$

donde $S[\Phi]$ es la acción Euclídea [3]:

$$S[\Phi] = \int dt\mathcal{L}(\Phi, \partial_\mu\Phi) \tag{1.2}$$

La formulación de la integral de camino no sólo proporciona una visión física llamativa de la evolución de un sistema cuántico como una suma sobre caminos clásicos, sino que abre el camino a cálculos tanto analíticos como numéricos. Además ayuda a comprender la relación entre TCC y fenómenos críticos en Mecánica Estadística (ME) clásica. Para ver esta relación consideremos la función de correlación a n puntos de una TCC escalar en el espacio Euclídeo:

$$\langle 0|\mathcal{T}(\Phi(x_1)\cdots\Phi(x_n))|0\rangle = \frac{1}{Z}\int [d\Phi]\Phi(x_1)\cdots\Phi(x_n)e^{-S[\Phi]} \ , \tag{1.3}$$

donde hemos incluido la normalización Z de manera que el valor medio de la identidad sea uno:

$$Z = \int [d\Phi]e^{-S[\Phi]} \ . \tag{1.4}$$

Estas ecuaciones se pueden interpretar como la función de correlación y la función de partición respectivamente de un sistema de ME clásica. La TCC en d_s dimensiones espaciales se puede hacer equivalente a un sistema de ME clásica en equilibrio en $d = d_s + 1$ dimensiones Euclídeas. La acción

Euclídea juega el papel de E/k_bT, donde con E se denota la energía clásica de la configuración [1].

Una primera aproximación a la solución de este tipo de integrales funcionales es considerar pequeñas fluctuaciones en torno al campo libre (integral gausiana), este es el contexto de la Teoría de Perturbaciones. La resolución perturbativa pasa por hacer un desarrollo en serie de la parte no gausiana de (1.3). Sin embargo al calcular la contribución de los distintos términos de la serie perturbativa aparecen divergencias asociadas a los grandes momentos como consecuencia de trabajar con un numero infinito de grados de libertad (la variable x es continua). En los cálculos perturbativos estas divergencias ultravioletas (UV) han de ser compensadas mediante la introducción de contratérminos en el lagrangiano de partida, lagrangiano desnudo, expresado en función de parámetros desnudos, acoplamientos y masas.

Para hacer cálculos hay que dar sentido a estas integrales divergentes, mediante un *cut-off* en momentos, trabajando en dimensión menor que 4, etc. Este procedimiento se denomina regularización. Una vez que se han hecho los cálculos se suprime la regularización, para ello se fijan un cierto número de parámetros (acoplamientos y masas) a sus valores renormalizados y se hace tender el *cut-off* a infinito o la dimensión a 4. En este proceso, los infinitos que aparecen al calcular los términos de la serie perturbativa son absorbidos en los parámetros desnudos y las constantes de renormalización que aparecen en los contratérminos. Una teoría se dice renormalizable cuando bastan un número finito de contratérminos para hacer la teoría finita a todos los ordenes de teoría de perturbaciones. En dimensión 4 las teorías gauge, como el SM, son renormalizables [4], y por tanto no hay ningún problema en dar sentido perturbativo a la definición (1.1).

Resumiendo, las integrales funcionales del tipo (1.1) no están definidas apropiadamente, su expresión es puramente formal y para darle sentido hay que regularizar la teoría de manera que no aparezcan infinitos en el UV. En teoría de perturbaciones son posibles varias regularizaciones que nos permiten dar sentido a las integrales.

Sin embargo, si se quiere dar cuenta de fenómenos no accesibles al cálculo perturbativo, como son por ejemplo la rotura espontánea de la simetría quiral, o la generación de masas para los hadrones, necesitamos una regularización que permita dar sentido al formalismo de la integral de camino en el regimen no perturbativo. Se obtiene una regularización no perturbativa introduciendo una longitud elemental "a" en el espacio-tiempo [5]. En este esquema las coordenadas del espacio-tiempo x_μ están

[1] Se ha usado el convenio $k_b = 1$ a lo largo de esta memoria

discretizadas:

$$x_\mu = a n_\mu, \quad n_\mu \in \mathcal{Z} \ . \tag{1.5}$$

Debido a la discretización, la transformada de Fourier de una función G(x)

$$\tilde{G}(k) = a^4 \sum_{n_\mu} e^{iak_\mu n_\mu} G(x) \ , \tag{1.6}$$

es periódica, es decir invariante bajo

$$k_\mu \to k_\mu + 2\pi/a \ . \tag{1.7}$$

Por lo tanto se puede restringir k_μ a todo intervalo de longitud $2\pi/a$, por ejemplo $-\pi/a < k_\mu \leq \pi/a$, que recibe el nombre de primera zona de Brillouin. Es decir, la consecuencia de haber introducido una longitud elemental "a", es que hemos regularizado la teoría en el UV puesto que ahora los momentos están restringidos a los valores del interior de una caja de arista $2\pi/a$. Esta regularización es más potente que las regularizaciones perturbativas, puesto que se espera que sirva como definición de la teoría completa, no sólo de su aspecto perturbativo.

1.2 Formulación en la red de la TCC

Para una teoría escalar hemos visto que si colocamos las variables dinámicas en los nodos de la red, el sistema es equivalente a un modelo de ME donde las variables son los valores de los campos.

En general en los nodos de la red se colocan los campos escalares y los fermiónicos, las derivadas se sustituyen por diferencias finitas y los campos vectoriales se colocan en los segmentos que unen nodos vecinos (links). En cuanto a estos últimos, parecería que la elección natural es colocar los campos vectoriales (potenciales gauge) en las links. Sin embargo hacerlo así rompe la invariancia gauge poniendo en peligro la renormalizabilidad. La forma de poner los campos gauge en la red es poner en las links no el mismo campo gauge, sino los elementos del grupo gauge. La link que conecta el site n con el site de coordenadas $\mathrm{n} + \hat{\mu}$ se denota por $U_\mu(\mathrm{n})$,

$$U_\mu(\mathrm{n}) = e^{iagA^b_{\mathrm{n},\mu}\mathcal{T}_b} \ , \tag{1.8}$$

donde $\hat{\mu}$ es el vector unitario en la direcion espacio-temporal μ, y $\mathcal{T}_b$ son los generadores del grupo gauge que estemos considerando.

En la red es conveniente trabajar con magnitudes adimensionales de manera que los operadores definidos en el continuo se redefinen en la red de la siguiente forma:

$$Q_{\mathrm{cont}} \to \hat{Q}_{\mathrm{lat}} = a^s Q_{\mathrm{cont}} \ , \tag{1.9}$$

donde s es la dimensión de $Q_{\rm cont}$ en unidades de energía.

La formulación de la integral de camino en TCC y su regularización en la red, permite la evaluación numérica de las integrales funcionales. En particular estaremos interesados en calcular el promedio de operadores invariantes gauge:

$$\langle \mathcal{O}(\Phi, A)\rangle = \frac{1}{Z}\int [d\Phi][dA]\mathcal{O}(\Phi, A)e^{-S[\Phi,A]} \ , \tag{1.10}$$

en una red finita cuadridimensional de lado L mediante integración numérica. Para obtener información sobre (1.10) numericamente definimos

$$\bar{\mathcal{O}} \equiv \lim_{\Theta\to\infty}\int_0^{\Theta} dt\mathcal{O}(\Phi(t), A(t))/\Theta \ , \tag{1.11}$$

donde t es un tiempo de ordenador, definido mediante la dinámica que nosotros hayamos elegido.

En estas condiciones, se evalua el operador $\mathcal{O}$ y se suma sobre las diferentes configuraciones de los campos $[\Phi(\tau), A(\tau)]$ generadas en el curso de la dinámica, que en general es discreta, es decir, se generan configuraciones numeradas 1,2,3 etc..., con lo cual la integral (1.11) será en realidad una suma del operador $\mathcal{O}$ evaluado sobre las diferentes configuraciones.

La dinámica se suele elegir definiendo una matriz de probabilidad de transición de una configuración a otra, que sea ergódica (para que el sistema no quede atrapado en un subconjunto del espacio fase), y que deje invariante la distribución de probabilidad de Boltzmann. Una tal dinámica se llama proceso de Markov y la secuencia de configuraciones generadas se llama cadena de Markov. Es posible demostrar que una dinámica que cumple estas condiciones converge a la distribución de equilibrio de Boltzmann definida en (1.10), y por tanto se tiene que:

$$\bar{\mathcal{O}} = \langle \mathcal{O}\rangle \tag{1.12}$$

En la practica hay dos problemas a tener en cuenta. El primero es que no se puede generar un número infinito de configuraciones. Cuando se considera un número finito de configuraciones N, la expresión (1.12) es cierta con un error que es del orden de $1/\sqrt{N}$ (teorema del límite central). El segundo problema es que la dinámica que usamos genera configuraciones que están correlacionadas. El tiempo que tarda el sistema en perder la memoria de la configuración de la que viene se denomina tiempo de autocorrelación y se denota por τ. Hablando cualitativamente, si se generan N configuraciones el número de configuraciones independientes es N/τ. Para una exposición detallada sobre los errores intrínsecos a una simulación de Monte Carlo vease [6].

Del mismo modo que se hace en teoría de perturbaciones, una vez que hemos dado sentido a las integrales hay que eliminar la regularización. El proceso de eliminar la regularización impuesta por la formulación en la red se denomina tomar el límite continuo. La forma precisa en que hay que tomar este límite la dicta el Grupo de Renormalización (RG). En particular cuando se está suficientemente proximo al límite continuo las magnitudes físicas no deben depender de los acoplamientos desnudos ni de "a". Es decir, la renormalizabilidad de la teoría implica la existencia de trayectorias de física constante en el espacio de acoplamientos desnudos.

En este contexto el proceso a seguir sería el siguiente. Se evalúa en la red el operardor $\hat{Q}(g)$ correspondiente al observable Q para distintos valores de los acoplamientos g. Después se restauran las dimensiones multiplicando $\hat{Q}(g)$ por la potencia adecuada de "a", obtenemos así $Q(g, a)$. La forma en que depende g de "a" la sabemos perturbativamente, de manera que al menos en la región perturbativa sabemos por donde pasan las trayectorias de física constante. Usando pues la predicción perturbativa podemos conocer $Q(g(a), a)$. Si el observable Q no depende de "a" podremos decir que estamos estudiando correctamente la física del continuo mediante nuestra formulación en la red. Esto es lo que se conoce como *scaling asintótico*. Una condición más suave que la anterior es lo que se conoce como *scaling*. Aquí se exige que cocientes adimensionales de cantidades con dimensiones (por ejemplo $m_{0^{++}}/m_{2^{++}}$) permanezcan constantes al variar los parámetros y acercarnos al límite contínuo. Por supuesto scaling asintótico implica scaling pero no a la inversa.

Supongamos que queremos calcular el espectro de masas de la teoría, calculando para ello el decaimiento en la red de las funciones de correlación apropiadas para largos tiempos Euclídeos. La masa más pequeña de la teoría está determinada por la longitud de correlación ξ más larga, que se define como la escala de longitud sobre la cual la partícula se puede propagar con una amplitud significativa. La renormalizabilidad de la teoría exige que la masa física sea finita, por lo tanto la masa en unidades de la red, $\hat{m} = am$, tiene que ser cero. Esto implica que la longitud de correlación medida en unidades de la red $\hat{\xi}$ debe diverger.

Resumiendo, el límite continuo de una teoría de campos en la red puede tener lugar sólo en un punto crítico del sistema de ME al cual es equivalente la TCC, y que está definido mediante la función de partición (1.4). Esta condición es por otra parte lógica, puesto que sólo cuando $\xi \to \infty$ el sistema pierde memoria de la red subyacente.

1.3 Transiciones de fase en el retículo

Los mecanismos de transición de fase aparecen frecuentemente en física de partículas para dar cuenta de las propiedades observadas en la naturaleza. Así por ejemplo, la generación de masa para los bosones vectoriales se entiende a través del mecanismo de Higgs, que se origina en una transición de fase producida por la ruptura espontánea de la simetría del campo de Higgs.

La ausencia de una transición de fase en SU(2) y SU(3) entre la región de acoplamiento fuerte y acoplamiento débil, sugerida por los trabajos pioneros de Creutz [7], se toma como criterio para pensar que la propiedad de confinamiento que puede ser demostrada en el régimen de acoplamiento fuerte [8], se mantiene en el régimen de acoplamiento débil, y por tanto dan fundamento a la creencia de que la QCD es una teoría razonable para estudiar la interacción fuerte.

Como se ha apuntado anteriormente la construcción de una teoría en el contínuo, implica la existencia de un punto crítico en el sentido de la teoría de transiciones de fase en ME.

Por lo tanto es fundamental el estudio del diagrama de fases de las TCC en el retículo, tanto desde el punto de vista de la caracterización de las fases en que se manifiesta la teoría, como para encontrar puntos críticos en los cuales la teoría es susceptible de definir una TCC en el continuo.

Las propiedades de un sistema físico dependen de parámetros como la temperatura, la presión, el campo magnético aplicado, etc... Sin embargo un cambio en las condiciones a que está sometido puede hacer que las propiedades del sistema varíen bruscamente. Este cambio brusco se denomina transición de fase. Un cambio brusco, en el lenguaje de las matemáticas es una discontinuidad, la cual se manifestará en las medidas de las funciones termodinámicas.

Vamos a centrarnos en las transiciones inducidas por la competición orden-desorden. Para tener un soporte concreto la discusión se hará para el modelo de Ising. A pesar de su simplicidad las conclusiones que se obtengan serán aplicables con gran generalidad. La acción del modelo de Ising en presencia de un campo magnético externo es:

$$S = -\beta \sum_{\langle i,j \rangle} \sigma_i \sigma_j - h \sum_i \sigma_i \ , \tag{1.13}$$

donde $\beta = J/T$ y $h = H/T$, siendo J la intensidad del acoplamiento entre espines y H el campo magnético externo aplicado. El espín σ toma los valores +1 ó -1. La notación $\langle i, j \rangle$ indica que la suma se extiende a las parejas de primeros vecinos.

La función de partición del sistema esta dada por:

$$Z_N = \sum_{\text{conf}} e^{-S(\text{conf})} \ , \tag{1.14}$$

donde el sumatorio en configuraciones significa:

$$\sum_{\text{conf}} = \sum_{\sigma_1=\pm 1} \sum_{\sigma_2=\pm 1} \cdots \sum_{\sigma_N=\pm 1} \ , \tag{1.15}$$

siendo N el número total de espines. Por tanto el número de términos en la función de partición es 2^N.

La densidad de energía libre está dada por:

$$F(\beta, h) = -\frac{1}{N} \log Z_N \ , \tag{1.16}$$

cuyas derivadas con respecto a β y/ó a h nos darán las magnitudes termodinámicas.

Definimos el valor medio del espín σ_i como:

$$\langle \sigma_i \rangle = \frac{1}{Z} \sum_{\text{conf}} \sigma_i e^{-S(\text{conf})} \ . \tag{1.17}$$

Debido a la invarianza traslacional de la acción, y trabajando en una red con condiciones de contorno periódicas, este promedio no depende del espín i particular para el que se calcula.

La magnetización del sistema estará dada por el valor medio de la suma de los espines individuales:

$$M(T, h) = N^{-1} \langle \sum_i \sigma_i \rangle \ , \tag{1.18}$$

Denotando por $w(E)$ el número de configuraciones con energía interna E, podemos reagrupar la función de partición, y expresarla como una suma sobre energías en lugar de como una suma sobre configuraciones:

$$Z = \sum_E w(E) e^{-E} = \sum_E e^{-[E - T\Omega(E)]} \ , \tag{1.19}$$

donde hemos usado la definición de entropía, $\Omega = \log w(E)$. La probabilidad de aparición de una configuración con energía interna E es proporcional a su factor de Boltzman multiplicado por la degeneración $w(E)$. Si el estado fundamental tiene una degeneración finita, la configuración correspondiente a $T = 0$ será aquella que corresponda al estado de mínima energía (todos los espines alineados) pues es infinitamente más probable que cualquier otra.

El modelo de Ising presenta una línea de transiciones de fase a campo magnético cero: $\{h = 0, 0 \leq T \leq T_c\}$. Que las transiciones de fase tienen que ocurrir a campo magnético nulo es una consecuencia de la simetría de la acción [9]:

$$\sigma_i \to -\sigma_i, \qquad h \to -h \ . \tag{1.20}$$

Por encima de T_c las fluctuaciones térmicas desordenan por completo al sistema y ya no hay transiciones de fase.

El parámetro conveniente para estudiar la aparición de la transición de fase es la magnetización, en particular la *magnetización espontánea* definida como:

$$M_0(T) = \lim_{h \to 0} M(T, h) \ . \tag{1.21}$$

Por encima de T_c la magnetización espontanea se anula, mientras que es distinta de cero para $T < T_c$.

Las transiciones de fase se clasifican de acuerdo con el comportamiento cualitativo de M_0 en el punto de la transición. En el modelo de Ising M_0 es continua en $T = T_c$, y acorde a ello la transición se dice que es continua en el punto $\{h = 0, T = T_c\}$.

Sin embargo, en el resto de puntos de transición de fase de la línea, es decir $\{h = 0, 0 \leq T < T_c\}$, M_0 se comporta de forma discontinua:

$$\begin{aligned} \lim_{h \to 0^-} M(T, h) &= -M_0(T) \\ \lim_{h \to 0^+} M(T, h) &= +M_0(T) \ . \end{aligned} \tag{1.22}$$

Correspondientemente se dice que las transiciones de fase son de *primer orden* o discontinuas.

Por ser la magnetización espontánea la magnitud que indica en que fase se encuentra el sistema, recibe el nombre de *parámetro de orden de la transición*.

Hablando con generalidad, se dice que una transición de fase es de primer orden cuando hay una discontinuidad en la primera derivada del potencial termodinámico, en el caso que estamos considerando, de la energía libre:

$$\begin{aligned} \text{Energía interna:} \quad U &= \partial F / \partial \beta \\ \text{Magnetización:} \quad M &= -(\partial F / \partial h) \end{aligned} \tag{1.23}$$

Si las primeras derivadas son continuas, pero aparecen discontinuidades en las derivadas segundas (al menos una de ellas es discontinua) la transición se dice de *segundo orden*. En general se habla de transiciones de fase continuas cuando la discontinuidad aparece en una derivada de orden igual o superior a dos, siendo todas las primeras derivadas contínuas.

En el caso Ising en el punto $(h = 0, T = T_c)$ la transición es de segundo orden por lo que aparecen divergencias en el calor específico y en la susceptibilidad magnética:

$$\begin{array}{lllll} \text{Calor Específico:} & C_v & = & \partial U/\partial\beta & = & (\partial^2 F/\partial\beta^2) \\ \text{Susceptibilidad:} & \chi & = & \partial M/\partial h & = & -(\partial^2 F/\partial h^2) \end{array} \tag{1.24}$$

La diferencia fundamental entre ambos tipos de transiciones es que las transiciones continuas presentan ordenamientos de largo alcance en el punto de la transición. Las divergencias que aparecen están ligadas a la divergencia de la longitud de correlación. Sin embargo en las transiciones de primer orden el sistema no anticipa la transición y la longitud de correlación permanece finita cuando nos aproximamos al punto de la discontinuidad.

Desde el punto de vista de la TCC las transiciones interesantes son por tanto las de segundo orden pues sólo en estos puntos se puede obtener una teoría estrictamente renormalizable. Puesto que en esta memoria estaremos especialmente interesados en la diferenciación de transiciones de fase de primer y segundo orden, veamos más detalladamente las características de ambas.

1.3.1 Transiciones de fase continuas

Para una descripción cualitativa de los fenómenos que ocurren en estas transiciones de fase tomemos como ejemplo el modelo de Ising (1.13) en ausencia de campo magnético externo ($h = 0$).

A temperatura elevada se observan espines hacia arriba y espines hacia abajo formando islotes cuyo tamaño promedio es la longitud de correlación entre espines. La correlación entre dos espines situados a una distancia r_{ij} tiende a cero exponencialmente con la separación:

$$\langle \sigma_i \sigma_j \rangle \sim e^{-r_{ij}/\xi(T)} \ , \tag{1.25}$$

con una longitud de correlación característica de la temperatura, $\xi(T)$. En estas condiciones la magnetización M es nula.

A medida que disminuye T, el tamaño de los islotes aumenta pues la correlación entre espines aumenta al disminuir la agitación térmica. Cuando se alcanza la temperatura crítica, $T = T_c$ los islotes tienen todos los tamaños posibles. Es decir, a T_c las fluctuaciones del sistema son de todas las longitudes, ya no hay una escala típica para el sistema, por eso se dice que la física es invariante de escala en el punto de la transición, que recibe el nombre de punto crítico.

Así mismo por debajo de T_c la función de correlación entre espines situados a distancia r_{ij} es el parametro de orden al cuadrado:

$$\lim_{r_{ij}\to\infty} \langle \sigma_i \sigma_j \rangle = \langle \sigma_i \rangle \langle \sigma_j \rangle = M^2 \ . \tag{1.26}$$

Se define la función de correlación entre dos espines de la siguiente forma:

$$\Gamma(\epsilon, r_{ij}) = \langle \sigma_i \sigma_j \rangle - \langle \sigma_i \rangle \langle \sigma_j \rangle \ , \tag{1.27}$$

donde $\epsilon = (T - T_c)/T_c$ recibe el nombre de temperatura reducida.

Con esta definición para $T > T_c$ y $T < T_c$, $\Gamma(\epsilon, r_{ij})$ decrece exponencialmente con la distancia: $\Gamma(\epsilon, r_{ij}) \sim \exp(-r_{ij}/\xi)$, siendo ξ la longitud de correlación asociada a la función de correlación entre dos espines. La definición precisa viene dada por:

$$\xi \equiv \lim_{|r_{ij}|\to\infty} \frac{-|r_{ij}|}{\log \Gamma(\epsilon, r_{0i})} \ . \tag{1.28}$$

Que exista una magnetización espontánea a campo exterior nulo, es de por si un hecho remarcable puesto que uno no esperaría en estas condiciones que el sistema elija una dirección privilegiada hacia la que apuntar. Sin embargo la más pequeña inhomegeneidad en los islotes, o un campo residual no nulo pueden hacer que una dirección resulte privilegiada frente a las demás, o dicho de otra forma el vacío con $M = 0$ no es estable. Este fenómeno se llama *ruptura espontánea de la simetría*.

El hecho de que la transición se produzca como un fenómeno cooperativo a gran escala induce a pensar que ciertas de sus características sólo dependen de las propiedades del sistema a gran escala, esto es, de sus propiedades generales, tales como la dimensión d del espacio, la dimensión del parámetro de orden o las simetrías de los acoplamientos, y no de los detalles de la interacción. Esta es la idea sobre la que descansa el concepto de *Universalidad*, que nos llevará a definir magnitudes para describir el comportamiento crítico de los sistemas dependiendo sólo de estas características generales, por ejemplo los exponentes críticos.

Los exponentes críticos caracterizan el comportamiento de los parámetros de orden, susceptibilidades, etc, en el entorno del punto crítico. La hipótesis que se hace es que el comportamiento de los observables en el entorno del punto crítico se puede describir como una potencia de la temperatura reducida, ϵ. Esta potencia se llama exponente crítico y cada observable físico dependiente de la temperatura tiene asociado uno. De esta manera dado un observable $f(\epsilon)$, se hace la hipótesis de que $f(\epsilon)$ es contínuo y positivo para valores pequeños y positivos del parametro ϵ. Se supone

además que el límite

$$\lambda = \lim_{\epsilon \to 0} \frac{\log f(\epsilon)}{\log \epsilon} \ , \tag{1.29}$$

existe y está bien definido. A λ se le llama exponente crítico asociado a $f(\epsilon)$.

Para sistemas magnéticos como el modelo de Ising, los exponentes se definen de la siguiente forma:

$$\begin{aligned} C_v(T) &\sim \epsilon^{-\alpha} \ ; \\ M(T) &\sim (-\epsilon)^{\beta} \ ; \\ \chi(T) &\sim \epsilon^{-\gamma} \ ; \\ \xi(T) &\sim \epsilon^{-\nu} \ . \end{aligned} \tag{1.30}$$

Por último se definen también exponentes para el comportamiento en el punto crítico (ϵ=0) de la función de correlación de dos espines situados a distancia r:

$$\Gamma(0, r) \sim r^{-(d-2+\eta)} \ , \tag{1.31}$$

En general la función de correlación se puede expresar como:

$$\Gamma(\epsilon, r) = \frac{g(r, \xi)}{r^{d-2+\eta}} \ . \tag{1.32}$$

Para $T \neq T_c$, $g(r, \xi) \sim \exp(-r/\xi)$ mientras que en el entorno del punto crítico ($\xi = \infty$) la función de correlación se comporta como una potencia de r.

Se introduce también un exponente crítico asociado al comportamiento del parámetro de orden en el punto crítico a campo externo distinto de cero:

$$M(T_c, h) \sim |h|^{1/\delta} \ . \tag{1.33}$$

En la dimensión crítica superior estas predicciones están modificadas por la existencia de correcciones logarítmicas [10].

Hay dos motivos esencialmente por los cuales estamos interesados en estas cantidades a pesar de que posean menos información que la función completa $f(\epsilon)$:

1. Cerca del punto crítico ($T \approx T_c$) domina el término con ϵ elevado a la potencia más baja. Esto se confirma experimentalmente en gráficas log-log puesto que se obtienen rectas en torno al punto crítico cuya pendiente es el exponente crítico. Por otra parte los fenómenos físicos en los que estamos interesados, tales como las existencia de largas correlaciones, ocurren en el entorno del punto crítico.

2. Existen relaciones entre los exponentes que trascienden a cualquier sistema particular pues dependen de características muy generales, en la línea del concepto de Universalidad mencionado anteriormente. Estas relaciones no han sido probada con la mayor generalidad sino sólo en el marco de ciertas hipótesis que conciernen a la forma de los potenciales termodinámicos.

En particular se supone que el potencial de Gibbs es una función homogenea generalizada (*hipótesis de escala*) es decir:

$$G(\lambda^{a_\epsilon}\epsilon, \lambda^{a_H} H) = \lambda G(\epsilon, H) \ . \tag{1.34}$$

Esta hipótesis permite establecer relaciones entre los exponentes críticos:

$$\begin{aligned} &\gamma = \nu(2-\eta) \ ; \\ &\alpha + 2\beta + \gamma = 2 \ ; \\ &\gamma = \beta(\delta - 1) \ ; \\ &\gamma = 2\beta\delta + \alpha - 2 \ . \end{aligned} \tag{1.35}$$

Si además se asume la *hipótesis de hiperescala* que consiste en suponer que las fluctuaciones que contribuyen a la parte singular de la densidad de energía libre van como:

$$F_{\text{sing}}(\epsilon) \sim \frac{1}{\xi(\epsilon)^d} \sim \epsilon^{\nu d} \ , \tag{1.36}$$

teniendo en cuenta que el calor específico es la segunda derivada de la energía libre, podemos escribir su ley de escalado como:

$$C_v \sim \epsilon^{\nu d - 2} \ . \tag{1.37}$$

Como consecuencia se obtiene la *relación de Josephson*:

$$\alpha = 2 - \nu d \ . \tag{1.38}$$

Si bien la hipótesis de escala no ha sido demostrada con rigurosidad, ésta surge de un modo natural en el marco de las hipótesis de trabajo del grupo de renormalización. En este contexto vamos a describir la línea argumental de Kadanoff que lleva a la plausibilidad de la hipótesis de escala.

Supongamos un Hamiltoniano tipo Ising como el descrito por la acción (1.13), es decir un sistema de N espines en una red de dimensión d. Consideremos la red dividida en celdas de lado aL, tenemos por tanto n $= N/L^d$ celdas cada una con L^d espines. Los argumentos de Kadanoff se aplican

sólo a la situación en que $\xi \gg aL$, es decir, en un entorno suficientemente pequeño del punto crítico. En estas condiciones dentro de un mismo islote de espines correlacionados hay un gran número de celdas.

Vamos a asociar a cada celda α ($\alpha = 1, 2, \ldots, \mathrm{n}$) un espín $\tilde{\sigma}_\alpha$ de acuerdo con la regla de la mayoría. Puesto que cada celda está enteramente dentro de un islote de espines correlacionados, es razonable asumir que los $\tilde{\sigma}_\alpha$ se comportarán como los espines individuales σ_i en el sentido de que actuarán como si tomasen los valores ± 1.

Podemos pensar que la acción escrita en términos de estos momentos $\tilde{\sigma}_\alpha$, tenga la misma forma que la acción original, excepto que los parámetros β y h serán en general distintos. Asociamos pues unos nuevos $\tilde{\beta}$ y $\tilde{h}$ a la acción construida con las $\tilde{\sigma}_\alpha$. Puesto que la temperatura crítica es una medida de la intensidad de la interacción J, no haremos la discusión en función de $\tilde{\beta}$ sino de la temperatura reducida $\tilde{\epsilon}$.

Ahora bien, si la acción tiene la misma forma funcional, es razonable pensar que lo mismo ocurrirá con los potenciales termodinámicos. Así por ejemplo el potencial de Gibbs de cada celda, $G(\tilde{\epsilon}, \tilde{h})$, será la misma función de $\tilde{h}$ y $\tilde{\epsilon}$ que el potencial de Gibbs correspondiente a cada site. Por ser éste una magnitud extensiva se tiene:

$$G(\tilde{\epsilon}, \tilde{h}) = L^d G(\epsilon, h) \ . \tag{1.39}$$

La dependencia de $\tilde{h}$ con h y $\tilde{\epsilon}$ con ϵ se puede pensar que será en general una función de L:

$$\begin{array}{l} \tilde{h} = H(L)h \\ \tilde{\epsilon} = T(L)\epsilon \ . \end{array} \tag{1.40}$$

En estas condiciones ya se puede argumentar el cumplimiento de la hipótesis de escala, sin embargo siguiendo con el argumento de Kadanoff, se asume que $H(L)$ y $T(L)$ se pueden expresar como una potencia de L: $H(L) = L^x$ y $T(L) = L^y$, con x e y arbitrarios. Esto nos permite reescribir (1.39) como:

$$\begin{array}{rcl} G(L^y\epsilon, L^x h) & = & L^d G(\epsilon, h) \\ \Rightarrow G(L^{y/d}\epsilon, L^{x/d}h) & = & LG(\epsilon, h) \ , \end{array} \tag{1.41}$$

que tiene la misma forma funcional que (1.34) excepto que L no es un parámetro libre como lo es λ en (1.34). En efecto L está sujeto a la condición $1 \ll L\xi/a$, sin embargo, puesto que ξ diverge en el punto de la transición siempre podemos ponernos tan proximos al punto crítico como queramos para lograr que L esté en ese intervalo. Es decir que (1.41) significa que el potencial de Gibbs es una función homogénea generalizada.

Una línea de argumentación análoga aplicada a la función de correlación a dos puntos, $\Gamma(\epsilon, r)$, muestra que ésta es también una función homogénea

generalizada. Teniendo en cuenta que la longitud de correlacón es función sólo de la temperatura reducida, podemos escribir $\Gamma(\epsilon, r)$ sustituyendo la dependencia en ϵ por la dependencia en ξ: $\Gamma(\xi, r)$. Puesto que es una función homogénea tenemos:

$$\Gamma(\lambda\xi, \lambda r) = \lambda^u \Gamma(\xi, r) \ . \tag{1.42}$$

Tomando $\lambda = 1/\xi$:

$$\Gamma(1, r/\xi) = \xi^{-u} \Gamma(\xi, r) \ . \tag{1.43}$$

Puesto que uno de los dos parámetros está fijo podemos escribir la función de correlación como dependiente de un solo parámetro, es decir $\Gamma(1, r/\xi) \equiv F(\xi, r)$. Es decir que podemos escribir:

$$\Gamma(\xi, r) = \xi^p \Gamma(1, r/\xi) \ . \tag{1.44}$$

Esta igualdad significa que la correlación entre dos espines situados a distancia r, depende de r sólo a través del cociente r/ξ. Dicho de otra forma, que sólo existe una longitud característica en el problema y que esta es la longitud de correlación.

Sin embargo a la hora de extraer información mediante métodos numéricos hay que tener en cuenta que las divergencias que marcan la existencia de una transición de fase ocurren sólo cuando el número de grados de libertad tiende a infinito. En un volumen finito, es decir dentro de los ordenadores, todas las cantidades se obtienen mediante sumas finitas siendo por tanto funciones analíticas en todo el espacio de acoplamientos. Como consecuencia aparecen dos fenómenos fundamentalmente: las divergencias son sustituidas por picos de altura finita, creciente con el tamaño de la red; la localización de estos picos se mueve en el espacio de acoplamientos conforme el tamaño de la red cambia.

La teoría de *Finite Size Scaling* (FSS) [11] está basada en que estos efectos que aparecen al aumentar el tamaño de la red son precursores del comportamiento del sistema en el límite termodinámico, y que pueden ser explotados para extraer las propiedades de la transición de fase. Consideremos un retículo de lado L. La teoría de FSS descansa sobre la hipótesis de que en el entorno del punto crítico el comportamiento del sistema se puede describir enteramente en funcion de la variable reescalada:

$$y = L/\xi(T) \ . \tag{1.45}$$

En una transición de fase continua $\xi(T)$ crece conforme nos acercamos a T_c. Es razonable suponer que los efectos de tamaño finito se harán palpables cuando ésta alcance el tamaño de la red L. Definimos la temperatura crítica

aparente $T_c^*(L)$ como aquella en la que $\xi(T_c^*(L)) \sim L$. En estas condiciones podemos estimar como depende de L la temperatura aparente puesto que:

$$\begin{aligned} \xi(T_c^*(L)) \propto L \quad &\sim \quad |T_c^*(L) - T_c|^\nu \\ \Rightarrow |T_c^*(L) - T_c| \quad &\sim \quad L^{-1/\nu} \ . \end{aligned} \tag{1.46}$$

En general si $Q_L(T)$ es un observable físico en el sistema finito, cuyo comportamiento en el límite termodinámico es:

$$Q_\infty(T) \sim C_\infty \epsilon^{-\rho} \quad \epsilon \to 0 \ . \tag{1.47}$$

En un volumen finito el comportamiento será del tipo:

$$Q_L(T) \sim \hat{C}_L \hat{\epsilon}^{-\rho} \ , \tag{1.48}$$

con $\hat{\epsilon} = |T - T_c^*(L)| \sim L^{-1/\nu}$.
Si introducimos ahora la hipótesis de FSS se tiene:

$$Q_L(T) \sim L^\omega f(y) \ . \tag{1.49}$$

Para determinar ω basta imponer que (1.49) reproduzca (1.47) en el límite de $L \to \infty$:

$$f(y) \sim C_\infty \epsilon^{-\rho} \quad L \to \infty \ , \tag{1.50}$$

para ello $\omega = \rho/\nu$.

Por otra parte puesto que en el sistema finito no hay transición de fase:

$$f(y) \to f_0 \quad \epsilon \to 0 \ , \tag{1.51}$$

es decir $f(y)$ debe aproximar una constante finita en el punto crítico.

Para resumir, el resultado significativo de este análisis, desde el punto de vista de extraer información numérica, es que la forma en que varían las magnitudes termodinámicas con el tamaño de la red está determinada por los exponentes críticos del sistema en el límite termodinámico: dado un observable $Q(\epsilon)$ que en $L = \infty$ diverge en el punto de la transición como $Q(\epsilon) \sim \epsilon^{-\rho}$, en L finito su comportamiento será de la forma:

$$Q_L(T_c^*(L)) \sim f_0 L^{\rho/\nu} \ . \tag{1.52}$$

1.3.2 Transiciones de fase de primer orden.

Como ya se ha señalado anteriormente, según el criterio básico de clasificación termodinámica las transiciones de fase de primer orden son aquellas

en las que la primera derivada de la energía libre presenta una discontinuidad.

Cuando un sistema realiza una transición de fase de primer orden de una fase de alta temperatura a otra de baja temperatura, éste desprende una cantidad no nula de calor (el *calor latente* C_l) a medida que se enfría en un intervalo infinitesimal de temperaturas alrededor de la temperatura de la transición. El valor de C_l se relaciona con el salto en la entropía que se produce en las transiciones de primer orden de la siguiente forma:

$$\Omega = -(\partial F/\partial T) \quad \Rightarrow \quad C_l = T_c \Delta\Omega \ . \tag{1.53}$$

Se tiene mucho menor conocimiento teórico sobre el comportamiento de las transiciones de fase de primer orden que sobre los fenómenos asociados a las transiciones continuas. Esto es debido a que al no haber una longitud de correlación divergente, no podemos restringir el estudio a los fenómenos asociados a largas longitudes de onda, por lo tanto el concepto de Universalidad no es aplicable. Las singularidades que aparecen en las transiciones de primer orden se deben exclusivamente a la coexistencia de fases, no hay región crítica, ni exponentes críticos. No podemos usar por tanto la teoría de FSS para estudiar el comportamiento de estas transiciones en un volumen finito.

Debido a la existencia de calor latente, el calor específico es una función $\delta(\epsilon)$. Analogamente a lo que ocurre con las transiciones continuas, en una red finita de lado L, las singularidades de las funciones en el punto de la transición, en este caso las δ's, serán suavizadas y sustituidas por picos de altura finita. De la misma forma esperamos un desplazamiento de la temperatura a la cual aparecen estos picos con el tamaño de la red, $T_c^*(L)$.

Para discutir cuantitativamente los efectos de tamaño finito asociados a una transición de primer orden vamos a utilizar la aproximación fenomenológica introducida por Binder [12]. Se asumirá que el tamaño de la red es mayor que la longitud de correlación de cada fase, de tal manera que los observables toman los valores asintóticos de la transición.

En una red de lado L y a una cierta temperatura T, la distribución de probabilidad de la energía, $P_L(E)$, es gausiana:

$$P_L(E) = \frac{A}{\sqrt{C}} \exp\{-\frac{(E-E_0)^2 L^d}{2T^2 C}\} \ , \tag{1.54}$$

donde E_0 es la energía del sistema en el límite de volumen infinito, y es característica de la temperatura T. La anchura de la distribución es proporcional al calor específico en este límite, denotado por C.

En el punto de la transición de fase la característica fundamental de las transiciones de primer orden es la coexistencia entre fases. Supongamos

que ocurre una transición en $T = T_c$ de un estado desordenado a un estado ordenado con degeneración q. Denotemos por E_+ (E_-) la energía interna de la fase desordenada (ordenada) a $T = T_c$, de manera que el calor latente es $E_+ - E_-$.

La generalización de (1.54) al caso en que hay coexistencia de fases es considerar que la distribución de probabilidad a T_c es una doble gaussiana. En el intervalo $\Delta T = T - T_c$ las gaussianas estarán centradas respectivamente en $E_+ + C_+\Delta T$ y $E_- + C_-\Delta T$:

$$P_L(E) \propto \frac{a_+}{\sqrt{C_+}} \exp\{-\frac{(E - E_+ - C_+\Delta T)^2 L^d}{2T^2 C_+}\} \tag{1.55}$$

$$+ \frac{a_-}{\sqrt{C_-}} \exp\{-\frac{(E - E_- - C_-\Delta T)^2 L^d}{2T^2 C_-}\} \ , \tag{1.56}$$

siendo C_+ y C_- el calor específico de las fases desordenada y ordenada respectivamente:

$$\lim_{T \to T_c^-} C_v(T) = C_- \tag{1.57}$$

$$\lim_{T \to T_c^+} C_v(T) = C_+ \ , \tag{1.58}$$

Puesto que se está considerando el comportamiento del sistema cerca de T_c se puede considerar que C_+ y C_- son constantes a lo largo de esta región. Los dos picos están pesados de acuerdo con la diferencia de energía libre entre las dos fases $\Delta F(T) = F_+ - F_-$, de manera que lejos de T_c sólo uno de los picos sobrevive, mientras que en el punto de la transición $\Delta F(T_c) = 0$ y ambos términos contribuyen con el mismo peso:

$$a_+ = \sqrt{C_+} e^x \tag{1.59}$$

$$a_- = q\sqrt{C_-} e^{-x} \ , \tag{1.60}$$

donde

$$x = \frac{-\Delta F L^d}{2T} \ . \tag{1.61}$$

Se puede aproximar x expandiendo en serie F_+ y F_- entorno a T_c hasta orden ΔT (orden mayor significaría considerar la variación de C_+ y C_-). Teniendo en cuenta que $F_\pm = U_\pm - TS_\pm$ y que $dF_\pm = -S_\pm dT$ se obtiene:

$$\Delta F = \frac{-(E_+ - E_-)\Delta T}{T_c} \tag{1.62}$$

El valor medio de la energía vendrá dado por el primer momento de la distribución de probabilidad (1.56):

$$\langle E\rangle = \frac{a_+E_+ + a_-E_-}{a_+ + a_-} + \Delta T \frac{a_+C_+ + a_-C_-}{a_+ + a_-} \ , \tag{1.63}$$

y por lo tanto el calor específico:

$$\begin{aligned} C_v(T,L) &= \frac{\partial\langle E\rangle_L}{\partial T} = \frac{a_+C_+ + a_-C_-}{a_+ + a_-} &(1.64)\\ &+ \frac{a_+a_-L^d}{T^2}\frac{[(E_+ - E_-) + (C_+ - C_-)\Delta T]^2}{(a_+ + a_-)^2} \ , &(1.65)\end{aligned}$$

cuyo máximo ocurre para:

$$\frac{T_c^*(L) - T_c}{T_c} = \frac{T_c \log q}{E_+ - E_-}\frac{1}{L^d} \ , \tag{1.66}$$

con una altura de:

$$C_v(L)^{\max} = \frac{(E_+ - E_-)^2}{4T_c^2}L^d + \frac{C_+ + C_-}{2} \ . \tag{1.67}$$

Cuando se está interesado en simulaciones de Monte Carlo hay errores asociados a la simulación que pueden hacer más aceptable una descripción de los efectos de tamaño finito en función de exponentes efectivos:

$$\begin{aligned} T_c^*(L) - T_c(\infty) &\propto L^{-\lambda} &(1.68)\\ C_v^{\max}(L) &\propto L^{\alpha_m} \ , &(1.69)\end{aligned}$$

donde hemos introducido los índices λ y α_m para estudiar esta dependencia con L. Es decir, el resultado que se encuentra es que los exponentes λ y α_m son igual a la dimensión del espacio, d, asintoticamente, es decir para L suficientemente grande ($L \gg \xi$).

Sin embargo la definición de estos exponentes es puramente formal, y no tienen nada que ver con las definiciones que hemos visto En una transición de primer orden L aparece sólo porque el volumen es L^d en d dimensiones: los máximos de las susceptibilidades y del calor específico crecen como L^d y la función δ se obtiene en el límite de volumen infinito porque la anchura de estas funciones decrece como L^{-d}.

Desde el punto de vista del estudio numérico, en las transiciones de primer orden, en general, cualquier observable termodinámico muestra en la evolución de MC saltos entre las dos fases (*flip-flops*) generando una distribución de doble pico.

Las transiciones fuertes (pequeña ξ) son fáciles de detectar. Las discontinuidades se observan ya a nivel de los ciclos de histeresis que muestran ramas metaestables. Las discontinuidades en la magnitudes termodinámicas son relativamente fáciles de detectar, y tanto el calor específico como las susceptibilidades en transiciones magnéticas divergen como L^d para redes de tamaño no muy grande.

La situación numérica es menos clara en las llamadas transiciones de primer orden débiles. La longitud de correlación es muy grande, y por tanto los efectos transitorios se prolongan hasta redes de tamaño respetable para nuestro actuales ordenadores. En estos casos uno debe simular redes de L creciente y tratar de ver si el comportamiento de primer orden anteriormente descrito se alcanza en el límite de volumenes muy grandes. En particular se pueden usar las técnicas desarrolladas de FSS para estudiar los exponentes críticos efectivos y ver como evolucionan con L las magnitudes termodinámicas. Dentro de este contexto se dice que en la región asintótica las transiciones de primer orden tienen asociado un exponente crítico "ν"$= 1/d$ o que "α/ν" $= d$, pero entendiendo bien que no son exponentes críticos definibles en sentido extricto.

Bibliography

[1] S.L. Glashow, *Nuc. Phys.***22** (1961) p 579
S. Weinberg, *Phys. Rev. Lett.* **19** (1967) p 1264

[2] K. Osterwalder and R. Schrader,
Commun. Math. Phys. **31** (1973) p 83
Commun. Math. Phys. **42** (1975) p 281

[3] K. Symanzik, J. Math. Phys. **7** (1966) p 510

[4] G. t'Hooft and M. Veltman, *Nuc. Phys.* **B44** (1972) p 189

[5] K.G. Wilson, *Phys. Rev.* **D10** (1974) p 2445

[6] A. Sokal,
"Bosonic Algorithms" en
Quantum Fields on the Computer
Ed. M. Creutz (World Scientific) (1992)

[7] M. Creutz, *Phys. Rev. Lett.* **43** (1979) p 553

[8] K. Osterwalder and E. Seiler, *Ann. Phys.* **110** (1978) p 440

[9] T.D. Lee and C.N. Yang, *Phys. Rev.* **87** (1952) p 410

[10] E. Brézin, J.C. Le Guillou and J. Zinn-Justin,
"Field Theoretical approach to critical phenomena" en
Phase Transition and Critical phenomena **Vol 6**
Ed. C. Domb and M.S. Green (Academic Press) (1976)

[11] M.N. Barber,
"Finite-size Scaling" en
Phase Transition and Critical phenomena **Vol 8**
Ed. C. Domb and J.L. Lebowitz (Academic Press) (1983)

[12] K. Binder, *Rep. Prog. Phys.* **50** (1987) 783

Chapter 2

El Modelo O(4) Anti-Ferromagnético

2.1 Introducción

En el Lagrangiano del Modelo Estándar el campo de Higgs está descrito por un campo escalar de cuatro componentes, el cual, aparte de interaccionar con los campos gauge y con los fermiones, interacciona consigo mismo a través de un autoacoplo cuártico. Si consideramos el límite en el que los acoplos gauge y los de Yukawa tienden a cero, los campos gauge y los fermiónicos se desacoplan. La acción correspondiente a este límite es el modelo $\lambda\mathbf{\Phi}^4$:

$$S_{\rm cont} = \int_\Omega \frac{1}{2}\sum_\mu (\partial_\mu \mathbf{\Phi}_{\rm B}(\mathbf{r}))^2 + \frac{1}{2} m_{\rm B}^2 \mathbf{\Phi}_{\rm B}(\mathbf{r})^2 + \frac{g_{\rm B}}{4!}\mathbf{\Phi}_{\rm B}(\mathbf{r})^4 \ . \tag{2.1}$$

Una forma conveniente de escribir la acción cuando estamos interesados en simulaciones de MC o expansiones de alta T es:

$$S_{\rm lat} = \sum_{\mathbf{r}} (-\kappa \sum_\mu \mathbf{\Phi}_{\mathbf{r}} \mathbf{\Phi}_{\mathbf{r}+\hat{\mu}} + \mathbf{\Phi}_{\mathbf{r}}^2 + \lambda[\mathbf{\Phi}_{\mathbf{r}}^2 - 1]^2) \ , \tag{2.2}$$

donde κ recibe el nombre de *hopping parameter*.

La correspondencia entre los parámetros en la red y en el contínuo es la siguiente:

$$\begin{aligned} \mathbf{\Phi}_{\rm B}(\mathbf{r})a &= \sqrt{2\kappa}\mathbf{\Phi}_{\mathbf{r}} \ ; \\ m_{\rm B}^2 a^2 &= (1-2\lambda)/\kappa - 8 \ ; \\ g_{\rm B} &= 6\lambda/\kappa^2 \ . \end{aligned} \tag{2.3}$$

El diagrama de fases del modelo (2.2) presenta una linea de transiciones de segundo orden $\kappa_{\rm c}(\lambda)$ separando la fase simétrica de la fase en que la simetría O(4) está rota a O(3)$\otimes$O(3). El límite contínuo hay que tomarlo aproximándose a esta línea crítica.

En $\lambda = 0$ se tiene el punto fijo Gaussiano infrarojo puesto que la teoría en este límite se reduce al campo escalar libre. El límite contínuo en el entorno de este punto fijo es trivial en el sentido de que la constante de acoplamiento renormalizada $g_{\rm R}$ se hace cero.

Para poder definir un límite contínuo no trivial ($g_{\rm R} \neq 0$) es necesario encontrar un punto fijo ultravioleta.

En dimensión $d > 4$ está probado rigurosamente [1, 2] que $\lambda\mathbf{\Phi}^4$ no tiene ningún punto fijo ultravioleta, la teoría es por tanto trivial para todo valor de λ.

En dimensión $d = 4$ las evidencias analíticas [3, 4] y numéricas [5, 6, 7] acumuladas soportan la conjetura de Wilson [3] apuntando a la trivialidad de las teorías $\lambda\mathbf{\Phi}^4$. Sin embargo una prueba rigurosa como la obtenida en

$d > 4$ no ha sido obtenida, a pesar de los serios intentos llevados a cabo (ver por ejemplo [8]).

Los teoremas existentes cubren sólo ciertos casos especiales, que por argumentos de plausibilidad, se supone que las QFT deben cumplir [9]. En particular se asume generalmente que la autointeracción del campo escalar se puede tratar perturbativamente. Sin embargo las teorías con acoplos negativos generan fuertes oscilaciones en los campos, que podrían dar lugar a que se generen no perturbativamente nuevos puntos fijos, donde eventualmente se podrían definir límites contínuos no triviales [10]. Desde este punto de vista el estudio de teorías Anti-ferromagnéticas (AF) es interesante puesto que nada impide formular una una QFT, "honesta" en el sentido de que cumple los axiomas de Osterwalder-Schrader, usando modelos antiferromagnéticos (AF) [11].

El antiferromagnetismo ha sido considerado en una amplia variedad de modelos con el objetivo de encontrar propiedades no presentes en teorías puramente ferromagnéticos. En el contexto de la superconductividad de alta temperatura el AF parece jugar un papel esencial [12]. En dimensión $d = 4$, interacciones competitivas como posibles agentes de nuevas clases de universalidad han sido investigadas para estudiar el punto multicrítico de modelos tipo Yukawa. Este punto multicrítico es el punto de encuentro de cuatro fases distintas (FM, AF, Ferrimagnética y Paramagnética (PM)). La cuestión de si es posible o no definir un límite contínuo no trivial en este punto permanece como un problema abierto [13, 14, 15, 16].

Así pues el estudio de modelos AF se presenta como una posibilidad interesante de estudiar en detalle. Estos modelos suelen presentar diagramas de fases muy ricos, y presumiblemente nuevas clases de universalidad podrían ser encontradas [17]. La existencia de acoplamientos de signo opuesto influencia el vacío de la teoría, en concreto en el estado fundamental se pueden observar fenomenos de frustración (la energía no puede ser minimizada simultaneamente para todos los acoplamientos) o de desorden (la entropía del vacío es distinta de cero).

En el trabajo que se presenta a continuación se considera la teoría $\lambda\mathbf{\Phi}^4$ en el límite en que $\lambda \to \infty$, lo cual equivale a fijar el módulo del campo de Higgs. Para introducir Antiferromagnetismo se ha añadido un acoplo negativo a segundos vecinos. El objetivo es la búsqueda y caracterización de puntos de transición de fase de segundo orden en el diagrama de fases.

Abstract

We study the phase diagram of the four dimensional O(4) model with first (β_1) and second (β_2) neighbor couplings, specially in the $\beta_2 < 0$ region, where we find a line of transitions which is compatible with second order. We also compute the critical exponents on this line at the point $\beta_1 = 0$ (F_4 lattice) by Finite Size Scaling techniques up to a lattice size $L = 24$, being these exponents different from the Mean Field ones.

2.2 Description of the model

Our starting point is the non-linear σ model, with action:

$$S_\sigma = -\beta \sum_{\mathbf{r},\mu} \mathbf{\Phi_r} \mathbf{\Phi_{r+\hat{\mu}}} \ . \tag{2.4}$$

Where $\mathbf{\Phi}$ is a 4-component vector with fixed modulus $\mathbf{\Phi_r} \cdot \mathbf{\Phi_r} = 1$.

The naive way to introduce AF in the non-linear σ model is to consider a negative coupling. In this case the state with minimal energy for large β is a staggered vacuum. On a hypercubic lattice, if we denote the coordinates of site $\mathbf{r}$ as (r_x, r_y, r_z, r_t), making the transformation

$$\mathbf{\Phi_r} \to (-1)^{r_x+r_y+r_z+r_t} \mathbf{\Phi_r} \ , \tag{2.5}$$

the system with negative β is mapped onto the positive β one, both regions being exactly equivalent.

Therefore to consider true AF we must take into account either different geometries or more couplings, in order to break the symmetry under the transformation (2.5). In four dimensions the simplest option is to add more couplings, we have chosen to add a coupling between points at a distance of $\sqrt{2}$ lattice units.

Following this we will consider a system of spins $\{\mathbf{\Phi_r}\}$ taking values in the hyper-sphere $S^3 \subset \mathbf{R^4}$ and placed in the nodes of a cubic lattice. The interaction is defined by the action

$$S = -\beta_1 \sum_{\mathbf{r},\mu} \mathbf{\Phi_r} \mathbf{\Phi_{r+\hat{\mu}}} - \beta_2 \sum_{\mathbf{r},\mu<\nu} \mathbf{\Phi_r} \mathbf{\Phi_{r+\hat{\mu}+\hat{\nu}}} \ , \tag{2.6}$$

The transformation (2.5) maps the semi-plane $\beta_1 > 0$ onto the $\beta_1 < 0$, and therefore only the region with $\beta_1 \geq 0$ will be considered. On the line $\beta_1 = 0$ the system decouples in two F_4 independent sublattices.

When $\beta_2 = 0$ the model is known to present a continuous transition between a disordered phase, where O(4) symmetry is exact, to an ordered

phase where the O(4) symmetry is spontaneously broken to O(3). This transition is second order, being the critical exponents those of MFT: $\alpha = 0$, $\nu = 0.5$, $\beta = 0.5$, $\eta = 0$ and $\gamma = 1$ up to logarithmic corrections. The critical coupling for this case can be studied analytically by an expansion in powers of the coordination number ($q = 2d$), being $\beta^c = 0.6055 + O(q^{-2d})$ [18].

From a Mean Field analysis, we observe that for $\beta_2 > 0$ the behavior of the system will not change qualitatively from the $\beta_2 = 0$ case but with higher coordination number. In fact, taking into account that the energy (for non-frustrated systems) is approximately proportional to the coordination number, there will be a transition phase line whose approximate equation is

$$\beta_1^c + Q\beta_2^c = \beta^c \ , \tag{2.7}$$

where Q is the quotient between the number of second and first neighbors, $2d(d-1)$ and $2d$, respectively. This line can be thought as a prolongation of the critical point at $\beta_2 = 0$ so the transitions on this line are expected to be second order with MFT exponents. This is also the behavior of the two couplings Ising model in this region [19].

When $\beta_2 < 0$, the presence of two couplings with opposite sign makes frustration to appear, and very different vacua are possible.

2.3 Observables and order parameters

We define the energy associated to each coupling:

$$E_1 \equiv \frac{\partial \log Z}{\partial \beta_1} = \sum_{\mathbf{r},\mu} \mathbf{\Phi}_{\mathbf{r}} \cdot \mathbf{\Phi}_{\mathbf{r}+\hat{\mu}} \ , \tag{2.8}$$

$$E_2 \equiv \frac{\partial \log Z}{\partial \beta_2} = \sum_{\mathbf{r},\mu<\nu} \mathbf{\Phi}_{\mathbf{r}} \cdot \mathbf{\Phi}_{\mathbf{r}+\hat{\mu}+\hat{\nu}} \ . \tag{2.9}$$

In terms of these energies, the action reads

$$S = -\beta_1 E_1 - \beta_2 E_2 \ . \tag{2.10}$$

It is useful to define the energies per bound as

$$e_1 = \frac{1}{4V} E_1, \ e_2 = \frac{1}{12V} E_2 \ , \tag{2.11}$$

where $V = L^4$ is the lattice volume. With this normalization e_1 , e_2 belong to the interval $[-1, 1]$.

We have computed the configurations which minimize the energy for several asymptotic values of the parameters. We have only considered configurations with periodicity two. More complex structures have not been observed in our simulations.

Considering only the $\beta_1 \geq 0$ case, we have found the following regions:

1. Paramagnetic (PM) phase or disordered phase, for small absolute values of β_1, β_2.

2. Ferromagnetic (FM) phase. It appears when $\beta_1 + 6\beta_2$ is large and positive.

   When the fluctuations go to zero, the vacuum takes the form $\mathbf{\Phi_r} = \mathbf{v}$, where $\mathbf{v}$ is an arbitrary element of the hyper-sphere.

   Concerning the definition of the order parameter let us remark that because of tunneling phenomena in finite lattice we are forced to use pseudo-order parameters for practical purposes. Such quantities behave as true order parameters only in the thermodynamical limit. In the FM phase, we define the standard (normalized) magnetization as

   $$\mathbf{M}_{\mathrm{F}} = \frac{1}{V} \sum_{\mathbf{r}} \mathbf{\Phi_r} \ , \tag{2.12}$$

   and we use as pseudo-order parameter the square root of the norm of the magnetization vector

   $$M_{\mathrm{F}} = \langle \sqrt{\mathbf{M}_{\mathrm{F}}^2} \rangle \ . \tag{2.13}$$

   This quantity has the drawback of being non-zero in the symmetric phase but it presents corrections to the bulk behavior order $1/\sqrt{V}$.

3. Hyper-Plane Antiferromagnetic phase (HPAF). It corresponds to large β_1, with β_2 in a narrow interval ($[-\beta_1/2, -\beta_1/6]$ in the Mean Field approximation). In this region the vacuum correspond to spins aligned in three directions but anti-aligned in the fourth (μ).

   In absence of fluctuations the associated vacuum would be $\mathbf{\Phi_r} = (-1)^{r_\mu}\mathbf{v}$, where μ can be any direction, and $\mathbf{v}$ any vector on S^4.

   We define an *ad hoc* order parameter for this phase as

   $$\mathbf{M}_{\mathrm{HPAF},\mu} = \frac{1}{V} \sum_{\mathbf{r}} (-1)^{r_\mu} \mathbf{\Phi_r} \ . \tag{2.14}$$

   $\mathbf{M}_{\mathrm{HPAF},\mu}$ will be different from zero only in the HPAF phase, where the system becomes antiferromagnetic on the μ direction. From the

four order parameters (one for every possible value of μ) only one of them will be different from zero in the HPAF phase. So, we define as the pseudo order parameter:

$$M_{\mathrm{HPAF}} = \sqrt{\sum_{\mu} \mathbf{M}^2_{\mathrm{HPAF},\mu}} \ . \tag{2.15}$$

4. Plane Anti-Ferromagnetic (PAF) phase for β_2 large and negative. In this region the ground state is a configuration with spins aligned in two directions and anti-aligned in the remaining two. It is characterized with by one of the six combinations of two different directions (μ, ν), and an arbitrary spin $\mathbf{v}$: $\mathbf{\Phi_r} = (-1)^{r_\mu + r_\nu}\mathbf{v}$. For the PAF region we first define

$$\mathbf{M}_{\mathrm{PAF},\mu,\nu} = \frac{1}{V}\sum_{r}(-1)^{r_\mu + r_\nu}\mathbf{\Phi_r} \ , \tag{2.16}$$

and the quantity we measure is

$$M_{\mathrm{PAF}} = \sqrt{\sum_{\mu<\nu} \mathbf{M}^2_{\mathrm{PAF},(\mu,\nu)}} \tag{2.17}$$

In order to avoid undesirable (frustrating) boundary effects for ordered phases, we work with even lattice side L as periodic boundary conditions are imposed.

From this data we can compute the derivatives of any observable with respect to the couplings as the connected correlation function with the energies

$$\frac{\partial O}{\partial \beta_j} = \langle O E_j \rangle - \langle O \rangle \langle E_j \rangle \tag{2.18}$$

An efficient method to determine β_{c} for a second order transition is to measure the Binder cumulant [20] for various lattice size and to locate the cross point in the space of β.

For O(N) models $U_L(\beta)$ takes the form [21]:

$$U_L(\beta) = 1 + 2/N - \frac{\langle (\mathbf{m}^2)^2 \rangle}{\langle \mathbf{m}^2 \rangle^2} \tag{2.19}$$

where $\mathbf{m}$ is an order parameter for the transition.

It can be shown [20, 21] that $U_L(0) \to O(1/V)$ and $U_L(\infty) \to 2/N$. The slope of $U_L(\beta)$ at β_{c} increases with L.

The value of the Binder cumulant is closely related with the triviality of the theory since the renormalized coupling (in the massless thermodynamical limit) at zero momentum can be written as:

$$g_{\mathrm{R}} = \lim_{L\to\infty} g_{\mathrm{R}}(L) = \lim_{L\to\infty} (L/\xi_L)^d U_L(\beta_{\mathrm{c}}) \tag{2.20}$$

where ξ_L is the correlation length in the size L lattice.

From this point of view triviality is equivalent to have a vanishing g_{R} in the thermodynamical limit. In this context it is clear that we can use the value of g_{R} to classify the universality class. Out of the upper critical dimension, L/ξ_L is a constant at β_{c} since $\xi \sim L$, and we could use the Binder cumulant for the same purpose [22]. At the upper critical dimension, ξ_L presents logarithmic corrections and L/ξ_L is no longer a constant at β_{c}. For the FM O(4) model in $d = 4$ (upper critical dimension) we have perturbatively $L/\xi_L \sim (\ln L)^{-1/4}$ [23]. In order to have a non trivial theory, the Binder cumulant should behave as a positive power of $\ln L$, but from its definition [20] we see that $U_L(\beta) \leq 1$. This is just another way of stating the perturbative triviality of the FM O(4) model.

2.3.1 Symmetries on the $\mathbf{F}_4$ lattice

In the $\beta_1 = 0$ case the system decouples in two independent lattices, each one constituted by the first neighbors of the other. So we consider two lattices with F_4 geometry. There are several reasons to choose the point $\beta_1 = 0$ for a careful study of the PM-PAF transition. The region with $\beta_1 > 1.5$ evolve painfully with our local algorithms; For small β_1 we expect very large correlation in MC time because the interaction between both sublattices is very small, and the response of one lattice to changes in the other is very slow. We also remark that the presence of two almost decoupled lattices is rather unphysical.

We also have the experience from a previous work for the Ising model [19] that the correlation length at its first order transition is smaller in the F_4 lattice, that means, we can find asymptotic critical behavior in smaller lattices.

However we should point out that the results in the F_4 lattice cannot be easily extrapolated to a neighborhood of the β_1 axis. Certainly, the geometry of the model is very modified when $\beta_1 \neq 0$, and perhaps continuity arguments present problems. Nevertheless, we have run also the case $\beta_1 \sim 0$, and as occurs in the Ising model we have not found qualitative differences.

In the following when we refer to the size of the lattice L on the F_4 lattice we mean a lattice with $L^4/2$ sites.

We have to find the configurations that maximize E_2 in order to define appropriate order parameters for the phase transition.

The system has a very complex structure. As starting point we have studied numerically the vacuum with $\beta_2 \ll 0$. For this values we have found in the simulation:

1. The vacuum has periodicity two. To check this, we have defined:

$$\mathbf{V}_i = \frac{1}{L^d/2^d} \sum_I \mathbf{\Phi}_{I_i} \ , \tag{2.21}$$

   where $i = 0, \ldots, 7$ stands for the i^{th} vertex of each 2^4 hypercube belonging to the F_4 lattice, and with I we denote the 2^4 hypercubes themselves.

   From these vectors we can define the 8 magnetizations associated to the elementary cell,

$$V_i = \langle \sqrt{\mathbf{V}_i^2} \rangle \ , \tag{2.22}$$

   We have checked that all V_i tends to 1 for the ordered phase in the thermodynamical limit, so we conclude that the ordered vacua have periodicity two.

   Let us remark for the sake of completeness that all order parameters we have defined can be written as an appropriate linear combination of the $\mathbf{V}_i$.

2. In the elementary cell, $\mathbf{\Phi}_{\mathbf{r}+\hat{\mu}+\hat{\nu}} = \mathbf{\Phi}_{\mathbf{r}}$ $\forall \mu, \nu$ with $\mu < \nu$. So, in this section we will restrict the study of the vacuum structure to the four sites ($i = 0, 1, 2, 3$) belonging to the cube in the hyper-plane $r_t = 0$.

3. We have measured the energy per bound associated to the second neighbors coupling. We check that in the thermodynamical limit $e_2 = -1/3$.

4. If we choose the symmetry breaking direction by keeping fix one vector, (eg. $\mathbf{\Phi}_0$) we find:

$$\sum_{i=1}^{3} ((\mathbf{\Phi_0} \cdot \mathbf{\Phi_i})\mathbf{\Phi_0} - \mathbf{\Phi_i}) = 0 \ , \tag{2.23}$$

The vacuum structure is not completely fixed by these three conditions since different symmetry breaking patterns are possible. For instance, a configuration $\mathbf{\Phi}_0 = (1, 0, 0, 0)$, $\mathbf{\Phi}_1 = (-1/3, \frac{2\sqrt{2}}{3}\mathbf{v_1})$, $\mathbf{\Phi}_0 = (-1/3, \frac{2\sqrt{2}}{3}\mathbf{v_2})$, $\mathbf{\Phi}_0 = (-1/3, \frac{2\sqrt{2}}{3}\mathbf{v_3})$, with v_i a 3-component unitary vector with the constraint $\sum_{i \neq j} \mathbf{v_i v_j} = 0$, breaks O(4), but an O(2) symmetry remains (for the different v_i).

To determine which is the vacuum in presence of fluctuations, we consider four independent fields in a 2^4 cell with periodic boundary conditions. Let us first consider an O(2) group. We can study the four vectors as a mechanical system of mass-less links of length unity, rotating in a plane around the same point, whose extremes are attached with a spring of natural length zero. The energy for the system is:

$$E = -\sum_{i,j=0,i>j}^{3} \cos(\theta_i - \theta_j) \ . \tag{2.24}$$

We consider the fluctuation matrix, $H = \partial E^2/\partial\theta_i\partial\theta_j$ in order to find the normal modes. The matrix elements of H take the form:

$$H_{i,j} = \delta_{ij}\sum_{k\neq i}\cos(\theta_i - \theta_k) - \cos(\theta_i - \theta_j)(1-\delta_{ij}) \ , \tag{2.25}$$

In the FM case the minimum correspond to $\theta_i = \phi$, for all i. The fluctuation matrix is

$$H_{FM} = \begin{pmatrix} -3 & 1 & 1 & 1 \\ 1 & -3 & 1 & 1 \\ 1 & 1 & -3 & 1 \\ 1 & 1 & 1 & -3 \end{pmatrix}$$

which has a single zero mode, and a three times degenerated non-zero mode with eigenvalue $\lambda = -4$.

For the AF (maximum energy) case, the maximum energy is found, up to permutations, at $\theta_0 = \phi$, $\theta_1 = \phi + \pi$, $\theta_2 = \phi + \alpha$ and $\theta_3 = \phi + \pi + \alpha$, $\forall\alpha$. In addition to the ϕ freedom that corresponds to the global O(2) symmetry, there is a degeneration of the vacuum in the α angle and this zero mode is double $\forall\alpha$.

The fluctuation matrix in the AF case is

$$H_{AF} = \begin{pmatrix} 1 & -1 & \cos\alpha & -\cos\alpha \\ -1 & 1 & -\cos\alpha & \cos\alpha \\ \cos\alpha & -\cos\alpha & 1 & -1 \\ -\cos\alpha & \cos\alpha & -1 & 1 \end{pmatrix}$$

The other two eigenvalues are $\lambda_{1,2} = 2(1 \pm \cos\alpha)$, so, an additional zero mode appears when $\alpha = 0$, obtaining in this case a three fold degenerated zero mode corresponding to: $\theta_0 = \theta_1 = \theta_2 + \pi = \theta_3 + \pi$.

The O(4) case is qualitatively similar. We have 12 degrees of freedom. Of all configurations that minimize the energy, that with a largest degeneration (9-times) consist of 2 spins aligned and 2 anti-aligned that correspond

to a PAF vacuum. We consider this degeneration as the main difference with the FM sector, and could be relevant to obtain different critical exponents.

In presence of fluctuations the configurations with largest degeneration are favored by phase space considerations, so we expect that the real vacuum is a PAF one. This statement will be checked below with Monte Carlo data in the critical region.

2.4 Finite Size Scaling analysis

Our measures of critical exponents are based on the FSS ansatz [24, 26]. Let be $\langle O(L,\beta)\rangle$ the mean value of an observable measured on a size L lattice at a coupling β. If $O(\infty,\beta) \sim |\beta - \beta_c|^{x_O}$, from the FSS ansatz one readily obtains [26]

$$\langle O(L,\beta)\rangle = L^{x_O/\nu} F_O(L/\xi(\infty,\beta)) + \dots \ , \tag{2.26}$$

where F_O is a smooth function and the dots stand for corrections to scaling terms.

To obtain ν we apply equation (2.26) to the operator $\mathrm{d}\log \mathrm{M_{PAF}}/\mathrm{d}\beta$ whose related x exponent is 1. As this operator is almost constant in the critical region, we just measure at the extrapolated critical point or any definition of the apparent critical point in a finite lattice, the difference being small corrections-to-scaling terms.

For the magnetic critical exponents the situation is more involved as the slope of the magnetization or the unconnected susceptibility is very large at the critical point.

We proceed as follows (see refs. [25] for other applications of this method). Let be Θ any operator with scaling law $x_\Theta = 1$ (for instance the Binder parameter or a correlation length defined in a finite lattice divided by L). Applying eq. (2.26) to an arbitrary operator, O, and to Θ we can write

$$\langle O(L,\beta)\rangle = L^{x_O/\nu} f_{O,\Theta}(\langle \Theta(L,\beta)\rangle) + \dots \ . \tag{2.27}$$

Measuring the operator O in a pair of lattices of sizes L and sL at a coupling where the mean value of Θ is the same, one readily obtains

$$\left.\frac{\langle O(sL,\beta)\rangle}{\langle O(L,\beta)\rangle}\right|_{\Theta(L,\beta)=\Theta(sL,\beta)} = s^{x_O/\nu} + \dots \ . \tag{2.28}$$

The use of the spectral density method (SDM) [27] avoids an exact a priori knowledge of the coupling where the mean values of Θ cross. We remark

that usually the main source of statistical error in the measures of magnetic exponents is the error in the determination of the coupling where to measure. However, using eq. (2.28) we can take into account the correlation between the measures of the observable and the measure of the coupling where the cross occurs. This allows to reduce the statistical error in an order of magnitude.

2.4.1 FSS at the upper critical dimension: logarithmic corrections

Being $d = 4$ the upper critical dimension of the FM O(4) model, logarithmic corrections to the Mean Field predictions are expected to set in. In particular, FSS in its standard formulation breaks at $d = 4$ because the essential assumption, namely $\xi_L(\beta_c) \sim L$ is no longer true. In fact, in four dimensions [29]:

$$\xi(\infty, t) \sim |t|^{-1/2} |\ln |t||^{\frac{1}{4}} \ . \tag{2.29}$$

The FSS formula for the correlation length was calculated by Brezin [23]. At the critical point one gets:

$$\xi(L, \beta_c) \sim L(\ln L)^{1/4} \ . \tag{2.30}$$

It has been suggested [28] that the usual FSS statement should be replaced by the more general one:

$$\frac{O(L, \beta_c)}{O(\infty, \beta)} = F_O \left(\frac{\xi(L, \beta_c)}{\xi(\infty, \beta)} \right) \ . \tag{2.31}$$

When applying the quotient method described above to systems in four dimensions one has to take into account the logarithmic corrections, so that the modified formula reads:

$$\left. \frac{\langle O(sL, \beta) \rangle}{\langle O(L, \beta) \rangle} \right|_{\Theta(L,\beta)=\Theta(sL,\beta)} = s^{x_O/\nu} \left(1 + \frac{\ln s}{\ln L} \right)^{1/4} \ . \tag{2.32}$$

This point is particularly important when measuring the magnetic critical exponents because as we have already mentioned, the slope of the magnetization and susceptibility are very large, and special care has to be taken when locating the coupling where to measure.

2.5 Numerical Method

We have simulated the model in a L^4 lattice with periodic boundary conditions. The biggest lattice size has been $L = 24$. For the update we have

employed a combination of Heat-Bath and Over-relaxation algorithms (10 Overrelax sweeps followed by a Heat-Bath sweep).

The dynamic exponent z we obtain is near 1. Cluster type algorithms are not expected to improve this z value. In systems with competing interactions the cluster size average is a great fraction of the whole system, loosing the efficacy they show for ferromagnetic spin systems.

We have used for the simulations ALPHA processor based machines. The total computer time employed has been the equivalent of two years of ALPHA AXP3000. We measure every 10 sweeps and store the individual measures to extrapolate in a neighborhood of the simulation coupling by using the SDM.

In the F_4 case, we have run about $2 \times 10^5 \tau$ for each lattice size, being τ the largest integrated autocorrelation time measured, that corresponds to M_{PAF}, and ranges from 2.3 measures for $L = 6$ to 8.9 for $L = 24$. We have discarded more than $10^2 \tau$ for thermalization. The errors have been estimated with the jack-knife method.

2.6 Results and Measures

2.6.1 Phase Diagram

We have studied the phase diagram of the model using a $L = 8$ lattice. We have done a sweep along the parameter space of several thousands of iterations, finding the transition lines shown in Figure 1. The symbols represent the coupling values where a peak in the order parameter derivative appears.

The line FM-PM has a clear second order behavior. It contains the critical point for the O(4) model with first neighbor couplings ($\beta_1 \approx 0.6$, $\beta_2 = 0$) with classical exponents ($\nu = 0.5$, $\eta = 0$). In the $\beta_1 = 0$ axis, we have computed the critical coupling ($\beta_2^c \approx 0.18$) and the critical exponents as a test for the method in the F_4 lattice. We have also considered the influence of the logarithmic corrections when computing the exponents.

The lines FM-HPAF, HPAF-PAF and PM-HPAF show clear metastability, indicating a first order transition.

The regions between the lower dotted line and the PAF transition line, and between the upper dotted line and the FM transition line, are disordered up to our numerical precision. We could expect always a PM region separating the different ordered phases, however, from a MC simulation it is not possible to give a conclusive answer since the width of the hypothetical PM region decreases when increasing β_1, and for a fixed lattice size there is a practical limit in the precision of the measures of critical values.

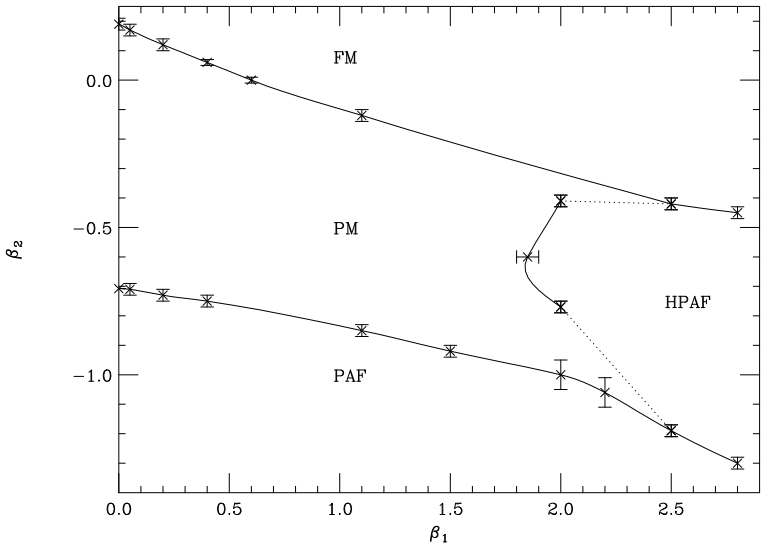

Figure 2.1: Phase diagram obtained from the MC simulation on a $L = 8$ lattice

The line PM-PAF has a very interesting behavior. To get ride of the influence of the HPAF region we have started the study at $\beta_1 = 1.5$. The energy distributions encountered at $\beta_1 = 1.5$ and $\beta_1 = 1.0$ are displayed in figure 2.2. We do not obeserve latent heat anymore in lattices up to L=16 in $\beta_1 = 0$. Two scenarios are suggested by this fact:

1. There exist a value of β_1 in which the order of the phase transition changes from being first order, to be continuous.

2. The phase transition line is first order everywhere, though increasily weak as the limit $\beta_1 = 0$ is approached.

The possibility of a second order behavior of the PM-PAF transition line contrast with the first order one found in the Ising model with two couplings in the analogous region [19]. This would not be that surprising because we are dealing now with a global continuous symmetry. The spontaneous symmetry breaking of such symmetries manifest in the appearance of soft modes or low energy excitations (long wavelength), the Goldstone bosons in QFT terminology [29]. In general, these low energy modes will perturb the mechanism of long distance ordering, softening in this way the phase transitions.

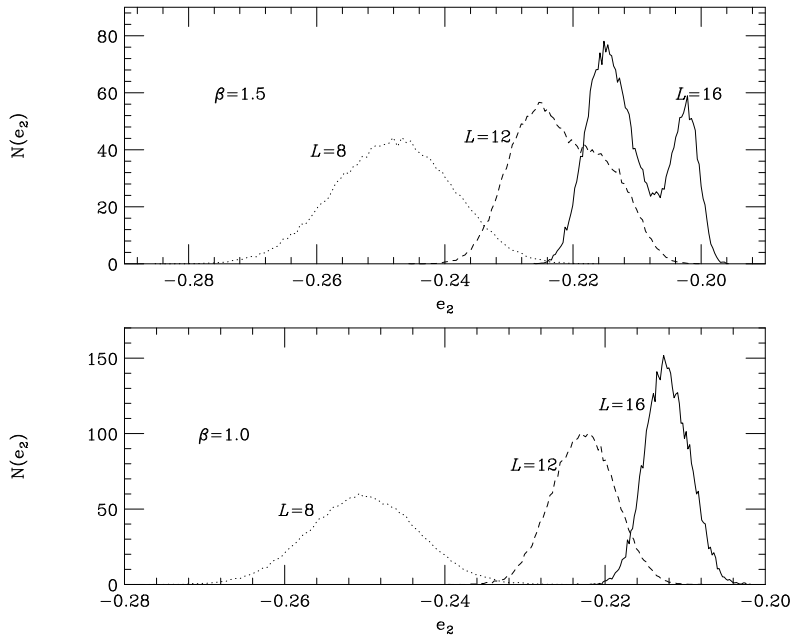

Figure 2.2: Energy distribution for L=8,12,16 measured at the peak of the specific heat at $\beta_1 = 1.5$ (upper window) and at $\beta_1 = 1.0$ (lower window).

Regarding the differences with the FM case, the most remarkable feature is the different vacuum structures appearing, specially the very large degeneration in the PAF transition, in contrast with the single degeneration of the FM O(4) mode.

For the reasons mentioned in section 1.3.1, the simpler point for studying the properties of the transition, namely the critical exponents is the F_4 limit. Most of the MC work has been done for this case.

2.6.2 Results on the F_4 lattice

Results on the FM region

Firstly, we have checked our method on the FM region of the F_4 lattice. In Figure 3 the crossing points of the Binder cumulant for various lattice sizes are displayed. The prediction for the critical coupling $\beta_c \sim 0.1831(1)$ agrees with an earlier study by Bhanot [30].

Concerning the measures of critical exponents, we have applied the quotient method, described in section 1.4 . In table 2.1 we quote the results when logarithmic corrections are included (formula (2.32)), and also for

sake of comparison, when they are neglected (formula (2.28)). We see how in fact the agreement of the critical exponents with the MFT predictions is better when the logarithmic corrections are taken into account.

L values	8/16	12/16	10/12
(without logarithmic corrections)			
α/ν	0.08(5)	0.02(2)	0.13(12)
β/ν	0.92(3)	0.94(3)	0.87(4)
γ/ν	2.16(2)	2.12(2)	2.24(4)
(with logarithmic corrections)			
α/ν	0.0	0.0	0.03(8)
β/ν	1.04(3)	1.06(3)	1.04(2)
γ/ν	1.94(3)	1.90(4)	1.93(3)

Table 2.1: Critical exponents for the FM-PM phase transition in the F_4 lattice.

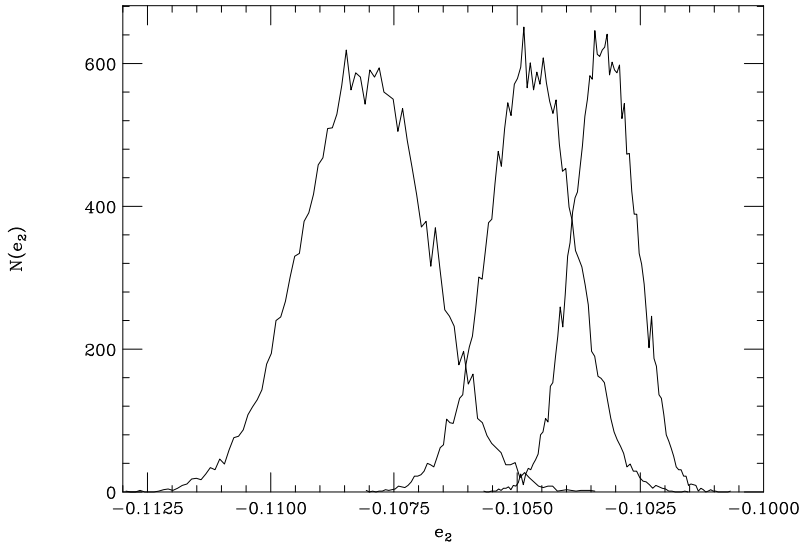

Figure 2.3: Energy distribution for L=16,20 and 24 at the peak of the specific heat on the F_4 lattice.

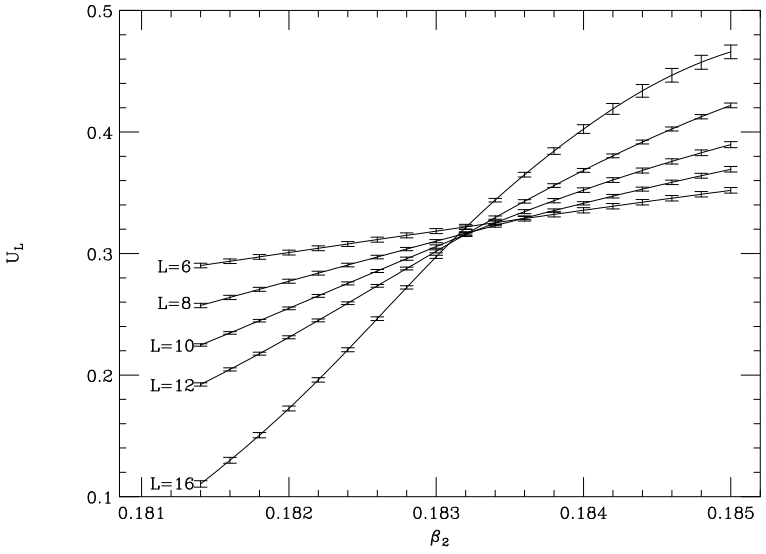

Figure 2.4: Crossing points of the Binder Cumulant for various lattice sizes on the FM-PM phase transition

From now on we will focus on the transition between the PM phase and the PAF phase on the F_4 lattice.

Vacuum symmetries on the PAF region

We will check using MC data that the ordered vacuum in the critical region is of type PAF.

Let us define

$$A_{ij} = \mathbf{V}_i \cdot \mathbf{V}_j \ . \tag{2.33}$$

The leading ordering corresponds to the eigenvector associated to the maximum eigenvalue of the matrix A, that should scale as $L^{-2\beta/\nu}$ at the critical point. The scaling law of the biggest eigenvalue agrees with the β/ν value reported in Table 2.3, and the associated eigenvector is, within errors, (1,1,-1,-1).

We also have found that the other eigenvalues scale as L^{-4}. This is the expected behavior if just the O(4) symmetry is broken, and it remains an O(3) symmetry in the subspace orthogonal to the O(4) breaking direction.

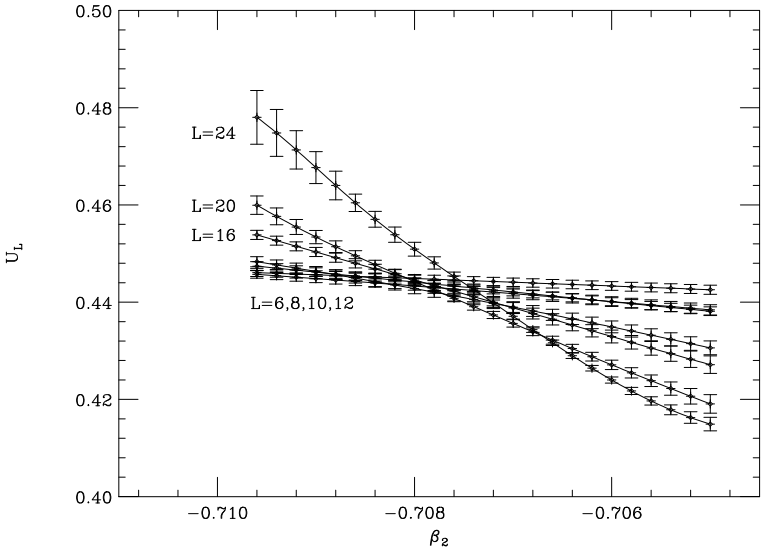

Figure 2.5: Crossing points of the Binder cumulant for various lattice sizes.

Critical Coupling

To obtain a precise determination of the critical point, β_c, we have used the data for the Binder parameter (2.19).

In Figure 4 we plot the crossing points of the Binder cumulants for the simulated lattices sizes. Extrapolations have been done using SDM from simulations at $\beta_2 = -0.7090$ for $L = 6, 8, 10, 12$ and 16; $\beta_2 = -0.7078$ for $L = 20$, and $\beta_2 = -0.7070$ for $L = 24$.

The shift of the crossing point of the curves can be explained through the finite-size confluent corrections. The dependence in the deviation of the crossing point for L and sL size lattices was estimated by Binder [20]

$$\beta_c(L, sL) - \beta_c \sim \frac{1 - s^{-\omega}}{s^{1/\nu} - 1} L^{-\omega - 1/\nu} \ , \tag{2.34}$$

where ω is the universal exponent for the corrections-to-scaling.

The infinite volume critical point the value

$$\beta_c = -0.7065(5)[+2][-2] \ , \tag{2.35}$$

where the errors in brackets correspond to the variations in the extrapolation when we use the values $\omega = 0.5$ and $\omega = 2$ respectively. In Figure 5

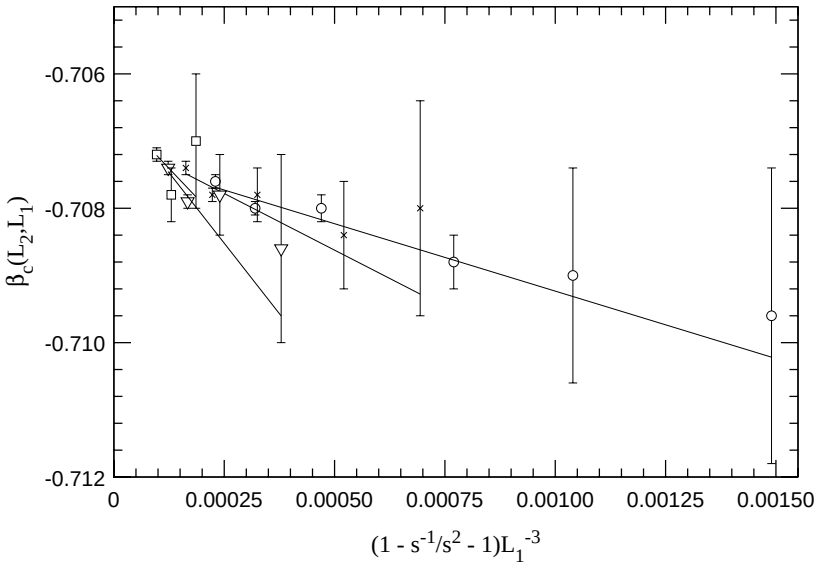

Figure 2.6: Extrapolation to $\beta_c(\infty)$ for $L_1 = 6, 8, 10, 12$ (circles, crosses, triangles and squares symbol respectively)

we plot eq. (2.34) for $\omega = 1$.

Using the previous value of β_c we can compute the Binder cumulant at this point. In table 2.2 we quote the obtained values. The result points to that the Binder cumulant stays constant in the critical region. This result would be compatible with a non zero value of the renormalized coupling when L increases.

Concerning the possibility of having logarithmic corrections in the determination of the critical coupling, from the numerical point of view, it is not possible to discern between the ω effect, and a logarithmic correction.

Thermal Critical exponents: α, ν

The critical exponent associated to correlation length can be obtained from the scaling of:

$$\kappa = \frac{\partial \log M}{\partial \beta} \ , \tag{2.36}$$

where M is an order parameter for the transition, $M_{\rm PAF}$ for our purposes. In the critical region $\kappa \sim L^{1/\nu}$. As κ is a flat function of β, is not crucial the

Lattice sizes	$U_L(\beta_c(\omega = 0.5))$	$U_L(\beta_c(\omega = 1))$	$U_L(\beta_c(\omega = 2))$
6	0.4435(15)	0.4437(12)	0.4438(12)
8	0.4406(15)	0.4409(12)	0.4413(12)
10	0.4407(14)	0.4411(16)	0.4414(14)
12	0.436(4)	0.437(3)	0.438(3)
16	0.435(3)	0.436(3)	0.437(3)
20	0.429(5)	0.431(5)	0.433(5)
24	0.428(6)	0.430(7)	0.433(7)

Table 2.2: Binder cumulant for various lattices sizes at the extrapolated critical point for $\omega = 0.5, 1, 2$.

point where we actually measure. The results displayed in table 2.3 have been obtained measuring at the crossing point of the Binder parameters for lattice sizes L and $2L$ using (2.28).

For measuring α/ν we study the scaling of the specific heat

$$C = \frac{\partial \langle E_2 \rangle}{\partial \beta_2} \ , \tag{2.37}$$

We expect that C scales as $A + BL^{\alpha/\nu}$, where A is usually non-negligible. In Figure 6 we plot the specific heat measuring at (2.35), as well as at the peak of the specific heat, as a function of L. We observe a linear behavior for intermediate lattices. For the largest lattice the slope decreases. The weak first order behavior [31] ($\alpha/\nu = 1$ for small lattices that becomes d for large enough sizes) seem hardly compatible with our data. If we neglect the A term (what is asymptotically correct), and compute the exponent using eq. (2.28) we obtain $\alpha/\nu \approx 0.3$ for intermediate lattices that reduces to $\alpha/\nu = 0.15(2)$ for the (20,24) pair.

However, to give a conclusive answer for the value of α statistics on larger lattices are mandatory.

Magnetic Critical exponents: γ, β

The exponents γ and β can be obtained respectively from the scaling of susceptibility and magnetization:

$$\chi \equiv V \langle M^2 \rangle \sim L^{\gamma/\nu} \tag{2.38}$$

$$M \sim L^{-\beta/\nu} \tag{2.39}$$

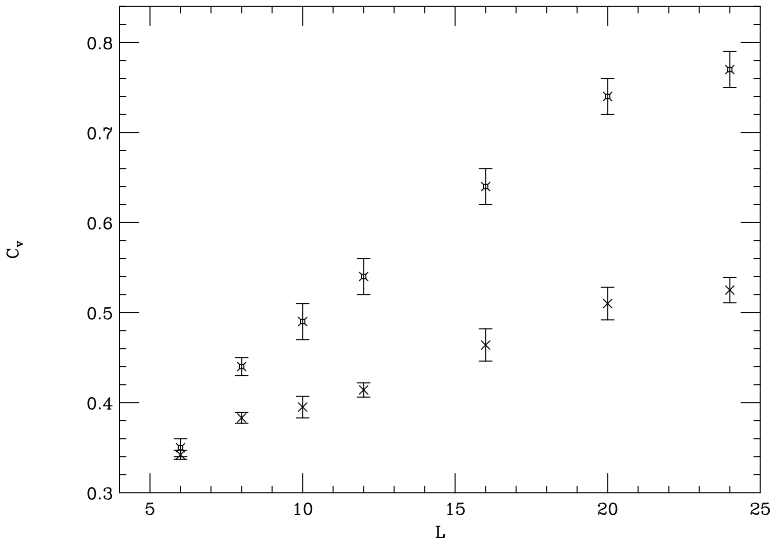

Figure 2.7: Specific heat at the peak (triangle symbols) and at $\beta = -0.7068$ (cross symbols) as a function of the lattice size.

Where M is an order parameter for the phase transition. In Figure 7 upper part, we plot the quotient between $M_{\rm PAF}$ for lattices L and $2L$ as a function of the quotient between the Binder cumulants for both lattice sizes.

For large L in the critical region we should obtain a single curve, the deviations corresponding to corrections to scaling. In the lower part of Figure 7 we plot the same function for susceptibility.

The values for γ and β are summarized in Table 2.3.

2.6.3 Logarithmic corrections

We now address the question of the possibility of logarithmic corrections in the AF O(4) model. For the thermal critical exponents, the situation seems clear, they are compatible with the classical exponent $\nu = 0.5$. For the magnetic exponents, the situation is more involved. In principle, one can think that they disagree from MFT due to logarithmic corrections. We have no perturbative predictions about the form in which these corrections would affect ξ_L for the AF case. However, one expects that such corrections

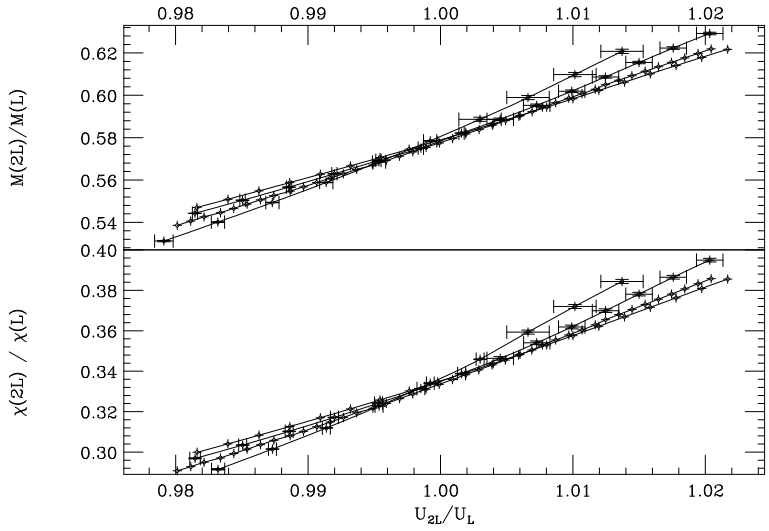

Figure 2.8: Quotients to obtain β/ν and γ/ν

slightly modify the critical exponents, as occurs in the FM case. It could be possible that logarithmic corrections modify largely the previous critical exponents and drift them to the FM ones. To sort this out, we have considered the possibility of a behavior FM like, so that $\xi_L \sim L(\ln L)^{1/4}$. In the lower part of Table 2.3 we quote the values of the critical exponents for the PAF phase transition when logarithmic corrections are included (formula (2.32)). We see how in effect the magnetic critical exponents are too far from the classical ones for being the result of a logarithmic correction to the MFT predictions. It is interesting to compare this situation with that in the RP^2 model in $d = 4$ [32] where small deviations from MFT exponents can be explained as logarithmic corrections.

2.7 Conclusions and open problems

We have studied the phase diagram of the four dimensional O(4) model with first and second neighbors couplings. We have found that the presence of couplings with opposite signs makes frustration to manifest in form of antiferromagnetism in different dimensionalities. Whether or not these

Lattice sizes	γ/ν	β/ν	ν
(without logarithmic corrections)			
6/12	2.417(3)	0.791(4)	0.474(10)
8/16	2.403(3)	0.792(6)	0.483(8)
10/20	2.410(2)	0.790(4)	0.471(6)
12/24	2.403(5)	0.797(5)	0.483(7)
20/24	2.398(5)	0.802(4)	0.487(6)
(with logarithmic corrections)			
6/12	2.301(3)	0.849(4)	0.484(9)
8/16	2.300(3)	0.850(5)	0.489(7)
10/20	2.315(2)	0.843(3)	0.488(5)
12/24	2.314(2)	0.842(5)	0.487(5)
20/24	2.317(5)	0.839(4)	0.498(5)

Table 2.3: Critical Exponents for the PM-PAF phase transition in the F_4 lattice

vacua have interest from the point of view of Quantum Field Theory is an open question. The transition between the paramagnetic phase, and the AF plane ordered one is compatible with very weak first order and with higher order. To shed some light on this question we have studied the evolution of the effective critical exponents in the limit $\beta_1 = 0$. We found that up to $L = 24$ the exponents are in disagreement with the Mean Field predictions. Specifically, from our γ/ν estimation (or β/ν using hyper-scaling relation) the exponent η asociated with the anomalous dimension of the field is $\eta \approx -0.4$. This fact itself would imply the non-triviality of the theory because Green functions would not factorize anymore. We have also measured the Binder cumulant at the critical point, finding that it stays almost constant when increasing the lattice size.

However, before claiming about the important issue of a non-trivial phase transition in four dimensions we have tried to acomodate the data in two possible scenarios: 1) logarithmic triviality; 2) weak first order scenario.

The mere observation of critical exponents different from the Mean Field ones is in principle still compatible with a logarithmic trivial theory. We have contrasted our data with the perturbative predictions derived in the FM case, which do not fit the results. It would be possible to obtain triviality also with a logarithmic exponent in equation (2.32) different from 1/4. We can fix the critical exponents to its mean field value and compute this parameter from the numerical data. The results obtained shown a non-

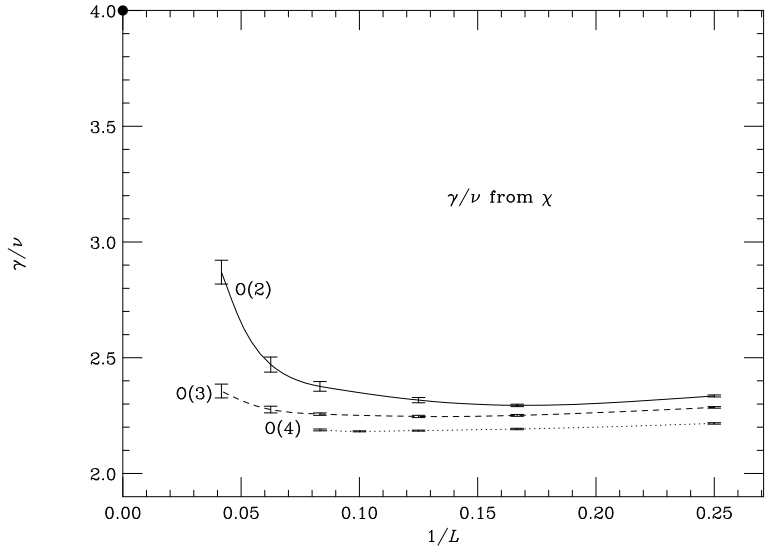

Figure 2.9: Effective γ/ν exponents in $O(N)$ with N=2,3,4.

asymptotic behavior with values ranging from 0.8 to 1.2 for the lattices used. In short, this model encounters the typical problems observed by other triviality studies, which make the numerical approach to this issue so difficult: one would need much stronger analytic insight to rule out logarithmic triviality.

In the other hand, the possibility of being behind a very weak first order phase transition is a possibility that cannot be discarded a priori. Our data do not evidence any two state signature. Moreover, the stability of our measure of γ/ν for lattices ranging from $L = 6$ to $L = 24$, which are more than a hundred standard deviations apart the MF value, makes this hypothesis rather unlikely. However the question is wether or not this hypothesis can be ruled out beyond any doubt. The phase transition in this region for the Ising case, O(1), has been shown to be first order [19]. Lately, the models O(2) and O(3) have been considered with the purpose of checking wether or not the order of the phase transition changes with N [33] in lattice sizes as larger as $L = 48$. Evidence is given for a first order character of the transition in O(2). In O(3) the transition is weaker, and despite no double peak structure is observed, the behavior of the effective exponents leaves little doubts about the first order character of O(3) as well

(see Figure 2.9). In the O(4) case we cannot observe any particular trend in the effective γ/ν . Indeed, since the transition seems to be continuous in the limit $N \to \infty$, $N = 4$ might be a sort of critical N value from which on the transition is second order.

However, from the observations in O(2) and O(3) we would be prone to consider the weak first order scenario as the most plausible. If the transition turns out to be first order, it would be weaker than the observed in O(3), and hence lattices larger than $L = 48$ would be needed to observe such asymptotic behavior in the critical exponents.

Bibliography

[1] M. Aizenman *Phys. Rev. Lett.* **47** (1981) p 1

[2] J. Frolich, *Nuc. Phys.* **B200 [FS4]** (1982) p 281

[3] K.G. Wilson and J. Kogut, *Phys. Rep.* **12** (1974) p 75

[4] G.A. Baker and J.M. Kincaid, *J. Stat. Phys.* **24** (1981) p 469

[5] M. Luscher and P. Weisz *Nuc. Phys.* **B290 [FS4]** (1987) p 25

[6] M. Luscher and P. Weisz *Nuc. Phys.* **B318 [FS4]** (1989) p 705

[7] C.B. Lang,
"Advances in lattice gauge theory"
Tallahasee conference 1985
Eds. D.W. Duke and J.F. Owens, World Scientific, Singapore, (1985)

[8] M. Aizenmann and R. Graham, *Nuc. Phys.* **B225** (1983) p 261

[9] R. Fernández, J. Frohlich and A. Sokal *"Random Walks, Critical Phenomena and Triviality in Quantum Field Theory" Texts and Monograph in Physics* Springer-Verlag (1992).

[10] G. Gallavotti and V. Rivasseau, *Ann. Inst. Henri Poincaré* **40, 2** (1984) p 185

[11] G. Gallavotti and V. Rivasseau, *Phys. Lett.* **B122** (1983) p 268

[12] J.L. Alonso, Ph. Boucaud, V. Martin-Mayor and A.J. Van der Sijs **hep-lat:/9706022**

[13] W. Bock, A.K. De, K. Jansen, J. Jersak, T. Neuhaus and J. Smit *Nuc. Phys.* **B344** (1990) p 207

[14] W. Bock, A.K. De, C. Frick, J. Jersak and T. Trapenberg *Nuc. Phys.* **B378** (1992) p 652

[15] T. Ebihara and K. Kondo *Prog. Theor. Phys.* **vol 87** (1992) p 4

[16] J.L. Alonso, Ph. Boucaud, F. Lesmes and E. Rivas. *Phys. Lett.* **B329** (1994) p 75

[17] J. Fingberg and J. Polonyi *Nuc. Phys.* **B486** (1997) p 315

[18] P.R.Gerber and M.E. Fisher, *Phys. Rev.* **B10** (1974) p 4697

[19] J.L. Alonso, J.M. Carmona, J. Clemente, L.A. Fernández, D. Iñiguez, A. Tarancón and C.L. Ullod, *Phys. Lett.* **B376** (1996) p 148

[20] K. Binder, *Z. Phys.* **B43** (1981) p 119

[21] E. Brezin and J. Zinn-Justin *Nuc. Phys.* **B257 [FS14]** (1985) p 867

[22] Giorgio Parisi, *Statistical Field Theory*, *Ed. Addison Wesley* (1992).

[23] E. Brezin *J. Phys.* **43** (1982) p 15

[24] C. Itzykson and J.M.Drouffe, *Statistical Field Theory*, **Vol. 1**, *Cambridge University Press* (1989)

[25] H. G. Ballesteros, L.A. Fernández, V. Martín-Mayor and A. Muñoz-Sudupe, *Nuc. Phys.* **B483** (1997) p 707

[26] *Finite size scaling, Current Physics - Sources and comments*, *vol. 2, Ed. J.L. Cardy*, *Elsever Science Publishers B. V.* (1988)

[27] A.M. Ferrenberg and R.H. Swendsen, *Phys. Rev. Lett.* **B61** (1988) p 2635

[28] R. Kenna and C.B. Lang *Nuc. Phys.* **B393** (1993) p 461

[29] Michel Le Bellac *Des phenomenes critiques aux champs de jauge* *Inter-Editions / Editions du CNRS, Paris* (1988)

[30] G. Bhanot *Nuc. Phys.* **B17** (Proc. Suppl.) (1990) 653

[31] L.A. Fernández, M.P. Lombardo, J.J Ruiz-Lorenzo and A. Tarancón, *Phys. Lett.* **B277**(1992) p 485

[32] H. G. Ballesteros, J.M. Carmona, L.A. Fernández, V. Martín-Mayor, A. Muñoz-Sudupe and A. Tarancón *Phys. Rev.* **D55** (1997) p 5067

[33] H.G. Ballesteros, J.M. Carmona, L.A. Fernández, A. Tarancón *Phys. Lett.* **B419** (1998) p 303

Chapter 3

La transición de fase en el modelo SU(2)-Higgs

3.1 Introducción

Los modelos Higgs describen la autointeracción del campo de Higgs y su acoplamiento con los campos gauge $\mathrm{SU}(2)_L$ y $\mathrm{U}(1)_Y$.

En la aproximación en la que se desprecian los acoplos de Yukawa entre el campo Higgs y los fermiones, estos modelos están considerados como una razonable descripción del sector electrodébil del Modelo Estándar. En particular se persigue mediante su formulación en la red dar cuenta de los aspectos no perturbativos de la teoría electrodébil, como por ejemplo la generación de masa mediante el mecanismo de ruptura espontánea de la simetría.

Los acoplamientos gauge de $\mathrm{U}(1)_Y$ y $\mathrm{SU}(2)_L$ se denotan respectivamente por $g'/2$ y g. La relación entre ellos es a través del ángulo de Weinberg, concretamente la relación es $g'/g = \tan\theta_{\mathrm{W}}$, puesto que este ángulo es pequeño ($\sin^2\theta_{\mathrm{W}} \approx 0.23$), podemos despreciar en un primer paso el grado de libertad $\mathrm{U}(1)_Y$. En este sentido SU(2)-Higgs puede considerarse como el modelo Higgs más simple.

El interés del estudio de estos modelos no es tanto la necesidad de determinar parámetros medibles en la naturaleza, sino más bien profundizar en el entendimiento teórico de la formulación de la teoría electrodébil. A diferencia de la QCD, esta teoría no es asintóticamente libre, el punto fijo gaussiano a acoplamiento cero es inestable ultravioleta, y la existencia de un punto fijo no trivial se hace necesaria para la formulación de la teoría en el continuo.

La acción del modelo SU(2)-Higgs consiste en una parte pura gauge más un término de interacción escalar-gauge:

$$S[U,\mathbf{\Phi}]_\lambda = S_{\mathrm{g}}[U] + S_{\mathbf{\Phi}}[U,\mathbf{\Phi}]\ . \tag{3.1}$$

La interacción entre la parte escalar y la gauge está controlada por el *hopping parameter*, κ. Una normalización adecuada cuando se está interesado en trabajar en el límite de autoacoplamiento cuártico infinito (regimen no perturbativo) es la siguiente:

$$\begin{aligned} S_{\mathbf{\Phi}}[U,\mathbf{\Phi}]_\lambda &= \sum_x \mathbf{\Phi}^\dagger(x)\mathbf{\Phi}(x) - \frac{1}{2}\kappa \sum_{x,\mu} \mathrm{tr}\ \mathbf{\Phi}^\dagger(x) U_\mu(x) \mathbf{\Phi}(x+\mu) \\ &+ \lambda \textstyle\sum_x [\mathbf{\Phi}^\dagger(x)\mathbf{\Phi}(x) - 1]^2\ , \end{aligned} \tag{3.2}$$

con esta normalización el límite $\lambda \to \infty$ equivale a fijar el modulo del campo Higgs a la unidad.

La parte pura gauge, $S_{\mathrm{g}}[U]$, se expresa como la suma sobre las plaquetas orientadas positivamente:

$$S_{\rm g} = \beta \sum_P (1 - \frac{1}{2} \,{\rm tr}\, U_{\rm P}) \ , \tag{3.3}$$

donde $\beta = 4/g^2$. En el límite $\beta \to \infty$ el campo gauge se desacopla y se recupera el modelo $\mathbf{\Phi}^4$, el cual presenta una transición de fase entre una región simétrica (pequeño κ) y una región en la que la simetría se ha roto espontaneamente (κ grande) [1].

Cuando β es finita ($g \neq 0$) esta transición de fase se prolonga en una línea de transiciones de fase en el interior del espacio de acoplos [3, 4, 5], como se muestra en la figura 3.1.

La continuación de la fase simétrica de $\mathbf{\Phi}^4$ cuando el acoplo gauge es distinto de cero es una región *confinante* en el sentido de que los campos gauge SU(2) confinan las partículas escalares de materia. En este sentido la fase simétrica de SU(2)-Higgs es análoga a QCD.

La continuación de la fase de simetría rota cuando el coupling gauge es distinto de cero es la fase *Higgs*. En esta fase, mediante el mecanismo de ruptura espontánea de la simetría, el campo de Higgs adquiere un valor esperado en el vacío distinto de cero. Los bosones vectoriales adquieren su masa a través de su acoplamiento con el campo escalar. Los tres bosones de Goldstone del modelo $\mathbf{\Phi}^4$ se hacen masivos al mezclarse con los bosones gauge vectoriales. El resultado es un isovector con spin 1, el boson W.

Esta línea de transiciones de fase termina en un valor finito del espacio de acoplamientos, estando las fases *Higgs* y *confinante* conectadas analiticamente.

En cuanto al orden de la transición de fase, para pequeños acoplamientos existen argumentos perturbativos debidos a Coleman y Weinberg [2] apuntando que la transición debería ser de primer orden. El estudio numérico de la transición de fase para pequeños e intermedios valores de λ parece confirmar esta conjetura [6, 7, 8].

Sin embargo se observa que la transición se debilita (las discontinuidades son más pequeñas) conforme λ aumenta. En el límite $\lambda = \infty$ la opinión generalizada es que la transición sigue siendo de primer orden aunque extremadamente débil, si bien no existen evidencias que justifiquen esta creencia. Los últimos resultados numéricos fueron obtenidos por Montvay en 1985, en redes no demasiado grandes y a pesar de observar metaestabilidades en los ciclos de histéresis no se pudieron obtener resultados concluyentes [11].

Tratando de arrojar algo de luz sobre este punto hemos enfocado el problema desde un punto de vista distinto, formulando el modelo SU(2)-Higgs en un espacio de parametros extendido. Sin embargo la motivación no es sólo hacer un estudio con alta estadística del modelo, sino tratar de

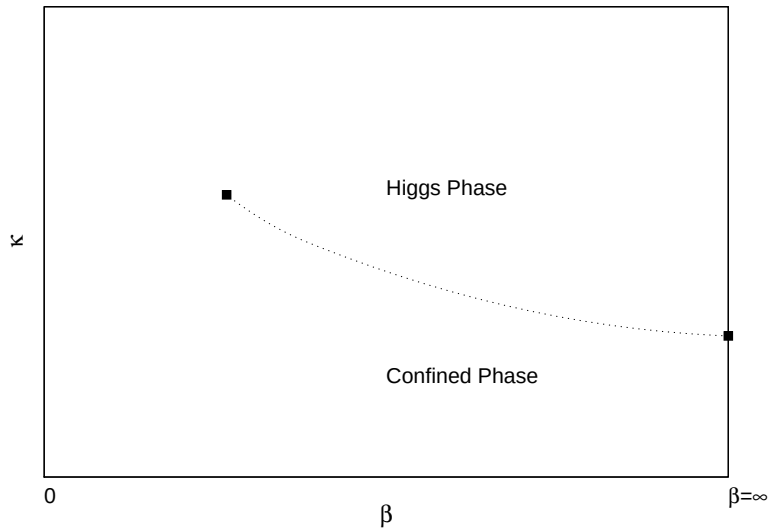

Figure 3.1: Gráfico esquemático del diagrama de fases del modelo SU(2)-Higgs con modulo fijo ($\lambda = \infty$).

extraer las propiedades generales que presentan las transiciones de primer orden débiles en la red en modelos gauge acoplados a campos escalares. Con este propósito se ha añadido a la acción estándard un acoplo extra entre el campo gauge y el campo escalar conectando segundos vecinos en la red. Este acoplamiento nuevo será usado como un parámetro para reforzar o debilitar la transición, permitiendo así estudiar su mecanismo de debilitamiento cuando este acoplamiento se hace tender a cero.

Abstract

The properties of the Confinement-Higgs phase transition in the SU(2)-Higgs model with fixed modulus are investigated. We show that the system exhibits a transient behavior up to L=24 along which, the order of the phase transition cannot be discerned. To get stronger conclusions about this point, without going to prohibitive large lattice sizes, we have introduced a second (next-to-nearest neighbors) gauge-Higgs coupling (κ_2). On this extended parameter space we find a line of phase transitions which become increasely weaker as $\kappa_2 \to 0$. The results point to a first order character for the transition with the standard action ($\kappa_2 = 0$).

3.2 The Model

The SU(2) lattice gauge model coupled to an scalar field, in the fundamental representation of the gauge field can be described by the action

$$\begin{aligned} S_\lambda \quad &= \beta \sum_p [1 - \frac{1}{2} \operatorname{tr} U_p] - \frac{1}{2}\kappa_1 \sum_{x,\mu} \operatorname{tr} \mathbf{\Phi}^\dagger(x) U_\mu(x) \mathbf{\Phi}(x+\mu) + \\ &+ \lambda \sum_x [\mathbf{\Phi}^\dagger(x)\mathbf{\Phi}(x) - 1]^2 + \sum_x \mathbf{\Phi}^\dagger(x)\mathbf{\Phi}(x) \ . \end{aligned} \tag{3.4}$$

Where $\mathrm{U}_\mu(x)$ represents the link variables, and U_p are their products along all the positive oriented plaquettes of a four-dimensional lattice of side L.

The scalar field at the site x is denoted by $\mathbf{\Phi}(x)$, being λ the parameter controlling its radial mode. In the limit ($\lambda = \infty$, $\beta = \infty$) the model becomes a pure O(4)-symmetric scalar model.

As we pointed out in the previous section, the PT line ends at some finite value of the parameters (β, κ_1) The endpoint moves towards larger β values as λ increases. For $\lambda \geq 0.1$ the endpoint crosses to the $\beta > 0$ region, and in the limit $\lambda = \infty$ the phase transition ends at ($\kappa_1 \approx 0.6$, $\beta \approx 1.6$) [6]. It is commonly believed that the transition at this point is second order with classical critical exponents [9], however a careful numerical study would be necessary.

In the scaling region, and for finite λ, the phase transition turns out to be first order. Also, the transition becomes weaker as β or λ increases. In particular in the limit $\beta = \infty$ (spin model) the transition is second order with classical critical exponents [1].

In the limit $\lambda = \infty$ the situation is less transparent, and it is not clear whether the transition is weak first order or higher order.

The study of the model with the parameter $\lambda = \infty$ is equivalent to fixing the modulus of the Higgs field, $\mathbf{\Phi}^\dagger \cdot \mathbf{\Phi} = 1$. In the pioneer work, [10], the PT was considered first order for finite λ and second order for $\lambda = \infty$. Later, larger statistics, and the hypothesis of a universal behavior of the PT for all values of λ, seem to point to a first order character of the PT in the scaling region. Nowadays, though it is generally believed that the transition is still first order in this limit, the numerical proofs [11, 7] on which rely these statements are not conclusive, as the authors safely conclude, because the statistic and lattice sizes are not enough for excluding the possibility of a higher order phase transition in the edge $\lambda = \infty$.

The model with fixed modulus is described by the action

$$S_\infty = \beta \sum_p [1 - \frac{1}{2} \operatorname{tr} U_p] - \frac{1}{2}\kappa_1 \sum_{x,\mu} \operatorname{tr} \mathbf{\Phi}^\dagger(x) U_\mu(x) \mathbf{\Phi}(x+\mu) \ . \tag{3.5}$$

As we shall show below, we have simulated this model up to lattices L=24, and the result is still compatible with a second or higher order PT, however, we have no indications of asymptoticity in the behavior of the observables, and the results are compatible with a very weak first order PT too. This means that larger lattices are needed to overcome these transient effects, but the added difficulty here is that such lattices would suffer of termalization problems, and severe autocorrelation times. Altogether makes this approach too CPU expensive for nowadays computers.

In order to get a more conclusive answer without going to prohibitive large lattice sizes, we have studied the model in an extended parameter space. For this purpose we have introduced a second coupling between the gauge and the scalar field connecting next-to-nearest neighbors on the lattice, in such a way that the new action reads

$$S = S_\infty - \frac{1}{4}\kappa_2 \sum_{x,\mu<\nu} Tr \mathbf{\Phi}^\dagger(x)[U_\mu(x)U_\nu(x+\mu)+U_\nu(x)U_\mu(x+\nu)]\mathbf{\Phi}(x+\mu+\nu) \tag{3.6}$$

Within this parameter space we expect to get a global vision on what the properties of the PT are, and also, to give a stronger conclusion about the order. In the region of κ_2 positive, (competing interaction effects appear if $\kappa_2 < 0$) this extended model is expected to belong to the same universality class than the *standard* one ($\kappa_2 = 0$) since both models posses the same symmetries. The effect of the new coupling $\kappa_2 > 0$ is to reinforce the transition but should not change the order if the system has not tricritical points. An example of such behavior appears in the O(4)-symmetric σ model with second neighbors coupling. This model presents a (κ_1^c, κ_2^c) line of phase transitions which is second order, since the model with $\kappa_2 = 0$ shows a second order PT too [12].

The action (3.6) has the following symmetries:

- $\kappa_1 = \kappa_2 = 0$.

$$\begin{aligned} \beta &\rightarrow -\beta \\ U_\mu(x) &\rightarrow (-1)^{\sum_{\rho\neq\mu} x_\rho} U_\mu(x) \end{aligned} \tag{3.7}$$

- $\kappa_1 \rightarrow -\kappa_1$, $\mathbf{\Phi}(x)$ fixed

$$U_\mu(x) \rightarrow -U_\mu(x) \tag{3.8}$$

- $\kappa_1 \rightarrow -\kappa_1$, $U_\mu(x)$ fixed

$$\mathbf{\Phi}(x) \rightarrow (-1)^{\sum_{\mu=0}^{d-1} x_\mu} \mathbf{\Phi}(x) \tag{3.9}$$

The action is not symmetric under the change $\kappa_2 \rightarrow -\kappa_2$. The existence of couplings κ_1 and κ_2 with opposite signs would make frustration to appear, and very different vacua are possible [12]. In this work we are interested in the regions free of frustration effects. Taking into account the symmetry properties of the action, the phase diagram in the region $\kappa_2 > 0$ will be symmetric with respect to the axis $\kappa_1 = 0$, and hence, we can restrict the study to the quadrant $\kappa_1 > 0$.

We define the normalized energy associated to the plaquette term

$$E_0 = \frac{1}{N_{l_0}} \sum_p (1 - \frac{1}{2} \operatorname{tr} U_p) \ , \tag{3.10}$$

and also the energies associated to the links

$$E_1 = \frac{1}{N_{l_1}} \sum_{x,\mu} \frac{1}{2} \operatorname{tr} \mathbf{\Phi}^\dagger(x) U_\mu(x) \mathbf{\Phi}(x+\mu) \ , \tag{3.11}$$

$$E_2 = \frac{1}{N_{l_2}} \sum_{x,\mu<\nu} \frac{1}{4} \operatorname{tr} \mathbf{\Phi}^\dagger(x) [U_\mu(x) U_\nu(x+\mu) + U_\nu(x) U_\mu(x+\nu)] \mathbf{\Phi}(x+\mu+\nu) \tag{3.12}$$

where $N_{l_0} = 6\mathrm{V}$, $N_{l_2} = 12\mathrm{V}$ and $N_{l_1} = 4\mathrm{V}$.

With these definitions $E_0 \rightarrow 0$ when $\beta \rightarrow \infty$ and $E_i \rightarrow 1$ when $\kappa_i \rightarrow \infty$.

On the three-dimensional (β, κ_1, κ_2) parameter space we consider the plane $\beta = 2.3$. On this plane there is a PT line (κ_1^c, κ_2^c). We expect to learn on the properties of this PT on the region $(\kappa_1^c \neq 0, \kappa_2^c \neq 0)$, where the signals are clearer, with regards to applying what we learn to the *standard* case $\kappa_2 = 0$.

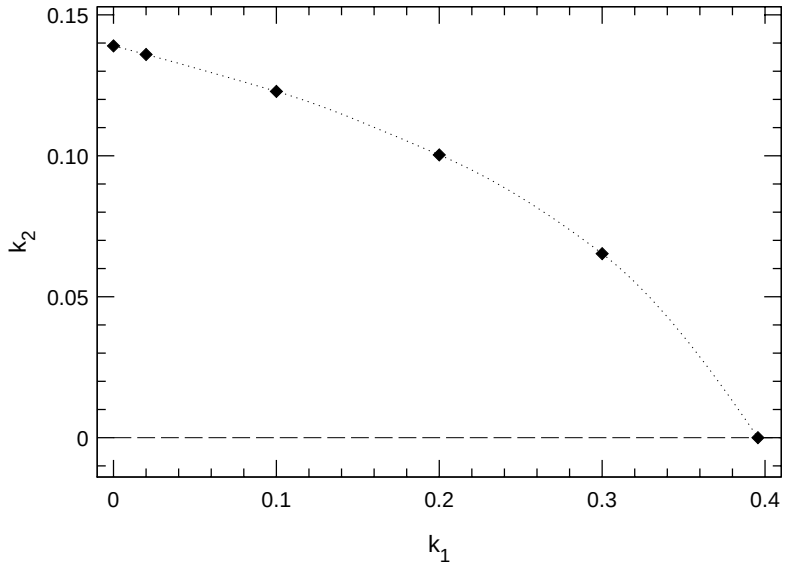

Figure 3.2: Phase diagram obtained from the MC simulation.

To monitorize the strength of the phase transition, we measure the existence of latent heat, and the behavior of the specific heat. As we shall see, for $\kappa_1 = 0$ the transition is first order, with a clearly measurable latent heat. We will see how this transition weakens along the PT line for increasing values of κ_1.

3.3 Numerical study

We have simulated the model in a L^4 lattice with periodic boundary conditions. For the update we have employed a combination of heat-bath and over-relaxation algorithms (ten over-relax sweeps followed by a heat-bath sweep). For the simulation we used the RTNN machine, consisting of a network of 32 PentiumPro 200MHz. processor. The total CPU time employed has been the equivalent of 3 years of PentiumPro.

Monte Carlo methods provide information about the thermodynamic quantities at a particular value of the couplings. We have used the Spectral Density Method (SDM) [13] to extract information on the values of the observables in a finite region around the simulation point. In particular it is

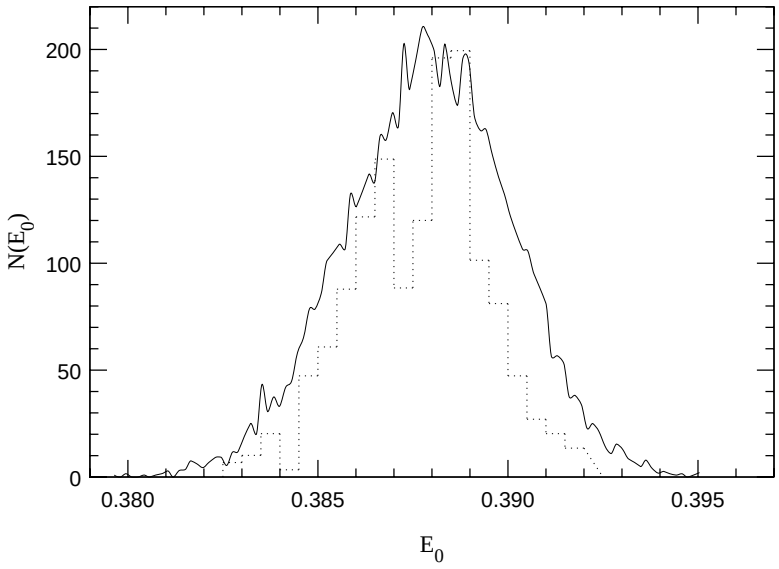

Figure 3.3: Normalized energy distribution for L=12, $\lambda = \infty$, κ_1=0.395, β=2.3 from [11] (dotted line), compared with the distribution we obtain at the same couplings (solid line) in L=12 too, when statistics is increased by one order of magnitude.

useful to have a precise location of the coupling where some observables have a maximum, as well as an accurate measure of the value of that maximum.

From the Monte Carlo simulation at some coupling κ, we got the histogram $H(E)$ which is an approximation to the density of states. Using the SDM approximation the probability of finding the system with an energy E at a different coupling κ' can be written as:

$$P_{\kappa'}(E) \propto H(E) e^{(\kappa' - \kappa) V E} \ . \tag{3.13}$$

The region of validity of the SDM approximation is $\Delta\kappa \sim 1/(V\sigma)$, being σ the width of the distribution $H(E)$. Although σ gets the maximum values in the critical region, the approximation has been very useful, specially for tuning the couplings where to measure.

Concerning the lattice sizes, we have used lattices ranging from L=6 to L=24. For the small lattices (L=6, 8 and 12) we have done $4{\times}10^5\tau$ iterations, being τ the largest autocorrelation time for the energy, which ranges from $\tau \approx 10$ in L=8 to $\tau \approx 35$ in L=24. For the largest lattices,

L=20 and 24, we run up to $10^5\tau$ MC iterations.

The statistical errors are computed with the jackknife method.

3.4 Results

We shall make the discussion with the first-neighbors link energy, E_1, but as far as the critical behavior is concerned, we could carry out the analysis with any of the energies. We remark that an appropriate linear combination of E_1, E_2 and E_0 could give slightly more accurate results [14].

We have considered fixed values of κ_1 (0, 0.02, 0.1, 0.2 and 0.3) and sought the κ_2 critical for every line, $\kappa_2^c(\kappa_1)$. We have also studied the case κ_2= 0 varying κ_1 which corresponds to the usual SU(2)-Higgs model.

The SDM has been used to locate the apparent critical point, defined through the specific heat behavior. From the specific heat matrix:

$$C_v^{i,j}(L) = \frac{\partial E_i}{\partial \kappa_j} \ , \tag{3.14}$$

we obtain the best signal for $C_v^{1,2}(L)$, which can be calculated as (we shall omit the superscript from now on)

$$C_v(L) = 4L^d(\langle E_1 E_2\rangle - \langle E_1\rangle\langle E_2\rangle) \ . \tag{3.15}$$

In a first order phase transition, $C_v^{\max}(L)$ behaves, asymptotically, proportional to the volume, L^d. If the PT is second order, the dominant behavior for $C_v(L)^{\max}$ is $L^{\alpha/\nu}$ which diverges too provided that $\alpha > 0$. At the upper critical dimension $\alpha = 0$, and one has to go further the leading order, appearing logarithmic divergences [15].

As a consequence of this divergent behavior, in a finite lattice $C_v(L)$ shows a peak at some value of the coupling which will be taken as apparent critical point, $\kappa_2^*(L)$.

In Figure 3.2 we plot the critical line (κ_1^c, κ_2^c). This line is obtained by extrapolation to the thermodynamic limit according to $\kappa_2^c(\infty) = \kappa_2^*(L) - AL^{-d}$. We point out that this extrapolation is valid only in first order phase transitions. If the PT is second order the power in L is $(-1/\nu)$.

In continuous PT scale invariance holds, and the thermodynamic magnitudes, such as the specific heat, or susceptibilities do scale. However if the transition is first order the correlation length remains finite and hence there is not scaling properties, and no critical exponents can be defined.

Nevertheless in a first order PT we can ask how large is the lattice we need in order to observe the asymptotic behavior of C_v. In particular, with abuse of language one can measure a *pseudo* α/ν exponent to get

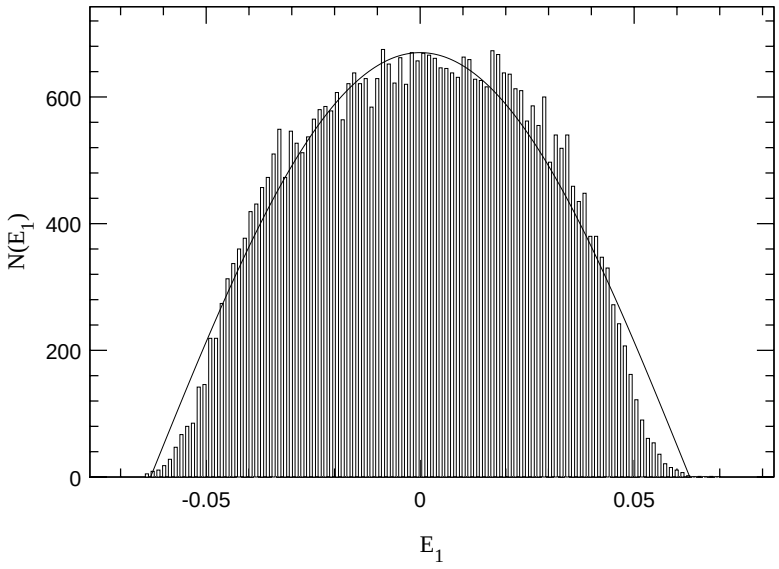

Figure 3.4: E_1 distribution on the axis $\kappa_1 = 0$ on a L=8 lattice at ($\kappa_2 = 0.15, \beta = 2.3$). The cosine fit is very accurate in spite of the finite β value, in this region of parameters the pure gauge term couples slightly both sub-lattices.

insight on the nature of the PT: the larger is the lattice we need to measure $\nu = 1/d$, the weaker the PT is. Following this, first order PT can be classified according to their degree of weakness.

However, the so called weak first-order PT appear often in literature (see [16, 17] and references there in) as PT characterized by a transient behavior with a non-measurable latent heat. Let be ξ_c the correlation length of the system at the critical point in the thermodynamic limit. In a finite lattice of size L, the first order behavior will be evidenced if $L \geq \xi_c$. For lattice sizes much smaller than ξ_c the system will behave like in a second-order PT, since the correlation length is effectively infinite. As an example, in Figure 3.3 we plot the energy distribution in a L=12 lattice at ($\beta = 2.3, \kappa_1 = 0.395$) obtained in [11], compared with the one we obtain at the same couplings and in the same L, when the statistics increases by one order of magnitude. We observe that the order of the PT can not be discerned at this volume, even when the statistics is enough. Termalization effects can also contribute to mistake the histogram structure.

The entire line (κ_1^c, κ_2^c) is first order, but the weak character increases

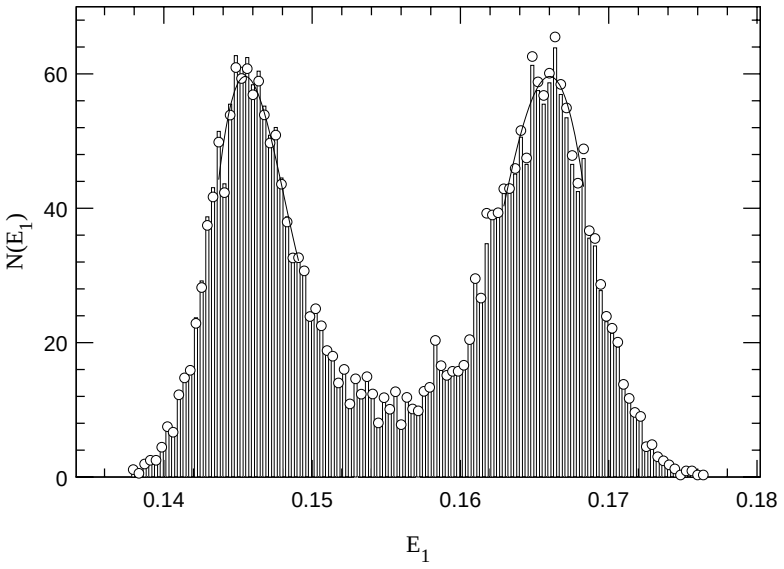

Figure 3.5: Normalized distribution of E_1 at ($\kappa_1 = 0.2$, $\kappa_2 = 0.10036$) in a L=16 lattice. The cubic fit at the maxima to get ΔE is superimposed.

as $\kappa_2 \to 0$. We will make a quantitative description of the weakening phenomenon by studying the specific heat, and the latent heat.

But before going on, we shall make a remark concerning the behavior on $\kappa_1 = 0$. As we pointed out, the system is symmetric under the change $\kappa_1 \to -\kappa_1$. The transformation (3.9) maps the positive κ_1 semi-plane with energy E_1, onto the negative κ_1 semi-plane with energy -E_1. The transition across this axis is first order because the energy is discontinuous. In the limit $\beta \to \infty$, and in $\kappa_1 = 0$, the system decouples in two independent sublattices, each one constituted by the first neighbors of the other. The first neighbors energy for this system is proportional to $\cos\theta$, being θ the angle between the symmetry breaking direction of the scalar field in both sub-lattices. In Figure 3.4 we plot the E_1 distribution for L=8 at ($\kappa_1 = 0, \kappa_2 = 0.15$) and $\beta = 2.3$. We see that the agreement with a cosine distribution is quite good in spite of the finite β value.

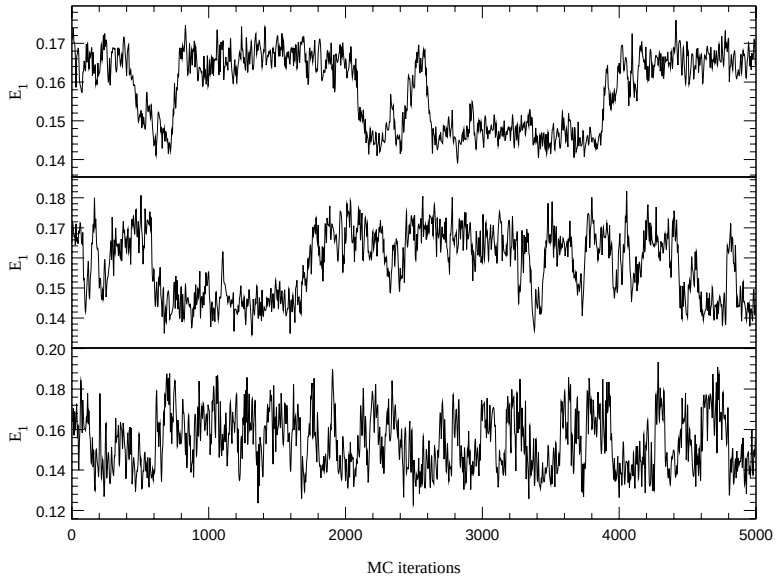

Figure 3.6: MC evolution of E_1 at $(\kappa_1 = 0.2, \kappa_2^*(L))$ for L=8 (lower part), L=12 (middle) and L=16 (upper part).

3.4.1 Latent Heat

Along the apparent critical line we have done simulations for different lattice sizes and stored the plaquette and links energies to construct the histograms for the energy distributions. In a first-order phase transition the energy has a discontinuity which manifest in the appearance of latent heat, ΔE. This quantity is not well defined in a finite lattice, so we measure the distance between the two maximum of the energy distribution, and extrapolate to the thermodynamic limit. The drawback of this approximation is that the maxima of the energy distribution are difficult to discern, since this function at the apparent critical point is very noisy We have used a cubic spline at the maxima in order to get a more reliable estimation (Figure 5).

In Figure 3.6 we show the MC evolution of E_1 for L=8, 12 and 16 at $\kappa_1 = 0.2$. In L=8 the latent heat is not clearly measurable. We observe in the MC evolution how the two-state signal becomes cleaner as the lattice size increases (see Figure 3.7).

In Figure 3.7 we plot the distribution of E_1 at $\kappa_1 = 0.2$ at the apparent critical point $\kappa_2^*(L)$ for L=6, 8, 12 and 16. A remarkable stability of ΔE_1

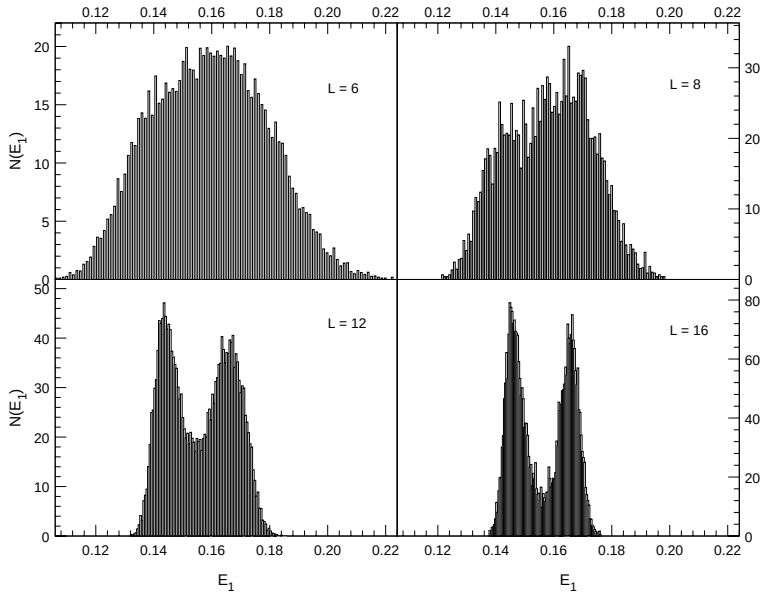

Figure 3.7: Normalized distribution of E_1 at $(\kappa_1 = 0.2, \kappa_2^*(L))$ for L=6, 8, 12 and 16.

with the volume is observed. This is a common feature for all values of κ_1.

As we have already pointed out, the transition weakens when increasing κ_1 and larger lattices are needed in order to observe a measurable latent heat. We give a quantitative description of this fact in Figure 3.8, where the distribution of E_1 for several values of $(\kappa_1, \kappa_2^*(12))$ is displayed. The two-state signal is no longer measurable in L=12 at $\kappa_1 = 0.3$. The first evidences of two-states appear in L=20 (see Figure 3.9). but from its energy distribution we can only give an approximate value for $\Delta E_1(L = 20)$ since the two-peaks appear too close to each other.

In Figure 3.10 we plot $\Delta E_1(L)$ and $\Delta E_2(L)$ as a function of $1/\mathrm{L}^4$, in order to get ΔE_i in the thermodynamic limit with a linear fit. Finally we quote these values in Table 3.1, together with the change in the action (3.6) between the two phases.

From the energy distributions at $\kappa_2 = 0$, see Figure 3.11 we have no direct evidences of the existence of latent heat. However, on the larger lattices one can observe non-gaussianities in the energy distributions. Such asymmetries could precede the onset of clear two-peak structures in larger lattices, however this is just a guess. We conclude that no information con-

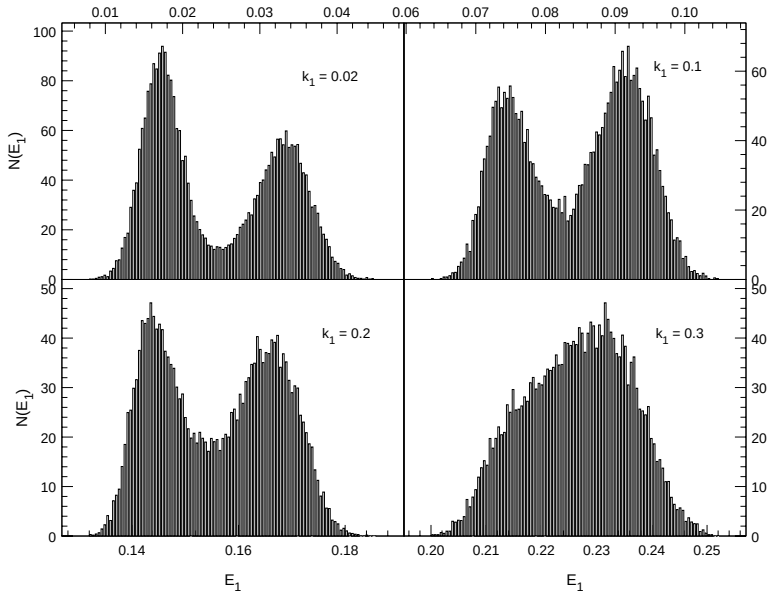

Figure 3.8: Normalized distributions of E_1 for $\kappa_1 = 0.02$, 0.1, 0.2 and 0.3 at $\kappa_2^*(12)$.

cerning the order of the PT can be obtained from the energy distributions up to L=24.

3.4.2 Specific Heat

We have done MC simulations at the points predicted by SDM, $(\kappa_1, \kappa_2^*(L))$, in order to measure accurately the peak of $C_v(L)$.

As an example we show in Figure 3.12 the value of $C_v(L)$ around its maximum for various lattice sizes at $\kappa_1 = 0.2$ (upper plane) and at $\kappa_1 = 0.3$ (lower plane). We observe that the maximum of the specific heat grows slower when increasing κ_1, indicating a weakening in the PT.

In Figure 3.13 we draw $C_v^{\max}(L)$ relative to $C_v^{\max}(6)$ as a function of the lattice size. The values have been normalized to $C_v^{\max}(8)/C_v^{\max}(6)$ in order to compare distinctly the behaviors for different κ_1. The slope of the segment joining the values of $C_v^{\max}$ in consecutive lattices gives the *pseudo* α/ν exponent. We observe that such slope is approximately 4 at $\kappa_1 = 0.02$, 0.1 and 0.2 for all the volumes we compare. However the transition at $\kappa_1 = 0.3$ evidences much more weakness. We do not have evidences

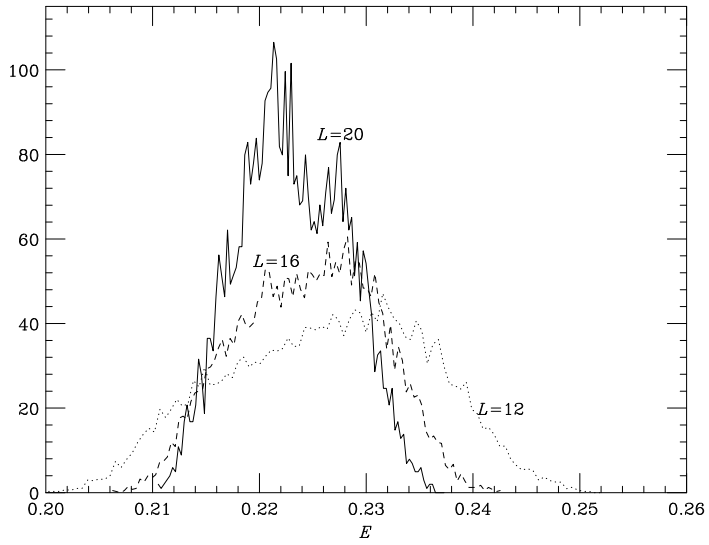

Figure 3.9: Normalized distribution of E_1 at $\kappa_1 = 0.3$ for L=12,16 and 20

of asymptoticity in $C_v^{\max}$ till L=20, as could be expected from the energy distributions (Figure 3.9). The slope of the segment joining $C_v^{\max}(16)$ with $C_v^{\max}(20)$ is 3.05(12) which is almost the asymptotic value expected for a first order PT.

As expected, only if the two-peak structure is observed in the energy distributions and ΔE is stable, the maximum of the specific heat will grow up like the volume, L^d.

At $\kappa_2 = 0$ we are within the transient region even for L=24. We remark that in this case C_v is defined by the element $C^{1,1}$ of the specific heat matrix (3.14) since this is the most natural choice at this point, and also is the best signal we measure. As we observe in Figure 3.13, at $\kappa_2 = 0$ $C_v^{\max}(L)$ seems to tend to a constant value as V$\rightarrow \infty$ up to L=20. From our previous discussions we should conclude that either the correlation length at the transition point ξ_c is much larger than the lattice size up to L=20, or the transition is second order with $\alpha = 0$ in the thermodynamic limit. However, in $L = 24$ things are changing, $C_v^{\max}(L = 24)$ starts to run away of this quasi-plateau, and the *pseudo* α/ν exponent grows again. As can be observed in Figure 3.13, at $\kappa_1 = 0.3$ the *pseudo* α/ν exponent decreases for the segment L = 12-16, with respect to the value in the segment L =

coupling	$\Delta E_1(\infty)$	$\Delta E_2(\infty)$	ΔS
$\kappa_1 = 0$	-	0.0366(8)	0.0134(12)
$\kappa_1 = 0.02$	0.0162(6)	0.0347(5)	0.0137(13)
$\kappa_1 = 0.1$	0.0162(7)	0.0345(9)	0.0094(10)
$\kappa_1 = 0.2$	0.0179(7)	0.0201(8)	0.0078(12)
$\kappa_1 = 0.3$	$\approx$0.006	≈ 0.012	≈ 0.0026

Table 3.1: $\Delta E(\infty)$ for E_1 and E_2, and variation of the action.

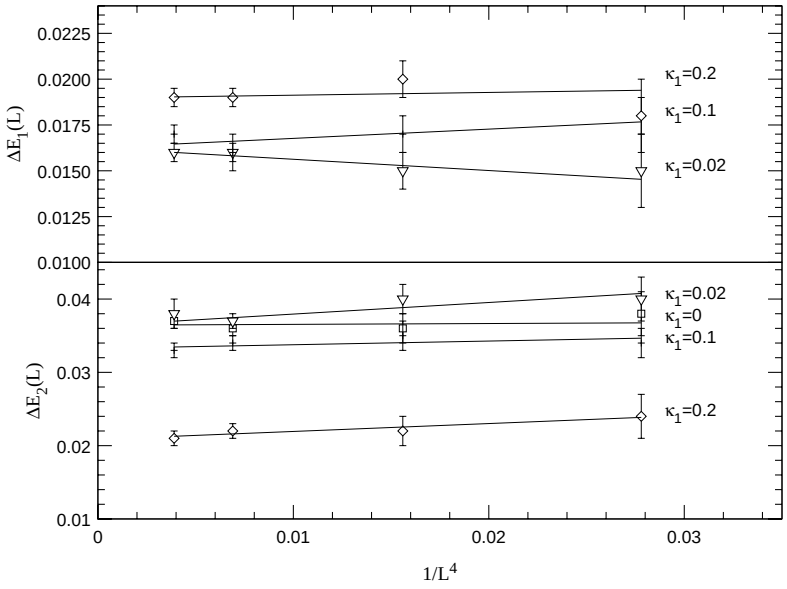

Figure 3.10: ΔE_1 (upper plane) and ΔE_2 (lower plane) as a function of $1/L^4$. The two-peak structure is not clearly observed in L=6 at any κ_1 value. The values quoted for this lattice size are upper bounds.

8-12. The lattice $L = 20$ is enough to overcome the transient region, but the behavior is qualitatively the same that in $\kappa_2 = 0$, though the transition is stronger.

We believe that this behavior is general for weak first order transitions in four dimensions. There exists a transient region in which the correlation length is effectively infinite compared with the lattice size, and the system behaves like suffering a second order PT with thermal index $\alpha \approx 0$ in the

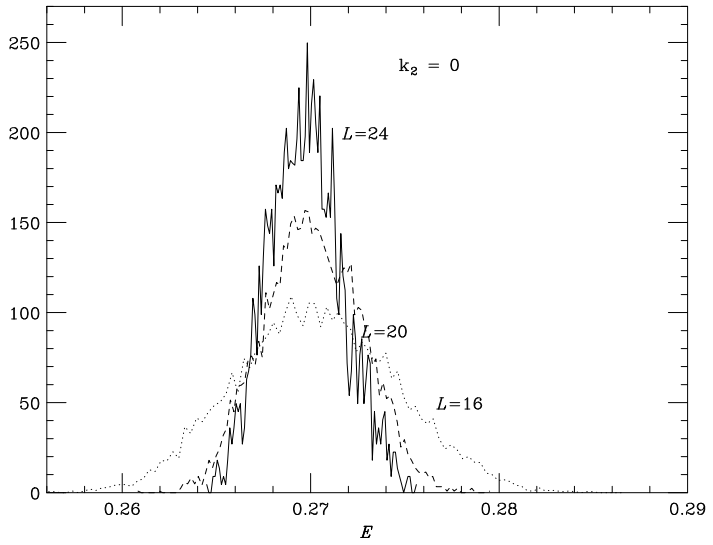

Figure 3.11: Normalized distribution of E_1 at κ_2=0, in L=16, 20 and 24 at the peak of the specific heat

thermodynamic limit.

3.4.3 Binder Cumulant

In order to check the consistency of our results we have also considered the behavior of the Binder cumulant

$$V_L = 1 - \frac{\langle E_1^4 \rangle_L}{3\langle E_1^2 \rangle_L^2} \ . \tag{3.16}$$

This quantity behaves differently depending on the order of the PT. If the transition is second order the minimum of the cumulant, $V_L^{\min}$ approach 2/3 in the thermodynamic limit. However if the transition is first order, $V_L^{\min}$ tends a value smaller than 2/3 reflecting the non-gaussianity of the energy distribution at the transition point.

In Figure 3.14 we plot $V_L^{\min}$ for several κ_1 values.

For those values of κ_1 in which the PT is distinctly first order, the minimum of the Binder cumulant stays safely away from 2/3, as we observe $V_L^{\min}$ extrapolated to L$\rightarrow \infty$ is 0.65401(4) at $\kappa_1 = 0.1$. However, this value

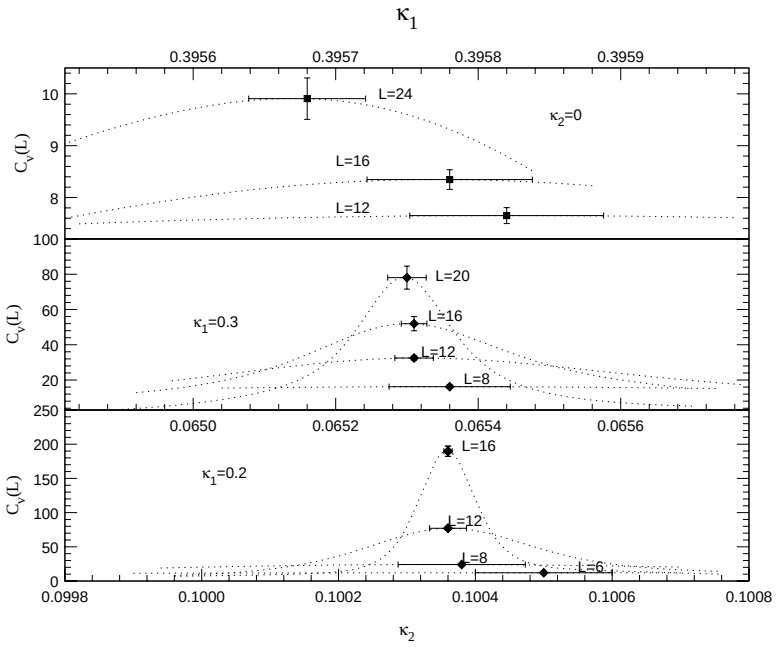

Figure 3.12: $C_v^{\max}(L)$ at $\kappa_1 = 0.2$ (lower plane), at $\kappa_1 = 0.3$ (middle) and at $\kappa_2 = 0$ (upper plane). The dotted line is the SDM extrapolation.

reachs 0.66637(5) at $\kappa_1 = 0.3$, and 0.66657(8) at $\kappa_2 = 0$. Again we find a tight difference between a very weak first order PT and a continuous one.

For the sake of discussing quantitatively the order of magnitude of the latent heat in the limit $\kappa_2 = 0$, from the energy distributions we find that at $\kappa_2 = 0$ one can approximately locate one the peaks of the energy at $\mathrm{E}_a \approx 0.273$. The other should be at certain $\mathrm{E}_b = \mathrm{E}_a - \Delta$, being Δ the latent heat.

In the thermodynamic limit the energy distributions are two delta functions situated at E_a and E_b, then

$$V_\infty^{min} = 1 - \frac{2(E_a^4 + E_b^4)}{3(E_a^2 + E_b^2)^2} \ . \tag{3.17}$$

If we use $\mathrm{V}_\infty^{\min} = 0.66657$ and E_a in (3.17) the value we got for the latent heat is $\Delta \approx 0.006$ which is of the same order as the one expected from the histograms.

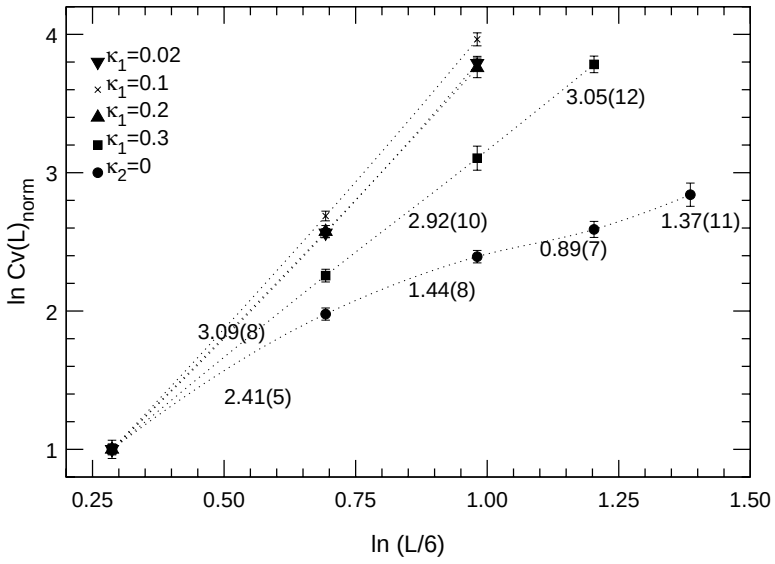

Figure 3.13: $C_v^{\max}$ for the various κ_1 values and $\kappa_2 = 0$. We have normalized the values with respect to $C_v^{\max}(8)/C_v^{\max}(6)$. The slope of the segments is indicated when smaller than 4.

3.5 Conclusions

The order of the Confinement-Higgs phase transition in the SU(2)-Higgs model with fixed modulus is a highly non trivial issue. We have used an extended parameter space, in order to get a global vision on the problem. On this extended parameter space we have found a line of first order phase transitions which get weaker as $\kappa_2 \to 0$. We have also observed that, because of the computer resources needed, it is too ambitious trying to measure two-peak energy distributions in the limit $\kappa_2 = 0$. However, on this point, we can extract conclusions from the behavior of the specific heat.

As we have discussed along the paper, a fake second order PT seems to exists for a range of L in very weak first order phase transitions. We have applied Finite Size Scaling properties along this transient region to compute a *pseudo* α/ν critical index. We want to be extremely careful at this point, this computation is completely meaningless when the transition is first order, since Scaling does not hold, but it can be used as a technical tool to catalogue the PT when there is no direct evidences, as in this case.

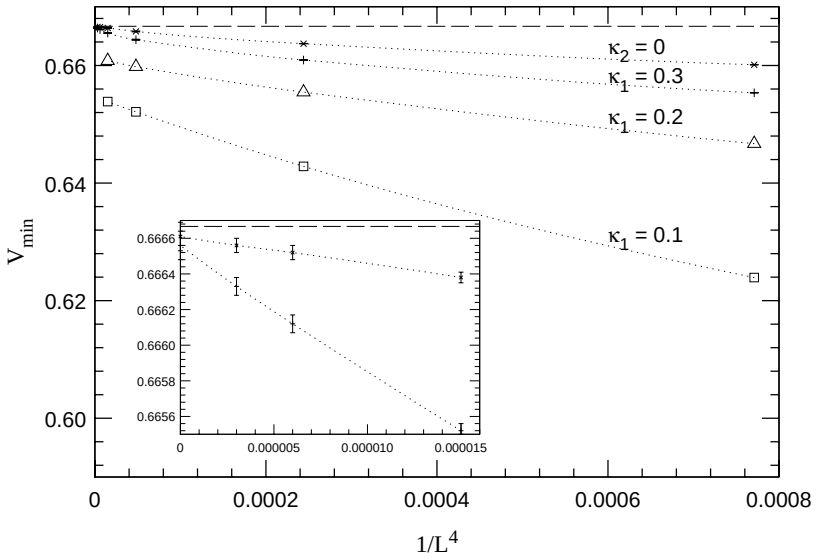

Figure 3.14: $V_L^{\min}$ for $\kappa_1 = 0.1$, 0.2,0.3 and $\kappa_2 = 0$, as a function of $1/\mathrm{L}^4$. The dashed line represents the value 2/3.

Using the relation $\alpha = 2 - \nu d$, we got ν varying in the interval (0.36, 0.41) in the range $L = 8, \ldots, 20$. Calculated from L=20 and L=24, $\nu \approx 0.35$. We expect this behavior to be transitory, and when going to larger lattices sizes, if the transition is second order, ν should reach its mean field value $\nu = 1/2$. If the transition is first order this value should go to 1/d, indicating that the specific heat maximum grows like the volume L^d. We believe that this is the case, since the *pseudo* ν exponent in L=24, instead of approaching 1/2, starts to decrease. An example of weak first order PT showing a similar behavior is described in [19].

In what concerning the motivation of introducing a second coupling, we pointed out that κ_2 should not change the order of the PT because do not change the symmetry properties. This argument is heuristic, but the phase diagram we found supports this assertion. As far as the order of the PT is concerned, we think that this approach can be useful when dealing with PT of questionable order in the sense that it is not clear whether the transition is weakly first order or higher order. The hope is that it could be applied to other more controversial models.

Bibliography

[1] C. Itzykson and J.M.Drouffe, *Statistical Field Theory*, **Vol. 1**, *Cambridge University Press* (1989)

[2] S. Coleman and S. Weinberg *Phys. Rev.* **D7** (1973) 1888

[3] J. M. Drouffe and J. B. Zuber. *Phys. Rep.* **102, p 1** (1983)

[4] E. Fradkind and E. Shenker. *Phys. Rev.* **D19, p 3682** (1979)

[5] M. Creutz, L. Jacobs and C. Rebbi. *Phys. Rep.* **95, p 201** (1983)

[6] J. Jersak, C.B. Lang, T. Neuhaus and G. Vones. *Phys. Rev.* **D32, p 2761**(1985)

[7] W. Langguth, I. Montvay and P. Weisz. *Nuc. Phys.* **B277, p 11**(1986)

[8] W. Bock, H. G. Evertz, J. Jersak, D.P. Landau, T. Neuhaus and J. L. Xu. *Phys. Rev.* **D41, p 2573**(1990)

[9] D.J.E. Callaway and R. Petronzio *Nuc. Phys.* **B267, p 253** (1986)

[10] C.B. Lang, C. Rebbi and M.A. Virasoro. *Phys. Lett.* **B104, p 294**(1981)

[11] W. Langguth and I. Montvay *Phys. Lett.* **B165, p 135**(1985)

[12] I. Campos, A. Tarancón and L.A. Fernández. *Phys. Rev.* **D55, p 2965** (1997)

[13] A.M. Ferrenberg and R.H. Swendsen, *Phys. Rev. Lett.* **B61** (1988) 2635

[14] RTN collaboration (J.L. Alonso et al.) *Nuc. Phys.* **B405, p 574** (1993)

[15] E. Brezin, J.C. Le Guillou and J. Zinn-Justin. *"Field Theoretical approach to critical phenomena"* in *Phase Transitions and Critical Phenomena* ed. C. Domb and M.S. Green (Academic Press, London) (1976).

[16] J.J. Ruiz-Lorenzo *Ph.D. Thesis U. Complutense de Madrid* (1993)

[17] L.A. Fernández, M.P. Lombardo, J.J Ruiz-Lorenzo and A. Tarancón, *Phys. Lett.* **B277**(1992) 485

[18] M.S.S. Challa, D.P. Landau and K. Binder. *Phys. Rev.* **B34, p 1841** (1986)

[19] J.L. Alonso, J.M. Carmona, J. Clemente, L.A. Fernández, D. Iñiguez, A. Tarancón and C.L. Ullod, *Phys. Lett.* **B376** (1996) 148

Chapter 4

El modelo U(1) gauge en D=4 con topologías toroidal y esférica

4.1 Introducción

La transición de la teoría libre de Dirac a la electrodinámica cuántica (QED) implica reemplazar una simetría global por una local es decir, hacer gauge la teoría. Concretamente de la acción correspondiente a la teoría libre de Dirac:

$$S_F^{(0)} = \int dx^4 \bar{\psi}(x)(i\gamma^\mu \partial_\mu - M)\psi(x) \ , \tag{4.1}$$

invariante bajo transformaciones globales de U(1), es decir del tipo $G = e^{i\Lambda}$, se pasa a la electrodinámica cuántica (QED) haciendo que la invarianza global sea tambien local, esto es, invariante bajo cambios locales de fase pertenecientes a U(1), es decir $G(x) = e^{i\Lambda(x)}$. Esta transformación implica introducir un potencial gauge $A_\mu(x)$ y reemplazar las derivadas ordinarias por derivadas covariantes: $D_\mu = \partial_\mu + ieA_\mu(x)$.

Sin embargo para que el campo gauge juegue un papel en la dinámica hay que añadir a la acción original un término cinético que permita su propagación. Para ello se introduce el tensor $\mathcal{F}_{\mu\nu}$:

$$\mathcal{F}_{\mu\nu}(x) = -\frac{i}{e}[D_\mu, D_\nu] = \partial_\mu A_\nu(x) - \partial_\nu A_\mu(x) \ , \tag{4.2}$$

de manera que la acción que describe la QED en el espacio euclídeo queda:

$$\begin{aligned} S_{QED}^{\text{cont}} &= S_G + S_F \\ &= \frac{1}{4}\int dx^4 \mathcal{F}_{\mu\nu}(x)\mathcal{F}_{\mu\nu}(x) + \int dx^4 \bar{\psi}(x)(i\gamma^\mu D_\mu + M)\psi(x) \end{aligned} \tag{4.3}$$

En lo que sigue estaremos interesados en el estudio de la parte pura gauge en la red, donde una posible formulación de la teoría del continuo está dada por la acción de Wilson [1]:

$$S_{\mathcal{W}} = \beta \sum_{\text{n}} \sum_{\mu<\nu} [1 - \frac{1}{2}(U_{\mu\nu}(n) + U_{\mu\nu}^\dagger(n))] \ , \tag{4.4}$$

donde $U_{\mu\nu}(n)$ es el usual producto ordenado de las links que forman cada plaqueta

$$U_{\mu\nu}(n) = U_\mu(n)U_\nu(n+\mu)U_\mu^\dagger(n+\nu)U_\nu^\dagger(n) \ . \tag{4.5}$$

En el límite en el que el espaciado de la red se hace tender a cero se recupera la acción del continuo, S_G, con la siguiente correspondencia:

$$U_\mu(n) = e^{ieaA_\mu(n)} , \tag{4.6}$$

$$\beta = \frac{1}{e^2} . \tag{4.7}$$

En efecto, usando la versión discretizada de $\mathcal{F}_{\mu\nu}$:

$$\mathcal{F}_{\mu\nu}(n) = \frac{1}{a}[(A_\nu(n+\mu) - A_\nu(n)) - (A_\mu(n+\nu) - A_\mu(n))] , \tag{4.8}$$

se tiene que la variable plaqueta se puede escribir como:

$$U_{\mu\nu}(n) \approx e^{iea^2\mathcal{F}_{\mu\nu}(n)} , \tag{4.9}$$

y por tanto la acción en el límite $a \to 0$ queda:

$$S_{\mathcal{W}} \approx \frac{1}{4}\sum_{\mathrm{n}}\sum_{\mu,\nu} a^4 \mathcal{F}_{\mu\nu}\mathcal{F}_{\mu\nu} . \tag{4.10}$$

El modelo U(1) compacto en $d = 4$ posee dos fases. Una es la región de acoplamiento fuerte en la cual los fotones están confinados, y la otra es la región de acoplamiento débil en la que los fotones son portadores de un potencial tipo culombiano. La transición de fase que separa ambas regiones tiene lugar en $\beta \sim 1$ y ha sido ampliamente estudiada debido a la relevancia del modelo U(1) para estudiar QED. Sin embargo el estudio de esta transición de fase ha resultado ser más complicado de lo que se podía esperar en un principio, de su al menos aparente simplicidad. En la actualidad, las cuestiones relacionadas con el orden de la transición de fase, y con los mecanismos que la provocan, siguen siendo temas controvertidos.

La mayoría de los estudios numéricos han sido realizados en redes cúbicas en $4D$ con condiciones de contorno periódicas, es decir en un hipertoro ($\mathcal{HT}$). Los estudios iniciales de este modelo apuntaban a que la transición era continua, puesto que las simulaciones numéricas no evidenciaron ninguna señal de metaestabilidad [2, 3, 4]. Las redes más grandes utilizadas en aquellos trabajos fueron $L = 4, 5$. Sin embargo, cuando los recursos de los ordenadores permitieron simular en redes más grandes, se empezaron a observar metaestabilidades e histogramas con doble pico de $L = 6$ en adelante, revelando que la transición tenía calor latente y por lo tanto sería de primer orden [6, 7, 8]. Esta idea fue corroborada por trabajos que aproximaron el problema desde el punto de vista del Grupo de Renormalización [10, 11].

Actualmente, quedan un cierto número de problemas abiertos.

1. Las simulaciones desde $L = 6$ hasta $L = 12$ revelan calor latente, pero su valor decrece con L.

2. El exponente crítico efectivo ν está en el intervalo (0.29,0.32) que es distinto de lo que se espera en primer orden, $\nu = 0.25$, y tambien del valor correspondiente al segundo orden trivial, $\nu = 0.5$.

Estos hechos llevaron a considerar la posibilidad de que el calor latente fuese a cero en el límite termodinámico. Es decir, la transición de fase en U(1) podría a pesar de todo ser continua si los dos picos que aparecen en las simulaciones fuesen un efecto de tamaño finito [13].

Aparte de la acción de Wilson, se consideraron acciones extendidas para tratar de clarificar el problema mediante su formulación en un espacio de fases extendido. En este contexto, una acción que incluye un término proporcional a las plaquetas al cuadrado fue propuesta por G. Bhanot a comienzos de los '80 [12]:

$$S_{\mathcal{EW}} = \beta \sum_{\mathrm{n}} \sum_{\mu<\nu} [1 - \frac{1}{2}(U_{\mu\nu} + U^{\dagger}_{\mu\nu})] + \gamma \sum_{\mathrm{n}} \sum_{\mu<\nu} [1 - \frac{1}{2}(U^{2}_{\mu\nu} + U^{\dagger 2}_{\mu\nu})] \ . \quad (4.11)$$

Esta acción posee el mismo límite continuo que la acción de Wilson con la identificación $\beta + 4\gamma = 1/g^2$.

En este trabajo se estudió el espacio de parámetros extendido (β, γ) en $L = 4, 5$. Se encontró que la linea transición de fase desconfinante se extiende para todo γ. En estas redes sólo se observaron metaestabilidades en $\gamma \geq +0.2$, sugiriendo que la linea de transiciones de fase $\beta_{\mathrm{c}}(\gamma)$ se hace de primer orden para $\gamma \geq +0.2$, mientras que en $\gamma < +0.2$ la transición aparecía como de segundo orden.

Simulaciones posteriores, siempre en redes $\mathcal{HT}$, han mostrado la existencia de calor latente para todo valor de γ, tanto positivo como negativo, para retículos suficientemente grandes. Por tanto, el trabajo de Bhanot no es exacto cuantitativamente, pero cualitativamente sus conclusiones si son correctas: los valores de γ positivos refuerzan la transición en el sentido que el calor latente crece cuanto más positivo es este parámetro, mientras que los valores negativos de γ debilitan la transición y calor latente decrece.

Actualmente se acepta con generalidad que la transición es de primer orden para valores positivos de γ. Sin embargo para $\gamma \leq 0$ son posibles dos escenarios: 1) la linea de transiciones $\beta_{\mathrm{c}}(\gamma)$ es de primer orden para todo γ finito, positivo o negativo; 2) Existe un $\gamma_{\mathrm{TCP}} \leq 0$ punto tricrítico a partir del cual la transición es de segundo orden [13].

Este problema fue estudiado desde el punto de vista del Grupo de Renormalización [14]. Los resultados dan soporte al primer escenario descrito, en

concreto se encuentra un debilitamiento de la transición al hacer γ más negativo, pero ello sin cambiar el caracter de primer orden, sino simplemente debilitándola.

Hasta aquí se han descrito los resultados existentes en la topología $\mathcal{HT}$.

Sin embargo a lo largo del estudio de esta transición de fase se han usado otras topologías aparte de la toroidal. El motivo para ello es la idea debatida hace algunos años sobre la influencia de los monopolos en la transición de fase de U(1). Concretamente se argumentó que debido a las condiciones de contorno periodicas existen monopolos no triviales, en el sentido de que no son contraíbles a un punto [15]. Al ser los monopolos configuraciones asociadas a mínimos locales de la acción, su existencia hace crecer la energía, y se sugirió que el salto en la energía observado en la transición de fase se debe a la desaparición de estos monopolos, que en la región desconfinada no existen.

Estas hipótesis indujeron a trabajar en redes con condiciones de contorno esféricas, puesto que en la esfera todos los monopolos son contraíbles a un punto [16, 17]. En concreto ha sido sugerido que los dos estados metaestables desaparecen cuando se trabaja en una red construída considerando la superficie de un cubo en $5D$ [16, 18], que tiene la misma topología que la esfera. La ausencia de doble pico, junto la estimación del exponente crítico $\nu \sim 0.37$ medido en $\gamma = 0, -0.2, -0.5$ ha inducido a los autores en [18] a decir que los dos picos observados en el toro son un efecto de tamaño finito, y que trabajando en la esfera se ve que la linea $\beta_{\rm c}(\gamma)$ es crítica para $\gamma \leq 0$ y está caracterizada por un exponente crítico $\nu \sim 1/3$.

El papel de los monopolos no triviales mencionados anteriormente parece estar descartado en cuanto a su influencia en el orden de la transición de fase [19]. Por lo tanto a primera vista la situación es bastante extraña. Puesto que que los monopolos no triviales no parecen jugar ningún papel, uno esperaría obtener antes el comportamiento asintótico en una red homogénea e invariante por traslaciones, es decir la toroidal, que en una red manifiestamente no homogenea, como la superficie de un cubo en $5D$, y en la cual la invariancia traslacional se recupera sólo en el límite de volumen infinito.

Como se ha venido exponiendo a lo largo de esta memoria, la ausencia de doble pico no prueba que una transición sea de segundo orden. Además la aparición de un exponente $\nu \sim 0.37$, intermedio entre el valor de primer orden y el de segundo orden trivial, ha sido encontrado en otros modelos como caracterizador del regimen transitorio de las transiciones de primer orden débiles [20, 21].

Para tratar de arrojar algo de luz sobre este problema se ha hecho un estudio sistemático de la linea de transiciones de fase $\beta_{\rm c}(\gamma)$ en el toro y en

la red con topología esférica empleada en [16, 18] y que denotaremos por $\mathcal{HS}$. Para esta red hemos empleado tamaños más grandes de los medidos anteriormente para ver si la señal de doble pico aparece. En la red $\mathcal{HT}$ hemos mejorado la estadística que había hasta la fecha, midiendo en redes hasta $L = 24$ para algunos valores de γ.

Abstract

We have performed a systematic study of the phase transition in the pure compact U(1) lattice gauge theory in the extended coupling parameter space (β, γ) on toroidal and spherical lattices. The observation of a non-zero latent heat in both topologies for all investigated $\gamma \in [+0.2, -0.4]$, together with an exponent $\nu_{\rm eff} \sim 1/d$ when large enough lattices are considered, lead us to conclude that the phase transition is first order. For negative γ, our results point to an increasingly weak first order transition as γ is made more negative.

4.2 Description of the model and observables

We shall consider the parameter space described by the extended Wilson action, which can be expressed in terms of the plaquette angle in the following way:

$$S = -\beta \sum_{\rm p} \cos\theta_{\rm p} - \gamma \sum_{\rm p} \cos 2\theta_{\rm p} \ . \tag{4.12}$$

We use for the simulations the conventional $4D$ hypercube with toroidal boundary conditions (hypertorus), and, for comparison we also consider the surface of a $5D$ cube which is topologically equivalent to a $4D$ sphere. Contrarily to the hypertorus, the surface of a $5D$ cube is not homogeneous. There are a number of sites which do not have the maximum connectivity, namely 8 neighbors. Due to this fact, uncontrolled finite size effects are expected to turn up. Their influence can be somehow alleviated by the introduction of appropriate weight factors in those inhomogeneous sites [18]. Since the topology remains unchanged and we do not expect the order of the phase transition to be affected by the rounding, we do not use weight factors.

As a notational remark, we label with L and N the side length for the $\mathcal{HT}$ topology and for the $\mathcal{HS}$ topology respectively.

Next we define the energies associated to each term in the action

$$E_{\rm p} = \frac{1}{N_{\rm p}} \langle \sum_{\rm p} \cos\theta_{\rm p} \rangle \ , \tag{4.13}$$

$$E_{\rm 2p} = \frac{1}{N_{\rm p}} \langle \sum_{\rm p} \cos 2\theta_{\rm p} \rangle \ , \tag{4.14}$$

where $N_{\rm p}$ stands for the number of plaquettes. On the hyper-torus this number is simply proportional to the volume, namely the forward

plaquettes are $N_{\rm p} = 6L^4$. On the sphere the number of plaquettes has a less simple expression, and can be computed as a function of N as $N_{\rm p} = 60(N-1)^4 + 20(N-1)^2$. In this case, the system is not homogeneous and $N_{\rm p}$ is not proportional to the number of points on the four dimensional surface, which is $N^5 - (N-2)^5$, some points having a number of surrounding plaquettes less than the possible maximum 12, as opposed to what happens on the torus . In order to allow comparison, we define $L_{\rm eff} = (\frac{N_{\rm p}}{6})^{1/4}$, in such a way that a hypertorus of $L = L_{\rm eff}$ has the same number of plaquettes as the corresponding hypersphere.

The specific heat and the Binder cumulant are useful quantities to monitorize the properties of a phase transition. At the critical point, they are known to posses different thermodynamical limits depending on whether the transition is first order or higher order, and hence, their behavior with increasing lattice size can give some clues as to the order of the phase transition. We have studied the Finite Size Scaling (FSS) of these two energy cumulants.

The specific heat is defined for both energies as:

$$C_{\rm v} = \frac{\partial}{\partial\beta} E_{\rm p} = N_{\rm p}(\langle E_{\rm p}^2\rangle - \langle E_{\rm p}\rangle^2) \ , \tag{4.15}$$

$$C_{\rm 2v} = \frac{\partial}{\partial\gamma} E_{\rm 2p} = N_{\rm p}(\langle E_{\rm 2p}^2\rangle - \langle E_{\rm 2p}\rangle^2) \ . \tag{4.16}$$

As we have observed a high correlation between both energies, the results being qualitatively the same, we shall only report on the observable defined for the plaquette energy $E_{\rm p}$.

In a second order phase transition, scaling theory predicts the specific heat maximum to diverge as $L^{\alpha/\nu}$. If the transition is first order it is expected to diverge like the volume L^d (or strictly like the number of plaquettes $N_{\rm p}$) reflecting that the maximum of the energy fluctuation has the size of the volume. This is expected to hold in the asymptotic region of the transition $L \gg \xi_c$. In the transient region, namely $L < \xi_c$, the specific heat is expected to grow more slowly than the volume.

We shall use the number of plaquettes $N_{\rm p}$ to study the specific heat behavior in order to have a single parameter for both the $\mathcal{HT}$ and the $\mathcal{HS}$ topologies. This is of course equivalent to doing the discussion as a function of L on the $\mathcal{HT}$ and $L_{\rm eff}$ on the $\mathcal{HS}$. We have in this case $C_v \sim (N_{\rm p})^{\alpha/d\nu}$.

We have also studied the behavior of the fourth cumulant of the energy

$$V_L = 1 - \frac{\langle E_{\rm p}^4\rangle_L}{\langle E_{\rm p}^2\rangle_L^2} \ . \tag{4.17}$$

When the energy distribution describing the system is gaussian $V_L \to 2/3$ in the thermodynamic limit. This is the case for a second order phase transition. If the transition is first order, far from the critical coupling β_c, V_L also tends to 2/3, reflecting the gaussianity of the energy distribution. However, at β_c the distribution can be described by two gaussians centered about the energy of each metastable state E_1 and E_2, and hence this quantity has the non-trivial thermodynamic limit:

$$V_{L\to\infty} \to 1 - \frac{2(E_1^4 + E_2^4)}{3(E_1^2 + E_2^2)^2} < 2/3 \ . \tag{4.18}$$

Another interesting quantity measurable from the density of states is the distribution of the partition function zeroes, or Lee-Yang zeroes [24]. To clarify the role of the partition function zeroes let us first stress a well known fact: there are no phase transitions on a finite volume, phase transitions arise in the thermodynamical limit and are signaled by non-analyticity in the free energy:

$$F(\beta, V) = -\frac{1}{\beta V} \log Z(\beta) \ . \tag{4.19}$$

$Z(\beta)$ is a linear combination of exponentials, and hence an analytical function. This implies that the free energy can be singular only where $Z(\beta) = 0$. However if the coupling β is real, and the volume is finite, that linear combination is a sum of positive terms and hence, the zeroes of $Z(\beta)$ are located in the complex plane of the coupling β. The onset of the phase transition in the limit of infinite volume is signaled by a clustering of the zeroes on the real axis at β_c.

Here follows the description of our procedure, for a general description of the method see [25].

As mentioned previously we work only with E_p, and then we consider only the spectral density method [26] for this variable. Since we work at fixed γ we consider only the β coupling derivatives.

From the MC simulation at β we obtain an approximation to the density of states which allows us to compute the normalized energy distribution $P_\beta(E)$. The energy distribution can be expressed as

$$P_\beta(E) = \frac{1}{Z} W(E) e^{-\beta E} \ . \tag{4.20}$$

We use the standard reweighting technique to obtain from the distribution measured at β the distribution at another coupling ω, which is complex in the more general case $\omega = \eta + i\xi$. The standard reweighting formula is:

$$P_\omega(E) = \frac{P_\beta(E)e^{-(\omega-\beta)E}}{\sum_E P_\beta(E)e^{-(\omega-\beta)E}} \ , \tag{4.21}$$

using (4.20) and the normalization condition $\sum_E P_\beta(E) = 1$ one obtains

$$\frac{Z(\omega)}{Z(\beta)} = \sum_E P_\beta(E)e^{-(\omega-\beta)E} \ . \tag{4.22}$$

We can factorize the contributions from the real and imaginary part:

$$\frac{Z(\omega)}{Z(\beta)} = \sum_E P_\beta(E)(\cos(E\xi) + i\sin(E\xi))e^{-(\eta-\beta)E} \ . \tag{4.23}$$

This is the standard reweighting formula extended to the complex parameter space of couplings. As a first observation we have a pure oscillating factor due to $Im(\omega) \neq 0$. Since E is $O(V)$ this is a rapidly oscillating function which makes it impossible to locate zeroes with large imaginary part.

The real part of the coupling contributes to the well known exponential damping, $e^{-(\eta-\beta)E}$, which is telling us that we can trust the extrapolation only in a small neighborhood $\beta \pm \eta$.

Since $Z(\mathrm{Re}\,\omega)$ has no zeroes in a finite volume, an easy way to locate the zeroes numerically is looking at the minima of the function $|G(\omega)|^2$, where:

$$G(\omega) = \frac{Z(\omega)}{Z(\mathrm{Re}\,\omega)} = \frac{\sum_E P_\beta(E)(\cos(E\xi) + i\sin(E\xi))e^{-(\eta-\beta)E}}{\sum_E P_\beta(E)e^{-(\eta-\beta)E}} \ . \tag{4.24}$$

The function to minimize is:

$$|G(\omega)|^2 = \frac{(\sum_E P_\beta(E)e^{-(\eta-\beta)E}\cos(E\xi))^2 + (\sum_E P_\beta(E)e^{-(\eta-\beta)E}\sin(E\xi))^2}{(\sum_E P_\beta(E)e^{-(\eta-\beta)E})^2} \tag{4.25}$$

One interesting property of the partition function zeroes concerns the estimation of critical exponents. Denoting by ω_0 the coupling where the first zero is located, the distance to the real axis scales with the ν exponent:

$$Im(\omega_0) \sim L^{-1/\nu} \ . \tag{4.26}$$

We shall use this property to compute the effective ν exponent.

From $P_E(\beta)_L$, we can measure the free energy gap, $\Delta F(L)$, which is the difference between the minima and the local maximum of the free energy [22]. We use the spectral density method to get, from the measured

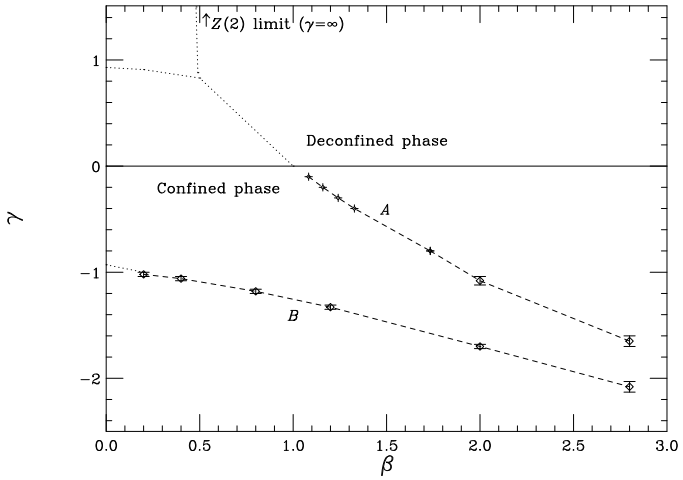

Figure 4.1: Phase diagram of U(1) in the extended (β, γ) parameter space. The dotted lines have been taken from [12]. The symbols correspond to our simulations on the torus. The crosses correspond to the peak of $C_{\rm v}(L = 16)$, the errors are not visible in this scale. The diamonds have been obtained with hysteresis cycles in $L = 8$.

histograms, a new histogram where both peaks have equal height. We take the logarithm of those histograms and measure the energy gap. A growing $\Delta F(L)$ in the asymptotic region of the transition implies a first order phase transition. An increase proportional to L^{d-1} is expected [22]. For the transition to be second order, $\Delta F(L)$ must stay constant with increasing lattice sizes.

4.2.1 Schwinger-Dyson Equations

As a further check we have implemented the Schwinger-Dyson equations (SDE) [26] which allow one to recover the simulated couplings from the Montecarlo data.

Let $\mathrm{A}(\theta)$ be an operator with null expectation value:

$$\langle A(\theta)\rangle = Z^{-1}\int [d\theta]A(\theta)e^{-S[\theta]} \equiv 0\ . \tag{4.27}$$

Derivating with respect to θ this equation trivially yields

$$\langle \frac{\partial A(\theta)}{\partial \theta} \rangle = \langle A(\theta) \frac{\partial S[\theta]}{\partial \theta} \rangle \ , \tag{4.28}$$

which is the equation of movement of the operator A(θ) or Schwinger-Dyson equation. When the action depends on several couplings the equation (4.28) can be expressed as:

$$\langle \frac{\partial A(\theta)}{\partial \theta} \rangle = \sum_i \beta_i \langle A(\theta) \frac{\partial S_i[\theta]}{\partial \theta} \rangle \ . \tag{4.29}$$

This equation relates the values of the couplings with the expectation values we measure from the MC simulation. We need as many independent equations as couplings we have to determine in the action. In our case, in order to measure both β and γ, we need two operators with null expectation value in order to have two independent tests. At each lattice site n and for every direction μ we consider the operators:

$$A(\theta) = \sin \theta_p = \sin(\theta_{n,\mu} - \theta_{stap}) \ , \tag{4.30}$$

$$B(\theta) = \sin 2\theta_p = \sin 2(\theta_{n,\mu} - \theta_{stap}) \ , \tag{4.31}$$

where θ_{stap} is the staple of the link labeled by (n,μ).

Applying equation (4.29) to those operators we get:

$$\langle \sum_{\rm p} \cos(\theta_{n,\mu} - \theta_{stap}) \rangle = \beta \langle \sum_{\rm p} \sin(\theta_{n,\mu} - \theta_{stap}) \sum_{\rm p} \sin(\theta_{n,\mu} - \theta_{stap}) \rangle + \\ + 2\gamma \langle \sum_{\rm p} \sin(\theta_{n,\mu} - \theta_{stap}) \sum_{\rm p} \sin 2(\theta_{n,\mu} - \theta_{stap}) \rangle \tag{4.32}$$

$$\langle \sum_{\rm p} 2\cos 2(\theta_{n,\mu} - \theta_{stap}) \rangle = \beta \langle \sum_{\rm p} \sin 2(\theta_{n,\mu} - \theta_{stap}) \sum_{\rm p} \sin(\theta_{n,\mu} - \theta_{stap}) \rangle + \\ + 2\gamma \langle \sum_{\rm p} \sin 2(\theta_{n,\mu} - \theta_{stap}) \sum_{\rm p} \sin 2(\theta_{n,\mu} - \theta_{stap}) \rangle \tag{4.33}$$

On the hypertorus $\sum_{\rm p}$ means the sum over the plaquettes in positive and negative directions ($\pm\mu$) bordering the link (12 plaquettes). On the sphere one has to be careful, since not all the links have 12 surrounding plaquettes, and the sum has to be understood as extended to the existing plaquettes.

These equations hold for all n in such a way that we can sum up the equations for every single link and average over the number of links. We quote in Table 4.1 for the tests done at $\gamma = -0.2$ using both topologies. They show a perfect agreement between the simulated couplings and the ones recovered from the MC expectation values.

$\mathcal{HT}$ topology			$\mathcal{HS}$ topology		
L	$\beta_{\rm sim}$	$(\beta,\gamma)_{\rm SD}$	N	$\beta_{\rm sim}$	$(\beta,\gamma)_{\rm SD}$
6	1.1460	1.1466(44),-0.2009(26)	6	1.1587	1.1592(14),-0.1998(12)
8	1.1535	1.1527(22) -0.1997(15)	8	1.1600	1.1599(12) -0.1999(8)
12	1.1582	1.1581(12),-0.1999(8)	10	1.1602	1.1602(7),-0.2001(9)

Table 4.1: Couplings obtained from the MC simulations at γ=-0.2 using the Schwinger-Dyson equations.

4.3 Numerical Simulation

$\gamma = +0.2$						
N	$L_{\rm eff}$	$\beta_{\rm sim}$	τ	N_τ	$\beta^*(L)$	$\mathrm{Im}(\omega_0)$
4	5.383	0.8910	70	29142	0.8906(2)	0.0169(1)
5	7.150	0.8855	210	8000	0.8855(2)	0.00604(6)
6	8.921	0.8834	520	3800	0.88330(5)	0.00244(6)
7	10.694	0.8818	790	2300	0.88182(3)	0.00090(3)
8	12.469	0.88095	930	1930	0.88097(3)	0.00040(2)
$\gamma = 0$						
N	$L_{\rm eff}$	$\beta_{\rm sim}$	τ	N_τ	$\beta^*(L)$	$\mathrm{Im}(\omega_0)$
6	8.921	1.0128	240	8300	1.01340(5)	0.00616(8)
8	12.469	1.0125	400	2300	1.0127(2)	0.00196(4)
10	16.021	1.0120	780	1200	1.01212(3)	0.00075(3)
12	19.574	1.0119	850	1150	1.01194(2)	0.00031(2)
14	23.123	1.0117	920	1900	1.01168(2)	0.00013(1)
$\gamma = -0.2$						
N	$L_{\rm eff}$	$\beta_{\rm sim}$	τ	N_τ	$\beta^*(L)$	$\mathrm{Im}(\omega_0)$
6	8.921	1.1587	160	2000	1.1587(4)	0.0107(3)
7	10.694	1.1600	320	2800	1.1597(1)	0.00550(7)
8	12.469	1.1597	510	1000	1.1603(2)	0.00321(4)
10	16.021	1.1602	680	1500	1.1604(2)	0.00171(2)
12	19.574	1.1604	820	1200	1.1602(1)	0.00083(1)
14	23.123	1.1605	900	1100	1.16048(5)	0.00044(1)
16	26.684	1.1604	1150	1200	1.16038(2)	0.00023(1)

Table 4.2: Statistics of the data obtained for the $\mathcal{HS}$ topology

Most of the work has been done by simulating the subgroup $Z(1024) \subset$

$\gamma = -0.1$					
L	$\beta_{\rm sim}$	τ	N_τ	$\beta^*(L)$	$Im(\omega_0)$
6	1.0720	350	1900	1.0716(2)	0.0097(1)
8	1.0784	640	1400	1.0786(2)	1.1539(2)
12	1.0820	820	750	1.0818(1)	0.00114(2)
16	1.08278	930	900	1.0827(1)	0.00040(2)
20	1.0833	1150	1100	1.0833(1)	0.00020(1)
$\gamma = -0.2$					
L	$\beta_{\rm sim}$	τ	N_τ	$\beta^*(L)$	$Im(\omega_0)$
6	1.1460	380	2000	1.1452(2)	0.0115(1)
8	1.1535	620	1900	1.1539(2)	0.00506(6)
12	1.1582	840	1200	1.1582(2)	0.00152(3)
16	1.15935	920	900	1.1593(1)	0.00060(2)
20	1.1599	1150	900	1.1599(1)	0.00028(1)
$\gamma = -0.3$					
L	$\beta_{\rm sim}$	τ	N_τ	$\beta^*(L)$	$Im(\omega_0)$
6	1.2255	340	2000	1.2237(4)	0.0138(1)
8	1.2344	560	1800	1.2340(1)	0.00623(4)
12	1.2395	770	1000	1.2395(2)	0.00190(3)
16	1.2410	900	900	1.2410(1)	0.00084(2)
20	1.2416	1100	1200	1.24156(5)	0.00041(2)
24	1.2417	1200	1100	1.24162(5)	0.00022(1)
$\gamma = -0.4$					
L	$\beta_{\rm sim}$	τ	N_τ	$\beta^*(L)$	$Im(\omega_0)$
6	1.3090	400	1800	1.3082(4)	0.0152(1)
8	1.3192	600	1600	1.3194(3)	0.00704(5)
12	1.3258	710	1400	1.3259(1)	0.00238(3)
16	1.32775	840	900	1.3278(1)	0.00108(2)
20	1.3285	930	1600	1.3284(1)	0.00054(2)
24	1.3286	1150	1500	1.3286(1)	0.00029(1)

Table 4.3: Statistics of the data obtained in the $\mathcal{HT}$ topology.

$U(1)$, since the phase transition associated to the discrete group lies safely far away. The overrelax algorithm can be applied only in the simulations with $\gamma = 0$ so that the gain in statistical quality due to the overrelax effect is limited to the Wilson action, where we have simulated both, the full group $U(1)$ and the discrete one for the sake of comparison. For $\gamma \neq 0$ we have simulated the discrete group since so the simulation is considerably

speeded up.

For every lattice size we consider, we perform trial runs to locate the coupling $\beta^*(L)$ where the specific heat shows a peak. We use the standard reweighting techniques to extrapolate in a neighborhood of the simulated coupling. Once the peak is located within an error in the fourth digit of the coupling, we perform an intensive simulation there to get $P_E(\beta^*)_L$. The statistics performed at these pseudo-critical couplings are reported in Table 4.2 and Table 4.3 for the $\mathcal{HS}$ and the $\mathcal{HT}$ topology respectively.

Typically we measure the energies every 10 MC sweeps in order to construct the energy histogram (4.20) From this energy distribution we obtain the cumulants of the energy we are interested in, and the critical exponents using Finite Size Scaling techniques. We remark that one of the main sources of systematic error when measuring critical exponents, is the indetermination in the coupling $\beta^*(L)$ where to measure.

The simulations have been done in the *RTNN* machine consisting of 32 Pentium Pro 200MHz processors. The total CPU time used is the equivalent of 6 Pentium Pro years.

We have updated using a standard Metropolis algorithm with 2 hits. The acceptance has always been between 65% and 75%.

In order to consider the statistical quality of the simulation, following [27] we define the unnormalized autocorrelation function for the energy

$$C(t) = \frac{1}{N-t} \sum_{i=1}^{N-t} E_i E_{i+t} - \langle E \rangle^2 \ , \tag{4.34}$$

as well as the normalized one

$$\rho(t) = \frac{C(t)}{C(0)} \ . \tag{4.35}$$

The integrated autocorrelation time for the energy, τ^{int}, can be measured using the window method

$$\tau^{int}(t) = \frac{1}{2} + \sum_{t'=1}^{t} \rho(t') \ , \tag{4.36}$$

for large enough t, which is in practice selected self-consistently. We use t in the range $5\tau^{int}$, $10\tau^{int}$, and we check that the obtained τ^{int} remains stable as the window in t is increased.

We have always started from hot and cold configurations in order to make sure that the system does not remain in a long living metastable state, which could be interpreted as a Dirac sheet. The results coming from both types of starts have always been indistinguishable.

4.4 The phase transition line $\beta_c(\gamma)$

We have studied the deconfinement-confinement phase transition line at several values of γ (Figure 4.1).

In the region of negative γ, apart from the deconfinement transition line, there is another transition line provoked by the competing interaction between the couplings (β, γ). In the limit $\gamma = -\infty$ the model is not dynamical since for all finite β, $\cos\theta_p = 0$. So we expect this line to end at the corner $(\gamma = -\infty, \beta = +\infty)$. We have not performed a deep study of this transition line, however the simulations at $L = 8$ revealed double-peak structures pointing to a first order character. The limit $\gamma = +\infty$ is equivalent to a $Z(2)$ theory and the critical point can be calculated exactly by self-duality.

We have studied carefully the region between lines A and B finding no signatures of the existence of additional lines.

We have focused on the transition line A, at several values of γ, on the hyper-torus and on the hyper-sphere.

The structure of this section is the following:

First, we describe the results at $\gamma = +0.2$ on the spherical topology. Our purpose is to observe how does the $\mathcal{HS}$ topology behave in a non controversial region, and comparing with the known results on the hypertorus.

Second, we study the point $\gamma = 0$ (Wilson action) on the spherical lattice. This coupling has been recently claimed to be the starting point of a critical line (infinite correlation length at the critical point) which extends in the range $\gamma \leq 0$, with an associated critical exponent $\nu \sim 0.37$ [18]. Since this assertion relies on the absence of two-state signals on spherical lattices up to $N = 10$, we shall check whether or not double peak structures set in when larger spheres are considered.

Third, we go to the region of negative γ values. We are aware of no previous systematic study on the hypertorus in this region, so we run simulations up to $L = 24$ at $\gamma = -0.1, -0.2, -0.3, -0.4$. Motivated by the results on the hyper-torus we have just run a single γ negative value on the hyper-sphere. For the sake of comparison with [18] we choose this value to be $\gamma = -0.2$.

Finally, we discuss the Finite Size Scaling behavior exhibited by both topologies.

4.4.1 Results at $\gamma = +0.2$ on the spherical topology

As we have pointed out, there is a general agreement on considering the phase transition first order in the region of positive γ.

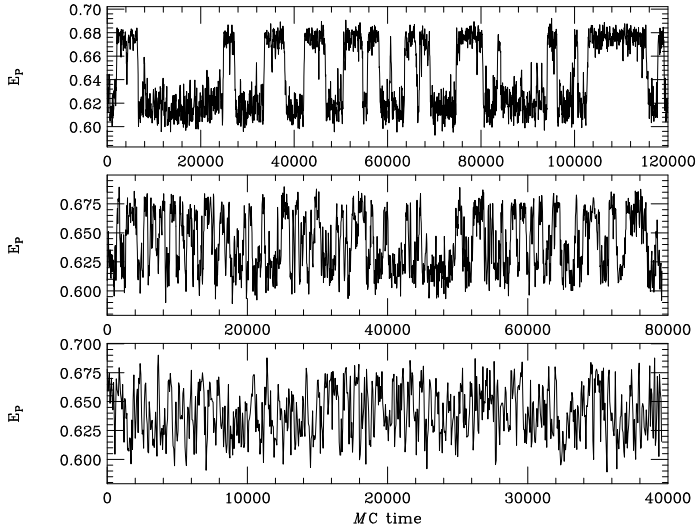

Figure 4.2: MC evolution of $E_{\rm p}$ at $\gamma = +0.2$ on the $\mathcal{HS}$ topology for $N = 6$ (lower window),$N = 7$ (middle) and $N = 8$ (top).

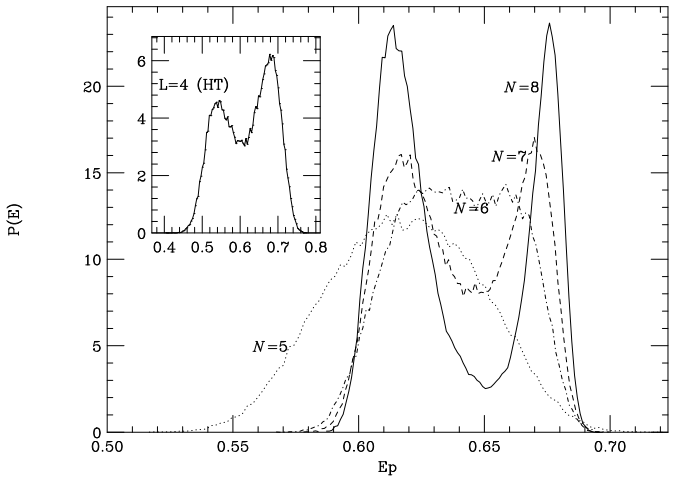

Figure 4.3: $E_{\rm p}$ distribution at $\gamma = +0.2$ on the $\mathcal{HS}$ topology. The small window is the distribution we obtained on the $\mathcal{HT}$ topology in $L = 4$ at $\beta = 0.8595$

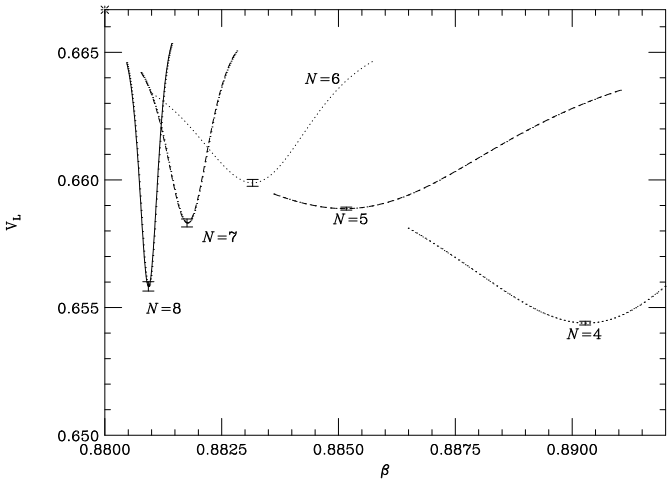

Figure 4.4: Binder cumulant at $\gamma = +0.2$ on the $\mathcal{HS}$ topology in $N = 4, 5, 6, 7, 8$. The cross in the upper corner signals the second order value 2/3.

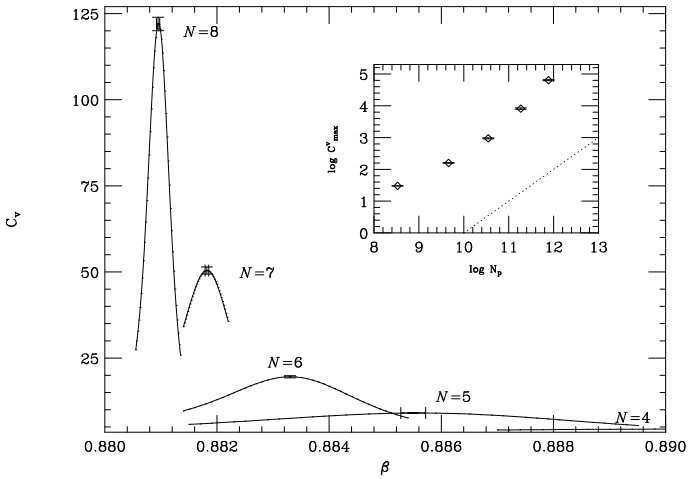

Figure 4.5: Specific heat maximum, and Ferrenberg-Swendsen extrapolation (solid line) at $\gamma = +0.2$ on the $\mathcal{HS}$ topology. The small window represents $C_{\rm v}^{\rm max}(N_{\rm p})$ The dotted line corresponds to the slope expected in a first order phase transition.

Figure 4.6: $E_{\rm p}$ distribution at $\gamma = +0.1$ on the $\mathcal{HS}$ topology.

The lattice sizes used range from $N = 4$ to $N = 8$, which correspond to $L_{\rm eff} \sim 5$ and $L_{\rm eff} \sim 12$ respectively see (Table 4.2).

In Figure 4.2, the MC evolution for $N = 6, 7, 8$ is shown. We remark that no multicanonical update is needed to obtain a very high rate of flip-flops up to $N = 8$. However, on the torus, for $L > 6$ the probability of tunneling between both metastable states is so tiny that a reasonable rate of flip-flops is not accessible to ordinary algorithms. Probably the inhomogeneity of the sphere is increasing the number of configurations with energies which correspond neither to the confined nor to the deconfined phase, but in between. These configurations make the free energy gap to decrease and hence the tunneling is easier on the $\mathcal{HS}$ topology. In short, the sites without maximum connectivity act as catalysts of the tunneling.

In Figure 4.3 the energy distributions are plotted. The distribution at $N = 6$ is distinctly non-gaussian, but a blatant two-peak structure is observed only from $N = 7$ ($L_{\rm eff} \sim 11$) on. So, when comparing with the result at $L = 4$ on the torus, (see small window in Figure 4.3) a first observation is that the onset of a two-state signal is particularly spoiled by the $\mathcal{HS}$ topology, at least in $4D$ pure compact U(1) gauge theory.

Concerning the latent heat, we remark its stability already at $N = 7$, or, if anything, its increase from $N = 7$ to $N = 8$. One would even say that the same happens between the positions of the would-be two states in

$N = 6$ and the position observed in $N = 7$. The behavior of the Binder cumulant reflects this fact (see Figure 4.4). We observe a rapid growth of $V_L^{\min}$ for small lattices sizes, apparently towards 2/3 (second order value). This growth stops when the splitting of the two peaks is observed. The splitting of the two peaks is reflected by smaller values in $V_L^{\min}$. We remark that the errors quoted for $V_L^{\min}$ are calculated taking into account the indetermination in the value of the minimum, but not the displacement in the position of the coupling where the minimum appears.

In our opinion, mainly two reasons can give account of this behavior. The first one comes from general grounds: at the very asymptotic region of a first order phase transition, the energy jump gets sharper and sharper, and a slightly increase of the latent heat could be expected. The second one would be the increasing restoration of homogeneity in the hypersphere when increasing the lattice size. The latent heat observed in small N might be affected by the inhomogeneity of the hyper-sphere.

At this point we cannot give a single reason for this to happen. We postpone a stronger conclusion to the section devoted to the Finite Size Scaling discussion.

The value of the latent heat when obtained with a cubic spline fit to the peaks in $N = 8$ is $C_{\rm lat} = 0.064(2)$. Results obtained with mixed hot-cold starts in $N = 9$ seems to give an energy jump around 0.067. However the reliability of this method is very limited and we do not dare to extract strong conclusions from it. Taking into account that he cubic spline at $N = 7$ gives 0.053(2) a possible scenario would be a slowly increasing latent heat towards its asymptotic value $C_{\rm lat}(\infty)$.

The peak of the specific heat for the different lattice sizes is displayed in Figure 4.5. The continuous line represents the FS extrapolation. The plot of the peak value, $C_v^{\max}(N_{\rm p})$ as a function of the plaquette number reveals a linear relationship, and hence a first order character.

We have also run simulations at $\gamma = +0.1$ in order to get an estimation for the latent heat. The results, being qualitatively similar to those encountered at $\gamma = +0.2$ are not reported in detail. We plot the energy distribution in Figure 4.6.

4.4.2 Results at $\gamma = 0$ on the spherical topology

Let us first situate the status of the studies using the toroidal topology with the Wilson action. As we have pointed out in the introduction, the transition was believed to be continuous till the simulation of a $L = 6$ lattice revealed the first signs of the existence of two metastable states [5]. Numerical simulations up to $L = 10$ showed a rapid decrease of the latent heat when increasing the lattice size, suggesting that the two metastable

states might superimpose in the limit $L \to \infty$ [6]. However, in [7], Azcoiti et al. suggest that the latent heat starts to stabilize at $L \sim 12, 14$.

When one tries to simulate large lattices the tunneling becomes scarce and the use of multicanonical simulations for those lattice sizes seems to be in order. However, in spite of its usefulness in spin models, as far as we know, there are no multicanonical simulation showing a substancial flip-flop rate improvement for this model.

Lattice sizes up to $L = 16$ have also been studied using multihistogramming techniques [8] and RG approaches [10, 11]. The results support the idea of a quasi stable latent heat for $L > 12$.

Topological considerations stressed already in the introduction led some authors to use lattices homotopic to the sphere. In the case of the Wilson action ($\gamma = 0$) the two-state signal is absent up to $N = 10$ [18]. Following this, we have simulated on the spherical topology in lattices ranging from $N = 6$ to $N = 14$, finding that the two-state signal sets in from $N = 12$ on.

The MC evolution for $N = 10, 12, 14$ is plotted in Figure 4.7. For the $N = 14$ lattice we have four independent runs, signaled by the dashed lines in the figure, all of them giving the same predictions.

In Figure 4.8 the distribution of $E_{\rm p}$ is plotted in lattices ranging from $N = 6$ to $N = 14$. We observe that a two-peak structure is revealed first time by the histogram in $N = 12$, which has a $L_{\rm eff} \sim 19$. On the toroidal topology the equivalent signal is observed already at $L = 6$ (see small window in Figure 4.8).

Having in mind the results of the previous section at $\gamma = +0.2$, it seems that the minimum $L_{\rm eff}$ required to observe a two-peak structure in the spherical topology is around three times the minimum lattice size L needed in the torus to observe two peaks.

The lattice sizes used in [18] at $\gamma = 0$ ranged from $N = 4$ to $N = 10$, so it is not surprising that they did not see any two-peak structure. Our results are in that sense compatible with theirs, though ours show a faster divergence for $C_{\rm v}^{\rm max}(N)$ with increasing N than the one observed in [18] in the lattice sizes we share (N=6,8,10). However we are particularly confident on this point because our simulation has been performed closer to the peak of the specific heat $\beta^*(L)$, and so we expect the Ferrenberg-Swendsen extrapolation to be more precise.

For the sake of comparison with the full group U(1), simulations with the Wilson action have been performed at $\gamma = 0$. At this coupling an implementation of overrelax is possible, and the global decorrelating effect should manifest itself in a better statistical quality.

In Figure 4.9 we show the histograms of $E_{\rm p}$ from $N = 6$ to $N = 12$ simulating the full group. The results are fully compatible with those obtained from simulations with $Z(1024)$.

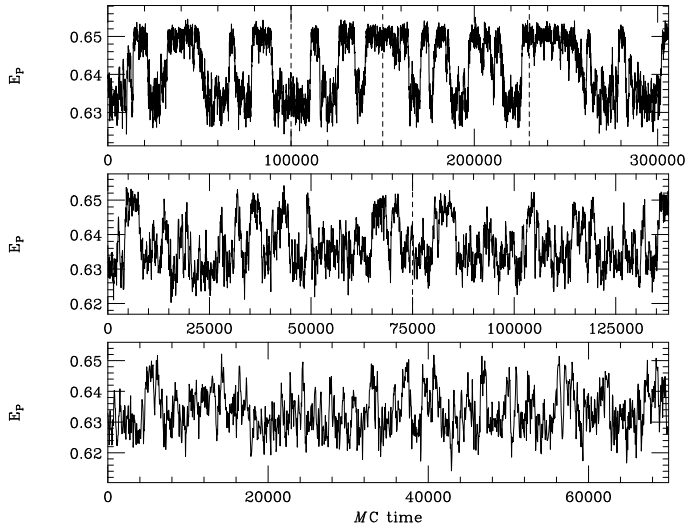

Figure 4.7: MC evolution of $E_{\rm p}$ at $\gamma = 0$ on the $\mathcal{HS}$ topology for $N = 10$ (lower window), $N = 12$ (middle) and $N = 14$ (top). The vertical dashed lines separate different runs

This test being performed, we go back to the description of the results obtained for the discrete group.

In Figure 4.10 we plot $C_{\rm v}(N)$ for different N's, together with the Ferrenberg-Swendsen extrapolation. The small window is a $\log - \log$ plot of $C_v^{\max}(N)$ as a function of $N_{\rm p}$. A linear behavior is observed from $N = 10$ on, which is even faster than linear when $N = 14$ is taken into account. This fact by itself implies the first order character of the transition since it means that the maximum in the energy fluctuation has the size of the volume. As a further check we have measured the ν exponent from the scaling of the Fisher zeroes (see Table 4.2).

In Figure 4.11 we plot $|G(\omega)|^2$ for several lattice sizes on the spherical topology at $\gamma = 0$. The different curves stand for the different ω we extrapolate. For small lattice sizes $Im(\omega_0)$ is larger, and the damping is more severe than for the larger lattices since in the later the imaginary part contributes with a faster oscillating function. Actually, we observe that for $N = 14$ even a second minimum could be measured before the signal is damped, while for $N = 10$ one can measure accurately only the first one.

The results for the effective ν are plotted in Figure 4.12 lower window. As could be expected from the behavior of the specific heat, for small lattices the effective exponent is somewhat larger than 0.25. It gets com-

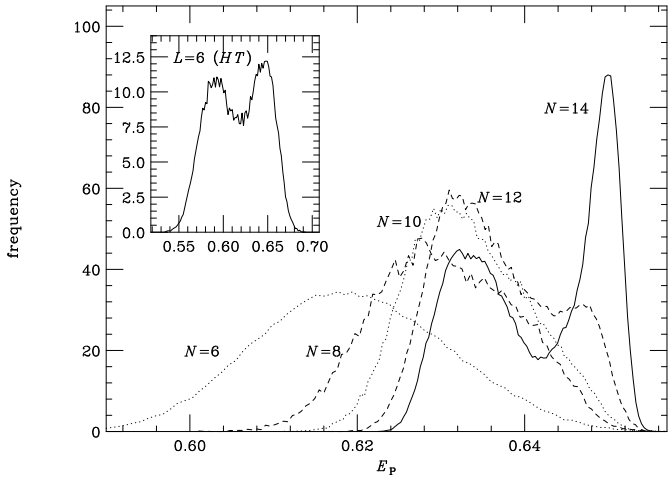

Figure 4.8: $E_{\rm p}$ distribution at $\gamma = 0$ on the $\mathcal{HS}$ topology. The small window corresponds to our simulation in the $\mathcal{HT}$ topology in L=6 at $\beta = 1.0020$.

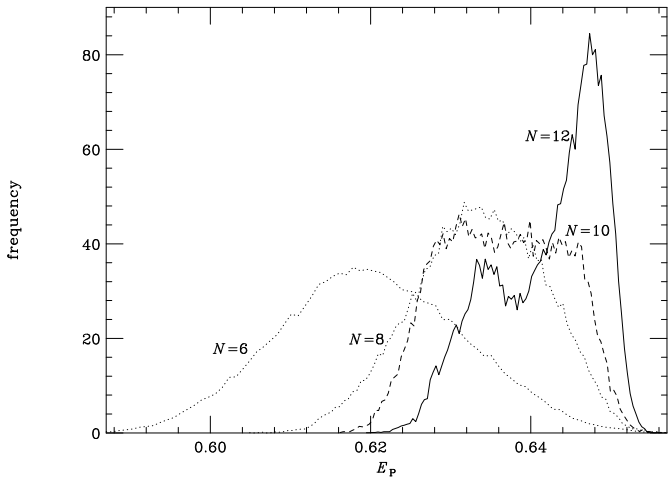

Figure 4.9: $E_{\rm p}$ distribution at $\gamma = 0$ on the $\mathcal{HS}$ topology simulating the full group U(1).

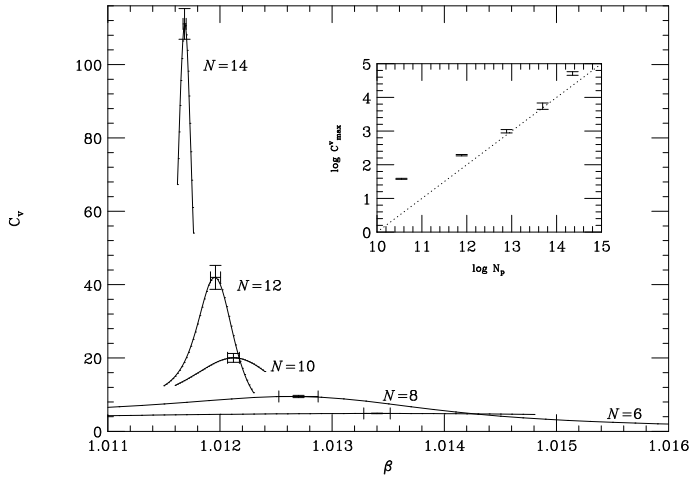

Figure 4.10: Specific heat maximum, and Ferrenberg-Swendsen extrapolation (solid line) at $\gamma = 0$ on the $\mathcal{HS}$ topology. The small window represents $C_{\rm v}^{\rm max}(N_{\rm p})$ The dotted line corresponds to the slope expected in a first order phase transition.

patible with the first order value from $N = 10$ on. In the largest lattices the distance between the two peaks slightly increases, and we measure a $\nu_{\rm eff}$ slightly smaller than the first order value. As a $\nu < 0.25$ is strictly impossible we expect this to be a transient effect due to finite size effects associated to the observed splitting up of the two peaks.

Concerning the latent heat, we observe a behavior completely analogous to the one observed at $\gamma = +0.2$. We do observe a two peak structure quite stable when comparing $N = 12$ and $N = 14$, but it slightly increases in $N = 14$. The plot of the Binder cumulant reflects again this fact (see Figure 4.13). The fast growth of $V_L^{\rm min}$ towards 2/3 is preempted by the onset of double peaked histograms from $N = 12$ on, and it even decreases in $N = 14$.

The cubic spline fit in $N = 14$ at the peaks gives a latent heat $C_{\rm lat} \approx 0.018(2)$. which is compatible with the results suggested by extrapolating to infinite volume the values obtained on the torus up to $L = 14$. Our results are hence supporting the conjecture stressed in [7] about a quasi stabilization of the latent heat on the torus from $L = 12$ on.

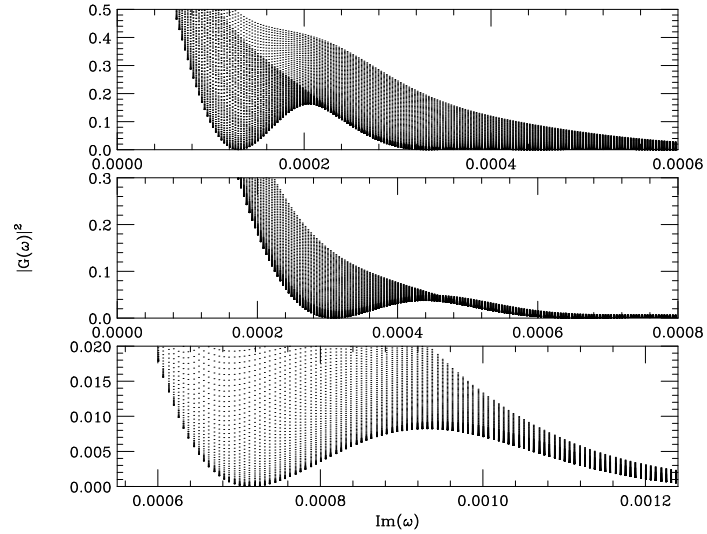

Figure 4.11: Plot of (4.25) for $N = 10$ (lower window), $N = 12$ (middle) and $N = 14$ (top) at $\gamma = 0$ in the $\mathcal{HS}$ topology.

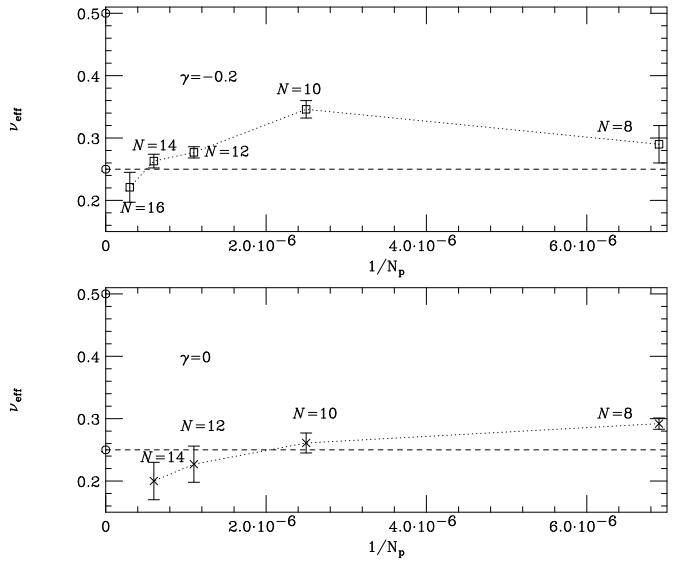

Figure 4.12: Effective exponent ν at $\gamma = 0$ (lower window), and at $\gamma = -0.2$ (upper window) on the spherical topology. In the smaller lattices an $\nu_{\text{eff}} \sim 1/3$ is observed which becomes $1/d$ when large enough lattices are considered.

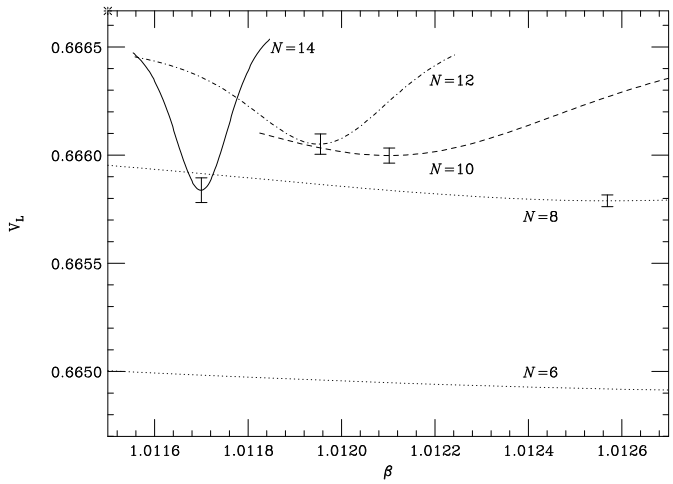

Figure 4.13: Binder cumulant at $\gamma = 0$ (Wilson action) on the $\mathcal{HS}$ topology in $N = 7, 8, 10, 12, 14$. The cross in the upper corner signals the second order value $2/3$.

Figure 4.14: MC evolutions at $\gamma = -0.2$ in L=12,16,20 on the $\mathcal{HT}$ topology.

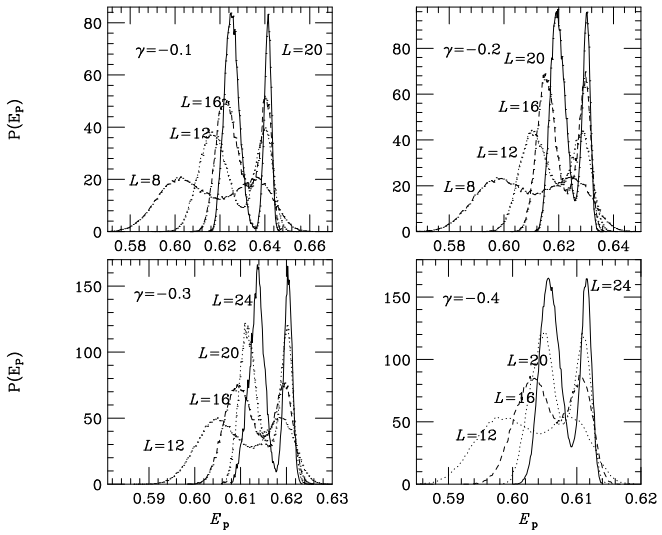

Figure 4.15: $E_{\rm p}$ distributions at the different negative γ on the $\mathcal{HT}$ topology. We have run up to $L = 20$ at $\gamma = -0.1, -0.2$ and up to $L = 24$ at $\gamma = -0.3, -0.4$.

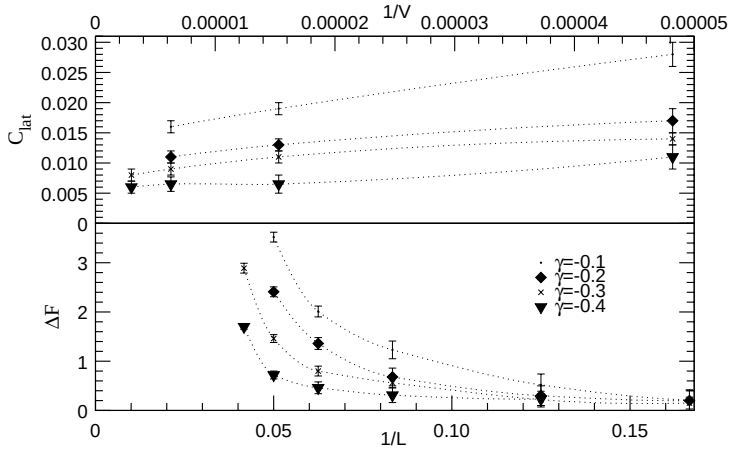

Figure 4.16: Free energy gap $\Delta F(L)$ (lower window) and latent heat (upper window) for the different negative γ in the $\mathcal{HT}$ topology.

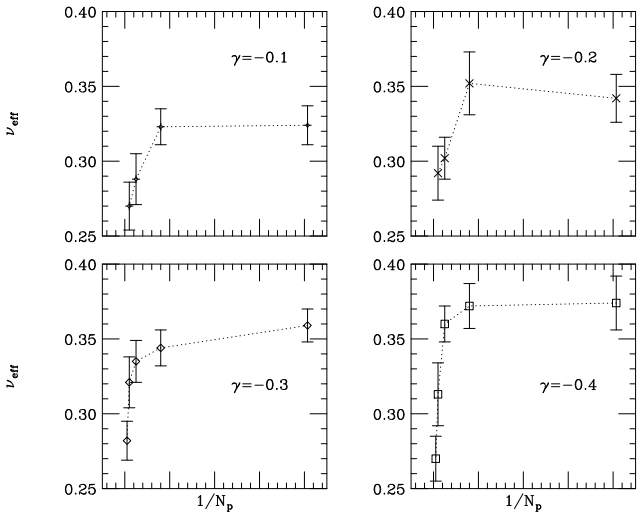

Figure 4.17: Effective ν exponent for the different negative γ in the $\mathcal{HT}$ topology.

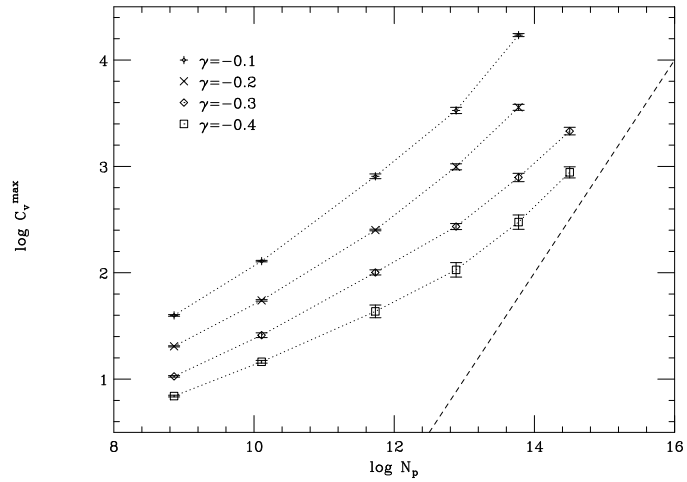

Figure 4.18: $C_v^{\max}(L)$ as a function of $N_{\rm p}$ for the different negative γ values on the $\mathcal{HT}$ topology. We have used $\log - \log$ scale for the clarity of the graphic sake. The dotted line corresponds to the first order slope.

4.4.3 Results for $\gamma < 0$

Toroidal topology

We have performed a systematic study of the transition at several negative values of γ on the toroidal topology.

We find that the two-state signal persists for all γ values we consider.

The MC evolution at $\gamma = -0.2$ is plotted for several lattices sizes in figure 4.14. As a general observation the more negative is γ, the flip rate becomes scarce for increasing lattice size. As an example, at $\gamma = -0.4$ the flip rate in $L = 20$ is comparable to the one observed in $L = 16$ at $\gamma = -0.2$.

The energy histograms reveal an increasing weakness of the transition when going to more negative γ values (see Figure 4.15). A double peak structure is clearly visible at $\gamma = -0.1$ in $L = 8$, while at $\gamma = -0.4$ one has to go to $L = 12$ to observe an equivalent signal.

In what concerns the behavior of the free energy gap $\Delta F(L)$, it grows for all investigated lattice sizes at all negative γ values (see Figure 4.16 lower window) signaling the first order character of the transition. The value of L at which $\Delta F(L)$ starts growing is certainly larger as the value of γ is more negative. This is another test of the increasing weakness of the transition as γ gets more negative.

The statistics performed on the torus are reported in Table 4.3. We also quote for the different negative γ, the value of $\beta^*(L)$ and the position of partition function zero closest to the real axis. We have computed from the imaginary part of the zeroes the effective ν exponent between consecutive lattice sizes following (4.26).

In Figure 4.17 we plot for the different γ values the $\nu_{\rm eff}$ we measure. In all cases a $\nu_{\rm eff} \sim 1/3$ is observed for small lattice sizes, which gets closer to 0.25 when the lattice is large enough. From this figure the trend of $\nu_{\rm eff}$ seems rather clear towards the first order value.

From the energy distributions we measure the latent heat through a cubic spline at the peaks. Taking into account the value $\nu_{\rm eff} = 0.25$ we measure, we plotted it as a function of the inverse of the volume L^{-4}, which is also the expected behavior of the latent heat when the transition is first order. The latent heat can be extrapolated to a value which is safely far from zero (see Figure 4.16 upper window).

In Figure 4.18 we plot $C_v^{\rm max}(L)$ as a function of $N_{\rm p}$. As could be expected from the behavior of the effective exponent ν, the maximum of the specific heat for small lattices diverges slower than the volume. For the smaller lattices the effective exponent is $\alpha/\nu \sim 1.4$. This value increases monotonically with the lattice size. In the largest ones we observe $\alpha/\nu \sim 3.5$.

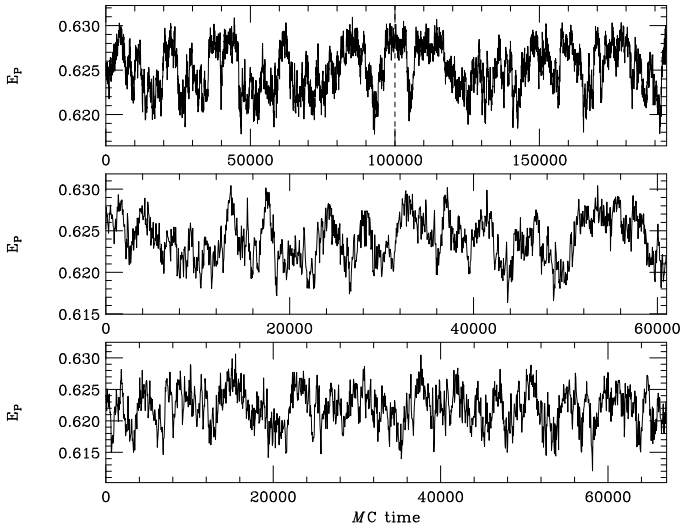

Figure 4.19: MC evolution of $E_{\rm p}$ in $N = 12$ (lower window), $N = 14$ (middle window) and $N = 16$ (upper window) at $\gamma = -0.2$ on the $\mathcal{HS}$ topology. The two different runs in $N = 16$ are separated by a vertical dashed line.

Spherical topology

On the toroidal topology we have found that the minimum lattice size required to observe a two state signal is obtained through an apropriate combination $(\gamma, L_{\rm min})$, with increasing $L_{\rm min}$ for increasingly negative γ, the behavior being qualitatively similar for all the γ values we have investigated. In view of this, we have studied a single $\gamma < 0$ value on the spherical lattice to check if the two state signal is absent on this topology. For the sake of comparison with [16, 18] we choose this value to be $\gamma = -0.2$.

We have run simulations on spheres ranging from $N = 6$ ($L_{\rm eff} \sim 8$) to $N = 16$ ($L_{\rm eff} \sim 26$). The MC evolution is plotted in Figure 4.19.

The distribution in $N = 14$ is distinctly non gaussian and the splitting of the peaks occurs in $N = 16$ (see Figure 4.20). We remark that the simulations in $N = 16$ are extremely expensive in CPU. In order to alleviate thermalization we have parallelized the code using shared memory in two PPro processors. In this lattice we have run two independent simulations starting from different configurations the results being fully compatible.

The behavior of the maximum of the specific heat is shown in Figure 4.21. We observe the same trend than in the previous values of γ in the sphere, i.e., an increasingly fast divergence of the specific heat with the

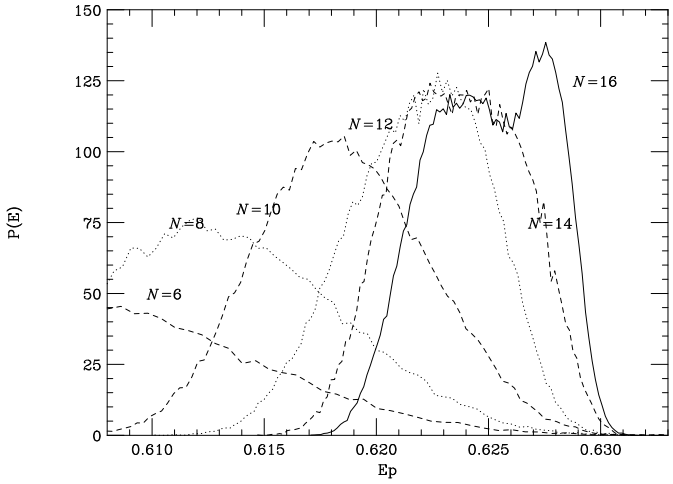

Figure 4.20: $E_{\rm p}$ distributions at $\gamma = -0.2$ on the $\mathcal{HS}$ topology.

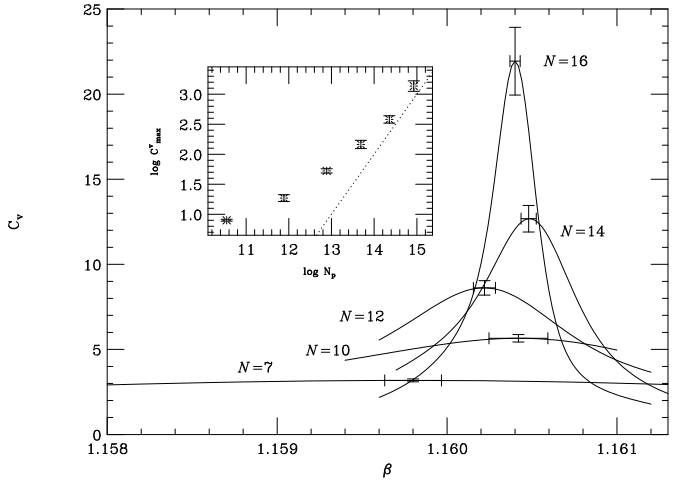

Figure 4.21: Specific heat maximum, and Ferrenberg-Swendsen extrapolation (solid line) at $\gamma = -0.2$. The small window represents $C_{\rm v}^{\rm max}(N_{\rm p})$ The dotted line correspond to the slope expected in a first order phase transition.

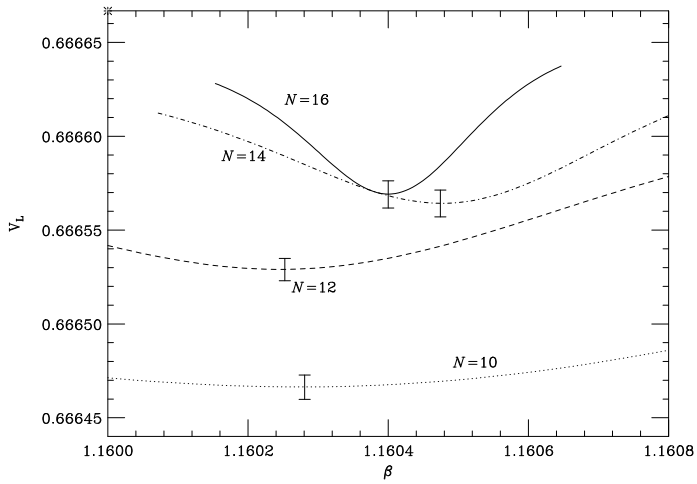

Figure 4.22: Binder cumulant at $\gamma = -0.2$ on the $\mathcal{HS}$ topology in $N = 10, 12, 14, 16$. The cross in the upper corner signals the second order value $2/3$.

lattice size, showing an effective $\alpha/\nu \sim 4$ already when the histogram width becomes constant with increasing lattice size.

At this value of γ we have a worse estimation for the latent heat to be, as the two peaks have not split enough to allow an accurate measurement.

Again the behavior of the Binder cumulant is very significant (see Figure 4.22. The value $V_L^{\min}$ shows a very fast trend towards $2/3$ in the small lattices. When increasing the lattice size the rate gets slower, and finally the value in $N = 16$ is compatible with the value in $N = 14$ preempting the extrapolation to $2/3$. Unfortunately lattices larger than $N = 16$ are unaccessible to our computers nowadays, and we cannot observe a decreasing $V_L^{\min}$ as we did for the other γ values. However from the behavior between $N = 14$ and $N = 16$ an increasing $V_L^{\min}$ for larger spheres seems to be very unlikely.

Concerning the effective critical exponent ν we have measured the position of the first Fisher zero (see Table 4.2) and compute ν_{eff} (see Figure 4.12). Again the first order value $1/d$ is reached in the largest lattices.

4.4.4 Toroidal versus Spherical topology

Due to the fact that on the sphere there are a number of points with less than the maximum connectivity, violations to standard FSS in the form of uncontrolled finite size effects are expected to appear on this topology.

We have observed all along this work that working on the spherical topology retards the onset of two-state signals. In terms of $L_{\rm eff}$, some qualitative prediction arising from our results would be that at fixed γ, the minimum lattice size required to observe a double peak structure, $L_{\rm min}$, is around three times larger on the sphere than on the torus. This one being the showier difference, is not certainly the only one.

When comparing $C_{\rm v}^{\rm max}(L_{\rm eff})$ on both topologies one finds always smaller values on the spherical topology (see small window in Figure 4.23). We did run on $L = 12$ on the torus and $N = 8$ on the sphere, which has an $L_{\rm eff} \sim 12$, sweeping an interval of β values including the phase transition. In Figure 4.23 we have plotted $E_{\rm p}$ in both topologies. In the region of low β the system is disordered, the entropy is higher and the system is not so sensitive to inhomogeneities of the lattice. However, in the region of high β the energy is in general smaller than for the homogeneous lattice since the system tends to be ordered, and the influence of the sites with less than

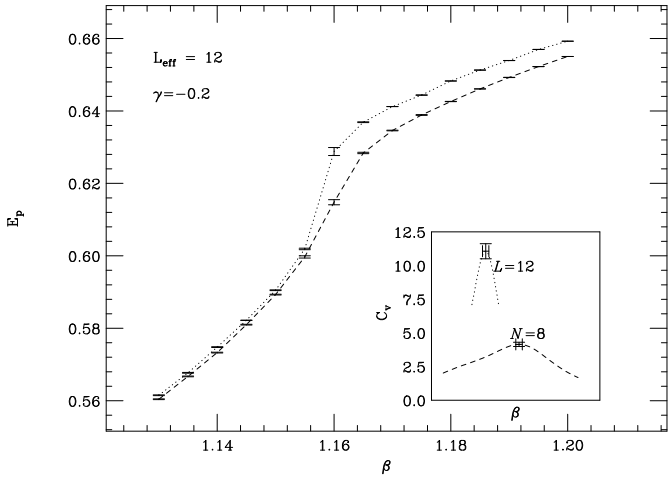

Figure 4.23: $E_{\rm p}$ at $\gamma = -0.2$ in $L_{\rm eff} \sim 12$. The dotted line corresponds to the toroidal topology, the dashed one to the sphere $N = 8$. The small window shows the difference in the specific heat between both cases.

maximum connectivity is more evident. This difference gets smaller when the lattice size is increased on the sphere, and hence the energy jump is larger. This feature explains the observed splitting of the two states on the spherical lattices when increasing lattice size.

Altogether, it is not recommended to work on spherical lattices to check the existence or not of two-state signals. However, there are a number of facts that make this topology not so dissapointing in spite of those uncontrolled finite size effects. The first one concerns the behavior of $\beta^*(L)$ and the second one the measure of the latent heat.

In Figure 4.24 we compare $\beta^*(L)$ on the torus and on the sphere. A first observation is that despite they not having the same values in finite lattices, both curves get closer when increasing the lattice size. This supports the idea of a common thermodynamic limit for both topologies. On the other hand, the shift in the apparent critical coupling with L is much less dramatic on the sphere than on the torus. It seems that finite size corrections to β_c are smaller in the case of the spherical topology. This behavior has also been observed in the Ising model on spherical lattices [28].

The behavior of the latent heat is very significant. In Figure 4.25 we compare the latent heat in finite volumes for both topologies. On the

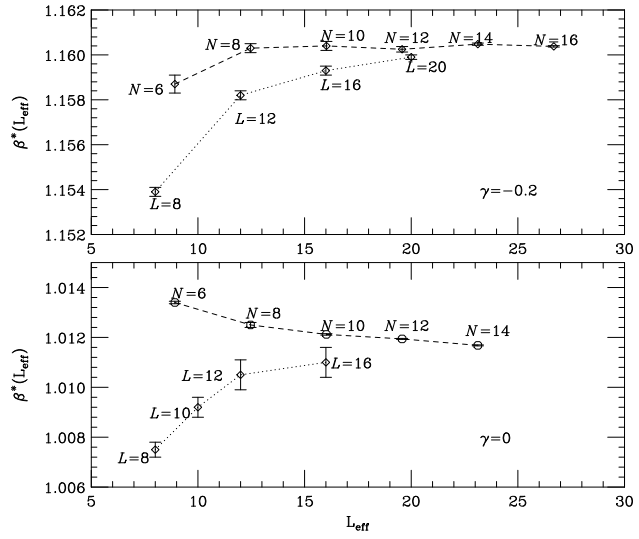

Figure 4.24: $\beta^*(L)$ for the different lattice sizes on the torus (dotted lines) and on the sphere (dashed lines) at $\gamma = 0$ (lower window) and at $\gamma = -0.2$ (upper window). The couplings for $\gamma = 0$ on the torus have been taken from [11].

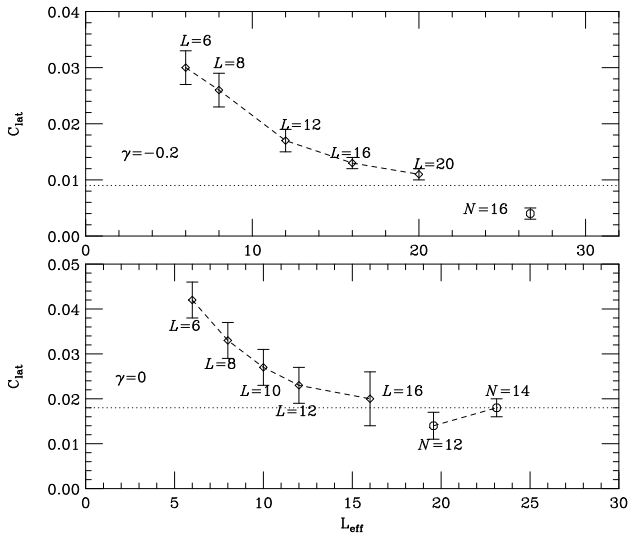

Figure 4.25: Latent heat for the different lattice sizes on the torus and on the sphere at $\gamma = 0$ (lower window) and at $\gamma = -0.2$ (upper window). The dotted line corresponds to $C_{\rm lat}(\infty)$ obtained by extrapolating the values on the torus through a linear fit as function of $1/V$. The values for $\gamma = 0$ on the torus have been taken from [11].

Wilson line, at $\gamma = 0$ the asymptotic value of the latent heat is obtained in the spherical topology. The inhomogeneity of the sphere has, paradoxically, helped us to run lattices with $L_{\rm eff} \sim 24$ without having to worry about the tunneling rate. From this graph we quote $C_{\rm lat}(\infty) = 0.018(1)$. In the upper window the same is plotted for $\gamma = -0.2$. Unfortunately we have just a single lattice size on the sphere to measure the latent heat, however, from the behavior exhibited by this topology, an increase of the latent heat on spheres larger than $N = 16$ seems rather likely. Altogether, at $\gamma = -0.2$ a $C_{\rm lat}(\infty) \sim 0.009$ is plausible.

In what concerns the latent heat, the spherical topology seems to afford an useful complement to the results obtained for the the toroidal lattice. In fact, on the Wilson line lattices larger than $L = 16$ cannot be studied due to the technical problem associated to the scarce tunneling. The spherical lattice alleviates this technical problem, and the results are supporting the value of the extrapolated latent heat as a function of the inverse of the volume, from the data on toroidal lattices up to $L = 16$. One could consider the possibility of simulating on spherical lattices at negative γ to solve the tunneling problem, but in our opinion, the price to pay is too high.

4.5 Conclusions

The first order character of the deconfinement transition in pure U(1) has been proved, up to the limits of a rather reasonable numerical evidence, in the interval $\gamma \in [+0.2, -0.4]$.

In $\gamma = +0.2$ we have been able to stabilize the latent heat. We are aware of no simulation on the torus showing a stable latent heat due to the scarce tunneling in lattices larger than $L = 6$. The spherical topology has helped to solve this problem. However, probably any lattice with inhomogeneities would produce the same catalysing effects.

In $\gamma = 0$ we have obeserved an increasing energy gap on the spherical lattice, and also, we have been able to measure the asymptotic value of the latent heat. We have proved the suggestions of several authors about a quasi stabilization on lattices larger than $L \sim 12$. The data on the spherical topology have been crucial to discard the possibility of a slowly vanishing latent heat. It follows that the discretization of pure compact U(1) LGT on the lattice using the Wilson action exhibits a first order phase transition with a latent heat in the thermodynamical limit $C_{\rm lat} \sim 0.018$.

On the toroidal topology things happen qualitatively in the same way than in $\gamma = 0$ up to $\gamma = -0.4$. We have run on spherical lattices in $\gamma = -0.2$ looking for an argument similar to the one found in the Wilson case concerning the stabilization of the latent heat. The simulation in $N = 16$ gives an estimation for the latent heat though rather imprecise because the splitting of the peaks is not good enough for the measurement to be accurate. However, in view of the behavior exhibited by the spherical topology concerning the trend of the two peaks on spherical lattices to separate, we are prone to consider the value measured in $N = 16$ as a lower bound for the latent heat in $\gamma = -0.2$. On the other hand, we would at present say that the latent heat extrapolated from the data on the torus up to $L = 20$ is rather accurate, in view of the behavior for the Wilson case. The possibility of running larger spheres surpasses our computer resources. A highly parallelized version of the code should be used to alleviate thermalization, which is a possibility we do not discard completely at medium term.

As for the evolution of the latent heat along the transition line as a function of γ. the scenario that follows from our results is plotted in Figure 4.26.

Either proving or discarding the possibility of a TCP at some finite negative $|\gamma_{\rm TCP}| > 0.4$ will be a very difficult task from the numerical point of view. An analytical argument would be welcome. A very tiny two-state signal, comparable with the one observed in $L = 8$ at $\gamma = -0.4$, is observed on the torus in $L = 16$ at $\gamma = -0.8$, which is the most negative value we

Figure 4.26: Extrapolated value for the latent heat as a function of γ. The values quoted for $\gamma < 0$ come from data on toroidal lattices, the ones for $\gamma \geq 0$ from data on spherical lattices.

have run on the torus. Taking into account the factor 3 in L_{eff} one would need a $N \sim 30$ sphere to observe a tiny double peak structure. Simulation with spherical lattices in this range of γ have no sense, and nothing can be concluded from the absence of two state signals from such negative γ values.

In view of these difficulties to stabilize the latent heat for very negative γ values, the only chance to discern the order of the phase transition is the study of effective critical exponents. Cumulants of the energy, such as the Binder cumulant, have been shown to behave like expected in the first order case only when the stable two-peak structure is almost setting in, and there, we do not need further evidences any longer. We could not expect additional information since by definition the Binder cumulant relies on the existence of stable latent heat in order to extrapolate to $V_{\text{L}=\infty}^{\min} < 2/3$.

The advantage of studying the effective exponents (which is nothing but studying the evolution of the histograms width) is that we do not need a direct observation of latent heat to conclude that a transition is first order [33, 30]. We have observed a ν_{eff} which evolves monotonically until it reaches the first order value, namely 0.25, in all cases. The statistics needed to observe a monotonous behavior, are order 1000τ at the coupling $\beta^*(L)$, which has to be located with high precision (four digits in our experience)

in order to accurately measure effective exponents. However, one has to make every effort to observe the trend of the effective exponents, since it is the only chance to discern the order of such tricky transitions.

In pure U(1), for the Wilson case, an exponent $\nu \sim 1/3$ was widely predicted [3, 4, 12] at the beginning of the eighties when the lattice sizes where too small to reveal two peaks. That ν was shown to become $\nu \sim 0.29$ when simulating $L = 14$ [7]. We have measured $\nu = 0.25$ on spherical lattices and stated its first order character. Within the approximation of effective potentials it can be shown that along the transient region of a weak first order phase transition, everything goes like in a second order one with a thermal exponent $\alpha = 0.5$ [20]. Together with Josephson law ($\alpha = 2 - \nu d$) it implies $\nu \sim 0.37$. This statement has been checked in 2D Potts [20], 3D and 4D $O(N)$ models [29, 30, 31, 32] and in the 4D SU(2)-Higgs at T=0 with fixed Higgs modulus [33]. Our results prove that pure compact U(1) theory behaves in the same way.

Bibliography

[1] K.G. Wilson *Phys. Rev.* **D10** 2445

[2] M. Creutz, L. Jacobs and C. Rebbi. *Phys. Rev.* **D20** (1979) 1915

[3] B. Lautrup and M. Nauenberg *Phys. Lett.* **B95** (1980) 63

[4] G. Bhanot *Phys. Rev.* **D24** (1981) 461

[5] J. Jersák, T. Neuhaus and P.M. Zerwas *Phys. Lett.* **B133** (1983) 103

[6] V. Azcoiti, G. di Carlo and A. Grillo *Phys. Lett.* **B238** (1990) 355

[7] V. Azcoiti, G. di Carlo and A. Grillo *Phys. Lett.* **B268** (1991) 101

[8] G. Bhanot, T. Lippert, K. Schilling and P. Ueberholz *Nuc. Phys.* **B378** (1992) 633

[9] D.J. Callaway and R. Petronzio *Nuc. Phys.* **B280** (1987) 481

[10] P. Hasenfratz and A. Hasenfratz *Nuc. Phys.* **B295** (1988) 1

[11] L.A. Fernández, A. Muñoz-Sudupe, R. Petronzio and A. Tarancón. *Phys. Lett.* **B267** (1991) 100

[12] G. Bhanot *Nuc. Phys.* **B205** (1982) 168

[13] H.G. Evertz, J. Jersak, T. Neuhaus and P.M. Zerwas *Nuc. Phys.* **B251** (1985) 279

[14] A. Hasenfratz *Phys. Lett.* **B201** (1988) 492

[15] R. Gupta, M.A. Novotny and R. Cordery *Phys. Lett.* **B172** (1986) 86

[16] C.B. Lang and T. Neuhaus *Nuc. Phys.* **B431** (1994) 119

[17] M. Baig and H. Fort *Phys. Lett.* **B332** (1994) 428

[18] J. Jersak, C.B. Lang and T. Neuhaus *Phys. Rev. Lett.* **77** (1996) 1933

[19] W. Kerler, C. Rebbi and A. Werber *Phys. Lett.* **B348** (1995) 565

[20] L.A. Fernández, M.P. Lombardo, J.J. Ruiz-Lorenzo and A. Tarancón. *Phys. Lett.* **B277** (1992) 485

[21] The APE collaboration *Nuc. Phys.* **B318** (1989) 553

[22] J. Lee and J.M. Kosterlitz *Phys. Rev. Lett.* **65** (1990) 137

[23] M.S. Challa, D.P. Landau, K. Binder *Phys. Rev.* **D34** (1986) 1841

[24] C. N. Yang and T. D. Lee. *Phys. Rev.* **87** (1952) 404

[25] E. Marinari in *1996 Budapest Summer School on Monte Carlo methods e-print: cond-mat//9612010*

[26] M. Falcioni, G. Martinelli, M.L. Paciello, G. Parisi and B. Taglienti *Nuc. Phys.* **B265** (1986) 187.

[27] A.D. Sokal *Bosonic Algorithms* in *Quantum Fields on the Computer*. Advanced Series on Direction in High Energy Physics Vol. 11, M. Creutz Editor. World Scientific, Singapore 1992.

[28] O. Diego, J. Gonzalez, J. Salas *J. Phys.* **A27** (1994) 2965.

[29] J.L. Alonso, J.M. Carmona, J. Clemente, L.A. Fernández, D. Iñiguez, A. Tarancón and C.L. Ullod. *Phys. Lett.* **B376** (1996) 148

[30] H.G. Ballesteros, J.M. Carmona, L.A. Fernández and A. Tarancón *Phys. Lett.* **B419** (1998) 303

[31] I. Campos, L.A. Fernández, A. Tarancón *Phys. Rev.* **D55** (1997) 2965

[32] J.L. Alonso, H.G. Ballesteros, L.A. Fernández, V. Martín-Mayor, A. Muñoz Sudupe and A. Tarancón *Phys. Rev.* **B53** (1996) 2537

[33] I. Campos, *Nuc. Phys.* **B514** (1998) 336

Chapter 5

Modelos bidimensionales de flujo de partículas

5.1 Introducción

En los últimos años está recibiendo una especial atención la formulación de modelos para describir por ejemplo el paso de mensajes a través de redes de ordenadores [1], el tráfico en grandes ciudades [2], la adsorción de moléculas en un cristal [3], conductores de iones rápidos [4].

Todos estos problemas tienen en común que pueden ser estudiados desde el punto de vista de la teoría de Random Walks. Sin embargo, el elevado número de grados de libertad hace imposble extraer información relevante mediante cálculos analíticos. La alternativa es el uso de simulaciones numéricas.

Desde este punto de vista uno podría pensar en formular modelos tan próximos a la realidad como sea posible, incluyendo todos los grados de libertad que se sea capaz de manejar. Sin embargo los modelos que resultan aplicando esta filosofía son demasiado complicados de estudiar, no sólo en lo que concierne a la descripción de fenómenos relevantes, sino también porque carecen de poder predictivo en general.

Una aproximación alternativa es formular modelos más simples, menos realistas pero manteniendo los rasgos fundamentales del sistema físico. Tales modelos están descritos por unos pocos parámetros, siendo por ello más faciles de tratar y haciendo posible un estudio global del espacio de parámetros sin perder intuición física.

Mediante la formulación de estos modelos se pretende obtener resultados relevantes sobre sistemas complejos, estudiando aproximaciones relativamente simples, como se suele hacer en Mecanica Estadística (ME) donde sistemas tan complicados como redes ferromagnéticas comparten muchas propiedades con modelos tan simples como el de Ising. En ME la relación entre ambos sistemas se entiende a través del Grupo de Renormalización. Desgraciadamente estamos lejos de poder probar una relación de este tipo para modelos de flujo de partículas, debido fundamentalmente a que no tienen un límite termodinámico bien definido. Sin embargo la modelización de estos sistemas es necesaria.

Los problemas que se encuentran cuando se estudian sistemas que envuelven flujo de partículas están relacionados con procesos de congestión. Los sistemas realizan una transición de una situación de tráfico fluido a otra caracterizada por el atasco.

Podríamos utilizar las herramientas de la ME para estudiar estos problemas si asimilamos este cambio a una transición de fase. Un primer paso es buscar las variables que gobiernan la transición.

El flujo en la red está condicionado por el número máximo de partículas que un nodo es capaz de contener, por la interacción entre las partículas y por la geometría de la red (por ejemplo el numero de coordinación).

En nuestro modelo hay una inyección continua de partículas en la red, para cada una de ellas se elije al azar un nodo que será su destino final. El movimiento de las partículas se implementa permitiendoles moverse en la red de acuerdo con determinadas reglas que definiremos más tarde. En el tráfico real las partículas encuentran a menudo obstaculos en su camino. Estos obstáculos se simulan limitando el número de partículas que un nodo de la red puede almacenar simultaneamente.

Volviendo a la discusión desde el punto de vista de la ME, vamos a enfocar la situación en la que la densidad de partículas es alta. Intuitivamente es claro que una partícula podría evitar zonas de atasco si le permitimos rodear el obstáculo. El sistema estará globalmente más descongestionado y esperamos una mejora en el número de partículas que alcanzan finalmente su destino. En términos de ME, la discusión previa significa que calentando el sistema ($T \neq 0$) se obtendran mejores resultados [5]

En lo que concierne a la interacción entre las partículas, hemos introducido un término de contacto, la existencia de obstáculos en forma de nodos completamente ocupados. Las consecuencias de esta interacción se pueden ver como si existiera un potencial infinito que actua en los nodos saturados.

Un término de interacción apropiado se obtiene asignando *carga eléctrica* a cada partícula. La repulsión alejará a las partículas de las regiones densamente cargadas. Consideraremos este tipo de repulsión actuando sólo sobre primeros vecinos en la red.

Este tipo de fuerzas repulsivas se consideran a menudo en problemas de polímeros [6].

Hemos introducido un modelo en el cual hay un término que controla la magnitud de las fluctuaciones térmicas y otro que simula una fuerza repulsiva. Los parámetros que controlan estos términos son respectivamente la temperatura y la *carga*. Veremos como ajustando ambos parámetros es posible mejorar el flujo de partículas.

Abstract

We study a particle flow model which may be used to get insight into various real traffic problems. The model is implemented using a discrete lattice, in which particles move towards their destination, fluctuating about the minimal distance path. A repulsive interaction between particles is introduced so as to avoid the appearance of a traffic jam. We have studied the parameter space finding regions of fluid traffic, and saturated ones, both regions being separated by abrupt changes. The improvement of the system performance is also explored by introducing a non-constant potential acting on the particles. Finally, we deal with the behaviour of the system when temporary failures in transmission occur.

5.2 The Model

We consider a two-dimensional lattice with coordination number 4, and periodic boundary conditions. The particles live in the lattice sites, labeled by $n \equiv (n_0, n_1)$ and can move from its site to one of its four nearest neighbors at every time step. The maximum number of particles that a site can contain will be denoted by B, and will be kept fixed for all the simulation at a value $B = 5$. We denote the occupation number of the site n by $\sigma(n)$. In this notation, the particles are prevented from moving to sites with $\sigma(n) = B$. In addition we consider an input queue at each site for the particles waiting to be injected on the lattice.

By analogy with statistical mechanics systems, we work with the inverse of the temperature, β. We denote the charge of the particles by κ and the probability of particle injection to the lattice by p.

The dynamic of the system is as follows:

1. A lattice site is chosen at random.

2. A particle is added, with fixed probability p, to the queue of the site, waiting to be introduced to the lattice [1]

3. If the queue of the site is not empty, and $\sigma(n) < B$, a new particle is introduced in the lattice, and an endpoint assigned to it at random.

4. All particles at the considered site, try to move towards one of its four neighbors. For a given particle located at the position n we

[1] The size of the queue is as big as necessary, so that it contains all particles waiting to be fed at that lattice site

must assign a probability of it jumping to each of its neighbouring locations. This probability is given by:

$$P(\pm\mu) = N \exp(\pm\beta \text{sign}({n^f}_\mu - n_\mu) - \kappa\sigma(n_\mu)) \ , \qquad (5.1)$$

where n_μ here signifies the μ coordinate of site n, n^f is the endpoint of the particle being considered, and N is the normalization constant. To choose between possible destinations we use a $Heat\ Bath$ [7] algorithm.

The factor multiplying β, is a potential term. It implies a constant force acting on the particle driving it to its endpoint. The κ term produces a repulsion between particles sitting in nearer neighbors sites. Obviously there is a wide range of potentials that could be considered, in order to produce more effective forces, and partial improvements will be expected.

5. Movement is allowed if the chosen site has $\sigma(n) < B$, otherwise the particle remains at its original site until a new movement is attempted in the next iteration.

6. A particle is removed from the lattice when it reaches its endpoint.

The smaller p is, the weaker is the effect of the interaction between the particles. For fixed (β, κ) the fluid flow of particles on the lattice only takes place for those values of p being less than a certain threshold which is (β, κ) dependent. Above this threshold, the density becomes too high and the transmission process is prevented. We say the system is saturated. The saturation mechanism begins with the appearance of saturated domains, which grows in size making the movement of the particles more and more difficult.

Our purpose is to quantify this threshold density, as well as to describe the flow properties along the parameter space (β, κ, p).

From the point of view of Telecommunication Networks, the lattice sites can be thought of as nodes of such networks, and *particles* here can be interpreted as *messages/packets*. Within this approach, B can be identified with the available buffer space at the considered node. In this way, our model can be considered as a first step towards an *abstract* modeling of packet/message Telecommunication Networks. In such networks, packets are routed by each node according to routing tables dynamically maintained by the network so as to minimize some *cost function* along the trajectory of the packets [8]. In the present model, this cost function is simply the traveled distance, and, as the network state does not change during simulations, routing tables need not be dynamically calculated. A natural extension of

this model would be to allow variable link lengths between the nodes and to compute routing tables according to the path lengths. The role of the temperature parameter is to quantify how firmly the network will try to stick to its policy of minimizing the cost along a trajectory: as will be shown below, implementing the routing according to the cost minimization procedure in a rigid way (*zero temperature*), although this is the best *naive* choice from an individual user point of view, can be detrimental to the global behavior of the network and thus to its collective utility (the total throughput offered by the network).

Congestion is an unavoidable phenomenon in uncontrolled packet networks, since packets introduced at one node have no guarantee of finding the necessary resources (available buffer space) in the transit nodes. If uncontrolled, congestion result in packet losses which, in the case of data transmission, are detected by upper layer protocols (the Transport Control Protocol, TCP, for instance in the case of the Internet) and are corrected by retransmision request. Hence these packet losses will trigger more packets to be introduced into the network, thus further amplifying the congestion Two approaches are possible to avoid this *vicious circle*: reducing the source emission rate when a congestion is detected (this is the TCP approach) or trying to control the congestion inside the network by preventing packets from accessing overloaded areas (this approach does not rely on any source behavior: in the extreme congestion case the source is simply denied any access to the network). This last option, congestion control inside the network, is presently a very active area of research in the networking community [9]. To implement such a control, the overload information should be transmitted by a node to its neighbors at least. This is precisely what is modeled by the repulsive charge term in the present model: access to a loaded node is discouraged, and access to an overloaded node is simply forbidden. It should be noted that in the model as it stands, a node is instantaneously aware of the load state of its neighbors. A more complex model should take into account the latency introduced by the node-to-node transit time, leading to a description of the congestion control by some kind of *retarded potential*. It will be particularly important to take this latency aspect into account for modeling high speed networks [10], but this is left for future work.

The system we are considering here is also related to a lattice gas with fixed number of particles in a constant electric field $\vec{E}$ [11]. The electric current is related to the traffic speed. Also in this model a transition appears, between a disordered phase and another one were particles move collectively in the $\vec{E}$ direction. In our case the electric field is no longer constant, it depends dynamically on the particle environment: the surrounding electrical charge and the end point associated with the particle. As is usual for

traffic models, the number of particles is not constant; as a consequence, the transition mechanism is different.

5.3 Numerical Simulation

We have performed Monte Carlo (MC) simulations in order to study the parameter space. Here we present results obtained using a $L \times L$ lattice with $L = 32$ and periodic boundary conditions. The computations have been carried out on workstations.

The starting configuration is obtained by generating a particle with probability p at each site of the lattice, therefore, the total number of sites occupied initially is about $p \times L^2$. The random number generator is based on one described in [12]. The time step is identified with a MC iteration, that is the update of L^2 lattice sites in the way described in section 2.

The temporal evolution of the system exhibits a transient regime, characterized by the instability in the observables (see next section). After this, the system falls into an extremely long-living metastable state, where the flow properties do not change significantly with the temporal evolution. We say the system has reached the asymptotic regime.

The time the system spends in the transient regime depends on the parameter space point (β, κ, p). In this regime, in the non-saturated region, the particle density is initially low and grows with the particle injection.

This transit time also grows near the parameter space points where an abrupt change in the properties is observed (e.g. near the threshold density), reaching in this case up to 2×10^4.

For each value of the parameters, we have performed typically 8×10^4 MC iterations. For β and $\kappa \in (0, 0.4)$ the transient regime takes around 5000 iterations, while above 0.5 for both parameters, this time falls to $400 - 600$ iterations. We have also performed the simulations starting from different configurations, allowing the system to evolve for up to 2×10^5 iterations. We have computed the errors by calculating the dispersion between the results obtained from starting from these different configurations.

5.4 Observables

A correct description of the system is obtained from the measurement of the relevant observables. From their temporal evolution we are able to evaluate when the asymptotic regime is reached, or even whether this regime will or will not be saturated. From the averaged value of these magnitudes we obtain a quantitative description of the flow process.

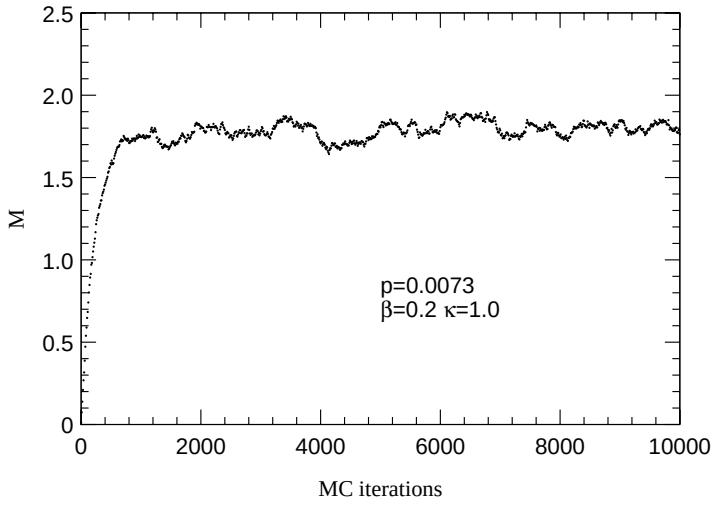

Figure 5.1: Temporal evolution of M bellow the critical injection p_c.

For a given configuration, we define the occupation M as:

$$M = (1/V) \sum_{i=1}^{V} \sigma(i) \ . \tag{5.2}$$

Where V is $L \times L$.

The statistical average over the configurations (labeled by j) is:

$$\langle M \rangle = \lim_{N \to \infty} (1/N) \sum_{j=1}^{N} M_j \ . \tag{5.3}$$

N being the number of averaged configurations.

During the time interval $t_j - t_i \equiv \triangle t$, n_e particles will reach their endpoint. We define the Band Width (B_W) as the number of particles that arrive at the endpoint per time unit.

$$B_W(\triangle t) = \frac{n_e}{\triangle t} \ . \tag{5.4}$$

The statistical average for B_W is obtained from its mean value over a number of time intervals N_T:

$$\langle B_W \rangle = \lim_{N_T \to \infty} (1/N_T) \sum_{j=1}^{N_T} B_W(j) \ . \tag{5.5}$$

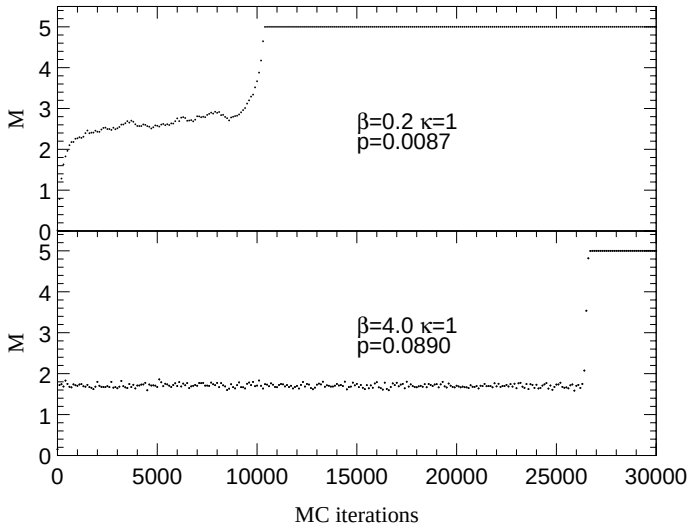

Figure 5.2: Temporal evolution of M above p_c.

We can obtain a good measure of the system performance from the mean time taken by the particles to reach their endpoint, T_M. We compute T_M in the time interval $\triangle t$ by adding the individual time spent by each particle (delay time), divided by n_f:

$$T_M(\triangle t) = \frac{\sum_{i=1}^{n_f} T_i}{n_f} \tag{5.6}$$

In the same way we define the statistical average as over N_T intervals as:

$$\langle T_M \rangle = \lim_{N_T \to \infty} (1/N_T) \sum_{j=1}^{N_T} T_M(j) \tag{5.7}$$

The occupation frequency of a certain occupation number, $\sigma(n)$, is defined as the number of times that the occupation $\sigma(n)$ appears at any lattice site.

5.5 Phase Diagram

We examine the parameter space (β, κ, p) searching for regions where sharp changes in the temporal evolution arise. At each (β, κ) value there is a p

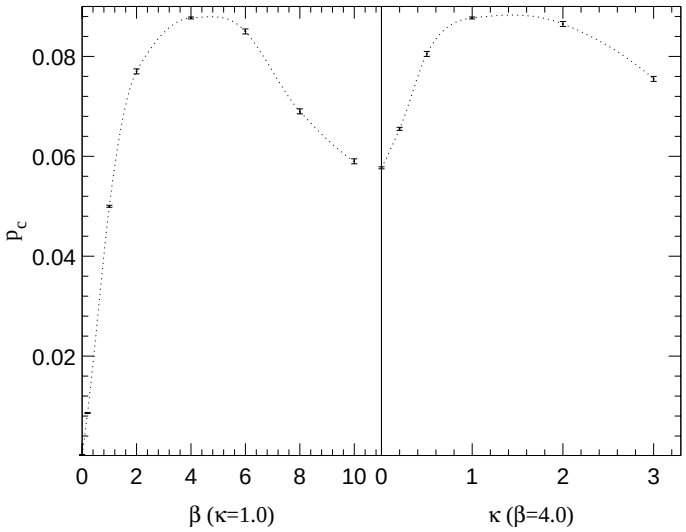

Figure 5.3: Sections through the phase space cube. On the left side is plotted p_c versus β, on the right one, p_c versus κ.

value denoted by p_c such that for $p < p_c$ the asymptotic regime presents a stationary flow, and for $p > p_c$ the asymptotic regime is saturated and the flow is no longer possible. We plot the temporal evolution of M below p_c (Figure 5.1) and above p_c (Figure 5.2) for some values of the parameters.

This change is similar to a phase transition. The temporal evolution leads the system to one or another phase depending on the parameter space point. Once in the asymptotic regime, the non-saturated phase exhibits a dynamic equilibrium: the number of injected particles, equals the number of those arriving at their end position. This is reflected by $\langle B_W \rangle = p \times L^2$. In this phase, $\langle T_M \rangle$ is constant, as well as $\langle M \rangle$ which is always less than B.

The parameter space is divided into two regions by the surface defined by (β, κ, p_c). Figure 5.3 shows two sections, for fixed β and κ respectively.

Above the surface, after the transient regime $\langle M \rangle = B$ and $\langle B_W \rangle = 0$, $\langle T_M \rangle$ diverges.

It is possible to give a simple interpretation of this congestion phenomenon; when the load increases so does the probability that two particles residing in two neighboring saturated sites will want to *exchange* their sites, but of course they cannot do so since one of the particles would have to move first and then have nowhere to go to as no resource is will be available at the desired site. This mutual blocking then tends to propagate to other

neighboring sites and once above a given load a complete congestion will develop at the scale of the network.

Such mutual blocking is well-known in most *no loss* routing schemes such as *wormhole* routing and is called *deadlock* [13]. Deadlock avoidance is a very active research area, specially for massively parallel system interconnections [14].

β dependence

The thermal fluctuations move particles away from their minimal distance path. The higher β is, the less the importance of these fluctuations.

As shown in Figure 5.3 (left side), there is an interval of β values where the reduction of fluctuations have a positive influence on the throughput: p_c rises, as well as $\langle B_W \rangle$, while $\langle T_M \rangle$ decreases, as shown in Figure 5.4.

When going to higher β values, the situation does not persist. The absence of thermal fluctuations damages the throughput because particles are not able of going round obstacles. As a consequence p_c and $\langle B_W \rangle$ decrease. $\langle T_M \rangle$ does not appreciably change from its minimal value, corresponding to the infinite directionality one.

Figure 5.2 shows how the thermal fluctuations influence the saturation mechanism. If they are important, M grows slowly until it reaches B. If they are not significant a sharp jump appears in the temporal evolution of M, between its value in the transient regime and B. We conclude from this that the saturated domains grow faster in the absence of fluctuations, as would be expected from the earlier discussions.

In particular, it is intuitive that a mutual deadlock will last longer if thermal fluctuations are disallowed (particles in mutual deadlock will repeatedly attempt to exchange their sites) hence creating a larger local congestion area which can eventually evolve towards a global congestion. This was clearly observed in [5] where only one buffer was available per site and this behavior is also exhibited in this model, hence illustrating the well-known fact [15] that deadlock is a consequence of our *no loss* routing scheme [2] and not a consequence of insufficient resources.

κ dependence

The dependence of p_c on κ presents two different regions (see Figure 5.3).

In the first one, p_c rises with increasing κ. For these κ values, the inclusion of the repulsion term helps the system to avoid congested regions. We denote by κ_{opt} the value at which p_c reaches its maximal value.

[2] movement is granted if and only if the available resource is available at the low end

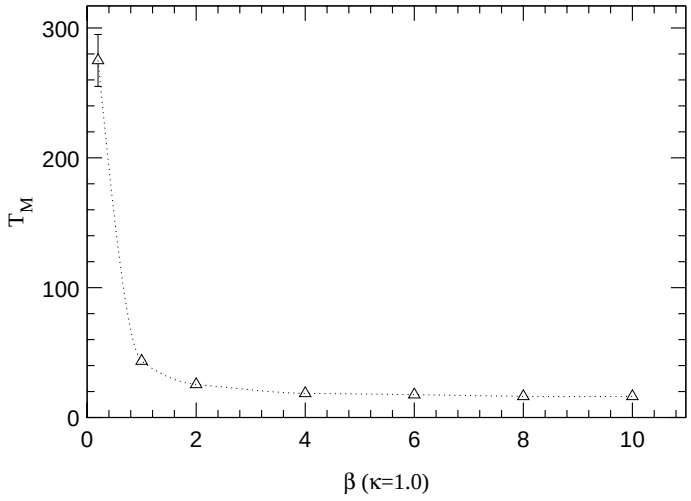

Figure 5.4: $\langle T_M \rangle$ dependence on β for $p \approx p_c$.

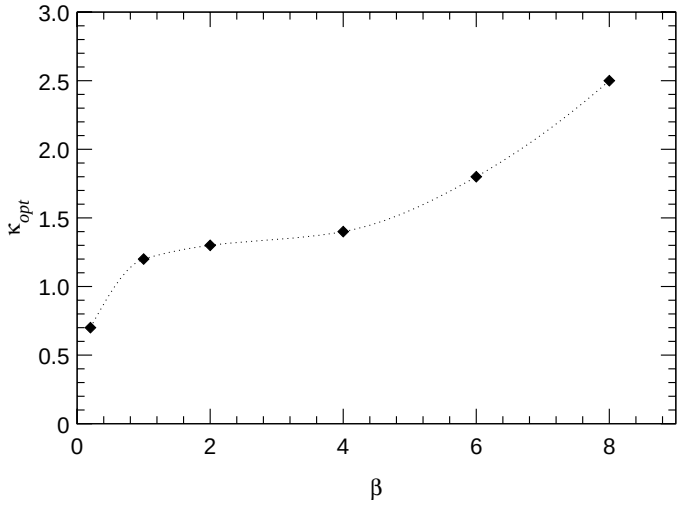

Figure 5.5: (β, κ_{opt}) line. The errors are of the size of the κ step measured, $(\triangle\kappa = 0.5.)$

In the second region, $\kappa > \kappa_{opt}$, p_c decreases with κ. Above κ_{opt} on, the repulsion is too strong and the particles move far away from their minimal paths. As a result, the collapse appears for smaller injection densities.

In Figure 5.5 we give the values of κ_{opt} for some β values. The more a particle is restricted to its minimal path, the stronger the repulsion needed to avoid obstacles in the lattice.

Therefore, there is a maximal value for the particle injection supported by each β value, which is reached for κ in a neighborhood of κ_{opt}.

5.6 General Behavior and Optimization

Let us focus on the behaviour of the other significant observables for the traffic flow, when β and κ have been tuned to obtain a maximal p_c.

Behavior of B_W

As we have already pointed out, B_W in the asymptotic regime is proportional to p by a factor L^2, as it may be checked in figure 6. Hence,at each (β, κ) value the maximum for $\langle B_W \rangle$ is reached when $p = p_c$.

Above p_c, $\langle B_W \rangle$ remains constant during the transient regime, and sharply falls to zero after it. B_W is a good measure to determine when

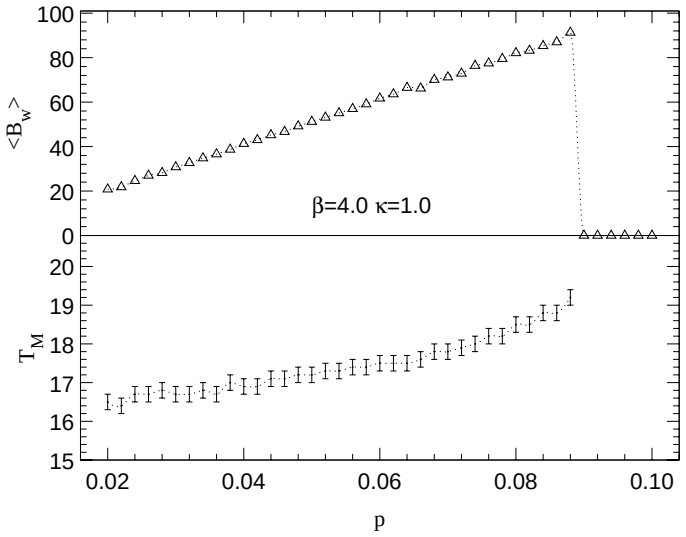

Figure 5.6: $\langle B_W \rangle$ (upper part) and $\langle T_M \rangle$ (lower part) versus p.

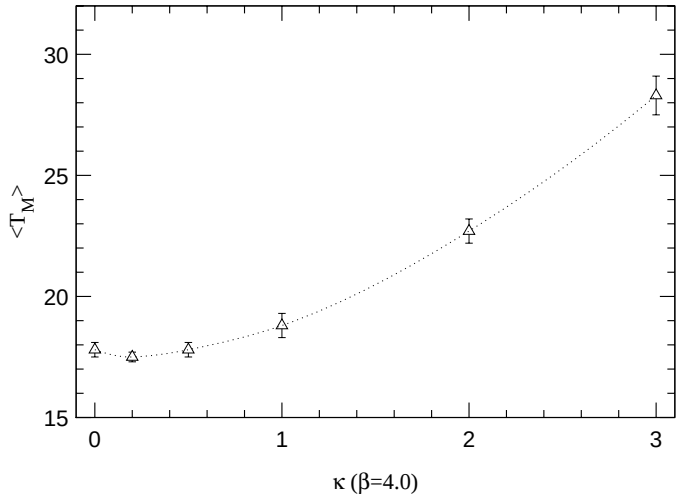

Figure 5.7: $\langle T_M \rangle$ dependence on κ.

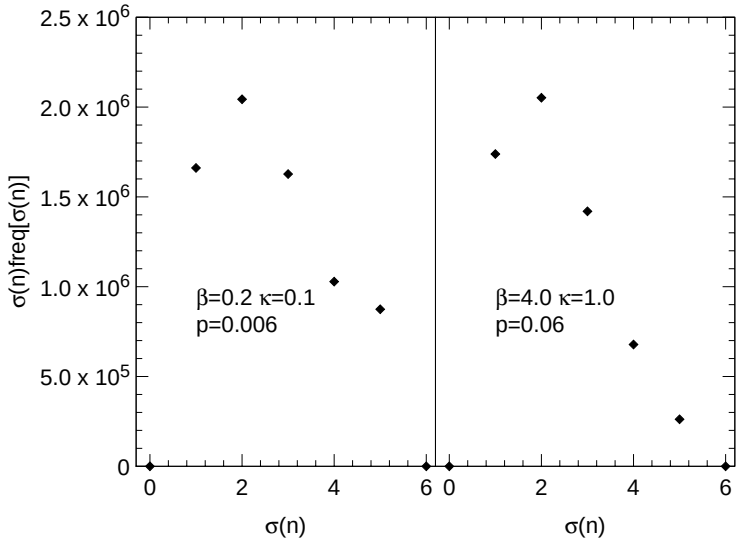

Figure 5.8: Distribution of the occupation number $\sigma(n)$ times the frequency of this state versus $\sigma(n)$ after 5×10^5 MC iterations. Transient regime contributions has been discarded.

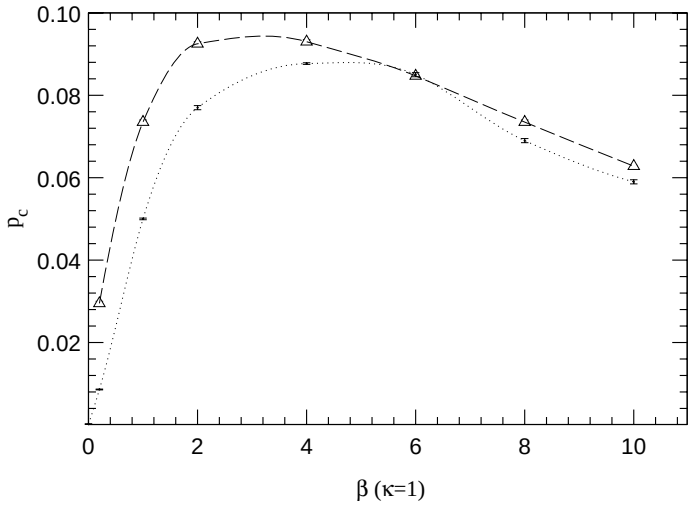

Figure 5.9: β dependence of p_c for the distance dependent force (dashed line). Dotted line represents the values obtained for the constant force.

the system has reached the asymptotic regime.

Behavior of T_M

The greater p the stronger the effect of the interaction over the particles: they move further and further away from their minimal path with increasing $\langle T_M \rangle$ (Figure 5.6). In Figure 5.7, we observe how $\langle T_M \rangle$ slightly increases with κ until κ_{opt} is reached From κ_{opt} on, $\langle T_M \rangle$ increases with a high slope.

We conclude that better performances are obtained for the maximal injection supported and for the bandwidth on the line (β, κ_{opt}). The repulsion term damages T_M: the greater κ, the larger the time the particles take to reach their destination. However, it is only for $\kappa > \kappa_{opt}$ that $\langle T_M \rangle$ increases in a dramatic fashion.

Figure 5.8 shows the particle distribution in the simulation for $\beta = 0.2$ and $\beta = 4.0$. The plot of $\sigma(n)\text{freq}[\sigma(n)]$ exhibits a maximum around $\langle M \rangle$, and also reveals a wider distribution of particles for small β values.

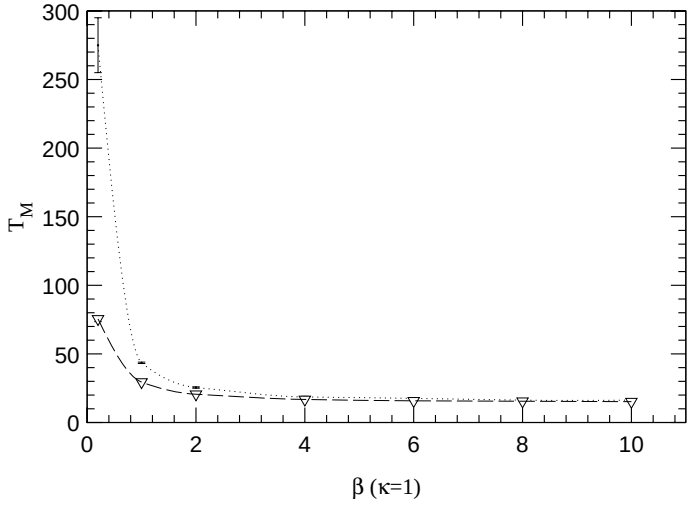

Figure 5.10: $< T_M >$ versus β for fixed $\kappa = 1$ in $p \approx p_c$ for the distance dependent force (dashed line) and constant force (dotted line).

5.7 Improving the throughput: distance dependent force.

Although our implementation of the physical system has been inspired by the search for the simplest model accomplishing the desired features, partial improvements are to be expected by taking into account details not included up to this point. As an example, we develop a possible improvement: quenching thermal fluctuations when they are no longer useful, that is, at the neighborhood of the endpoints.

In the primary implementation, we have used a constant force and therefore the particles support thermal fluctuations of the same strength no matter what the remaining distance to the endpoint is. We can expect a globally less congested lattice if particles which are only a few sites away from their destination are prevented from fluctuating. We will see how the inclusion of this feature does not spoil the good properties of the throughput, and also that the general behaviour of the system is not altered.

A possible implementation to take this fact into account is obtained by introducing a distance dependence in the probability distribution, such that contributions of the fluctuations decrease with decreasing distance to the endpoint.

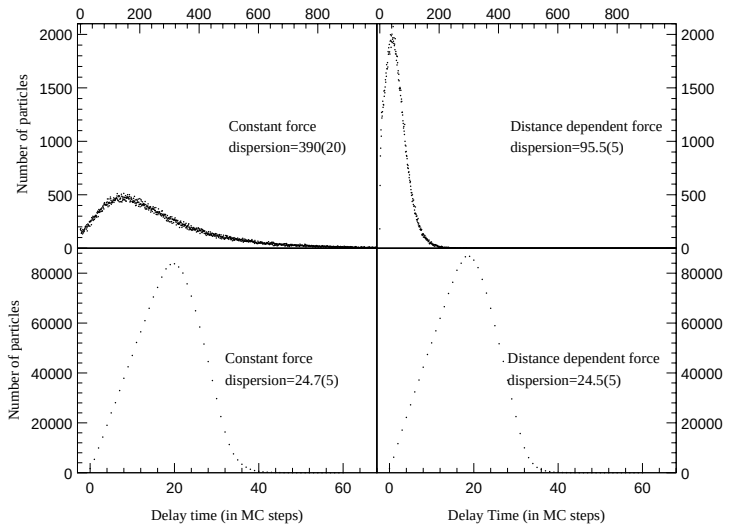

Figure 5.11: Delay distribution for the whole particles after 4×10^4 MC iterations. Graphics on the left (constant force) must be compared with the right side ones (distance dependent force). The distributions in the top are calculated in $(\beta = 0.2, \kappa = 1, p = 0.08)$ in the bottom they correspond to $(\beta = 4, \kappa = 1, p = 0.008)$.

A straightforward way of doing this is to include a dependence on the relative distance to the endpoint: the probability distribution now reads:

$$P(\pm\mu) = N \exp(\pm\beta \text{sign}(n^f{}_\mu - n_\mu) - \kappa\sigma(n_\mu)) \left(\frac{r_n}{r_{n+\mu}}\right) . \tag{5.8}$$

Where r_n is defined by:

$$r_{(n_0,n_1)} = \sqrt{(n^f{}_0 - n_0)^2 + (n^f{}_1 - n_1)^2} , \tag{5.9}$$

In Figure 5.9 the evolution of p_c with β is shown. A global throughput improvement is reflected by higher p_c values. This effect is more remarkable when the size of the thermal fluctuations is important (small β values), corroborating our first intuition on the effect of fluctuations in the steps preceding the endpoint.

In Figure 5.10 we plot the β dependence of T_M. We observe a global decrease in this time for all β values.

The improvements concerning the delay time, are not restricted to a smaller $\langle T_M \rangle$. Figure 5.11 shows the delay distribution for all particles, compared with the delay distribution obtained with the constant potential. We see at $\beta = 0.2$ how the dispersion of the distribution strongly decreases when using a distance dependent force. So, the particles arrive in more similar times, increasing the uniformity and the reliability of the traffic flow.

Shift	$n = 10$	$n = 100$	$n = 200$
$\beta = 4.0$ $\kappa = 1.0$			
$\triangle_r p_c$	0.09	0.40	0.58
$\triangle_r \langle T_M \rangle (\approx p_c)$	-0.05	-0.38	-0.89
$\triangle_r \langle M \rangle (\approx p_c)$	0.00	0.37	0.55
$\beta = 0.2$ $\kappa = 1.0$			
$\triangle_r p_c$	0.04	0.24	0.41
$\triangle_r \langle T_M \rangle (\approx p_c)$	-0.00	-0.08	-0.37
$\triangle_r \langle M \rangle (\approx p_c)$	0.00	0.43	0.50

Table 5.1: Shifted values of relevant observables for some values of the number of failures n.

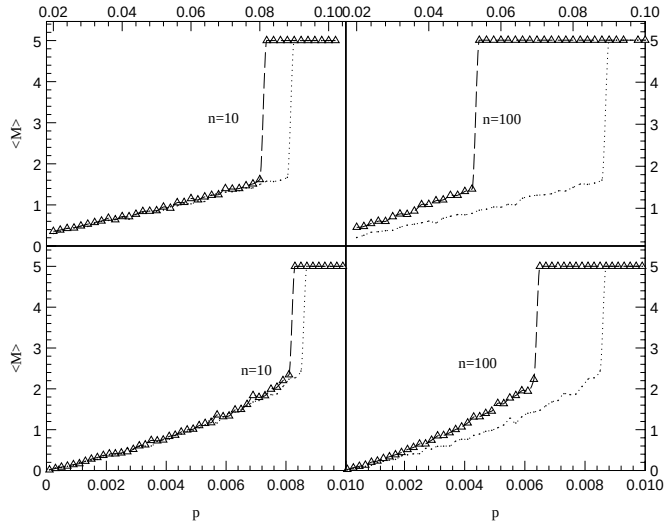

Figure 5.12: $\langle M \rangle$ versus p for values of the fault percentage. Dotted lines represent $\langle M \rangle$ values obtained for an ideal lattice. On the top diagram the parameter space point is $(\beta = 4, \kappa = 1)$, and on the bottom frames the plotted point is $(\beta = 0.2, \kappa = 1)$.

5.8 Fault tolerance

As we have pointed out, the lattice sites may simulate the control nodes of an information flow system. Needless to say the sites here are idealizations of nodes in real system because the possibility of communication failures is not allowed. Real nodes are subject to external factors, such as technical constraints or outside influences, that often damage the communication ability between some nodes. These nodes are then temporarily out of order, and cannot communicate or receive information from other nodes. It is therefore of interest to have an estimate of how robust a system is when temporary problems in the transmission occur.

To implement the ocurrence of communication problems, information exchange is prevented at n randomly chosen sites during an interval of $\triangle t \equiv 10\ MC$ iterations in the simulation. After this time interval these n sites are again allowed to communicate and another n sites are broken at random [3].

In general, the measured values for observables will be shifted by an

[3] In this section the probability distribution (5.1) is used

amount depending on n and in the parameter region. For each p value, we define the shift in the observable O as its value relative to the one obtained in the ideal system:

$$\triangle_r O(p) = \frac{O(p, n=0) - O(p, n)}{O(p, n=0)} \ . \tag{5.10}$$

We have studied the influence on the relevant parameters of communication failures for $n = 10$, 100 and 200 with $\beta = 0.2$ and $\beta = 4.0$.

Figure 5.12 shows the comparative evolution of $\langle M \rangle$ for $n = 10$ and $n = 100$.

The first consequence of a bad transmission is that the system must support globally higher occupation numbers. We measure smaller $\triangle_r p_c$ values for lower β, because, as has been already demonstrated, the lattice supports higher occupation numbers when the fluctuations are important.

$\triangle_r \langle M \rangle$ is almost zero for both β values with $n = 10$ (around 1% of nodes out of order), while with $n = 100$ and 200 $\triangle_r \langle M \rangle$ is always large.

In Table 5.1 we give the results obtained. As would be expected $\langle T_M \rangle$ increases for all n values even though it is almost zero for $n = 10$.

5.9 Summary and Outlook

We have studied a model useful for describing the relevant processes occurring in traffic flow systems with immediate applications to network message passing and traffic problems in general.

The introduction of the parameters β and κ as controllers of the system behavior allows us to go a step further from purely descriptive models, because we are able to give prescriptions to improve the performance of the flow process.

Deeper studies are also possible. Concretely an accurate study of the scaling with L of the relevant magnitudes as well as a detailed description of how the saturation time behaves, could lead us to the definition of quantities analogous to critical exponents. Also non-equilibrium states could be studied in order to monitor the parameters controlling the saturation process.

The introduction of the κ parameter has implied that the particles are able to avoid congested regions. The study has been limited to short-ranged interactions, because the particles at a site only see the occupation of its nearest neighbors. By informing the particles about the occupation of wider surrounding regions improvements in the throughput are expected.

Bibliography

[1] A. G. Greembergand, B. Hajek, *IEEE Transactions on Communication* **40**, 1070, (1992).

[2] J. A. Cuesta, F. C. Martínez, J. M. Molera and A. Sánchez, *Phys. Rev. E* **Vol. 48**, R4175 (1993).

[3] When-Shyan Sheu and Katja Lindenberg, *Phys. Lett. A* **147**, 437 (1991).

[4] S. Katz, J.L. Lebowitz and H. Spohn, *Phys. Rev. B* **28**, 1655 (1983).

[5] I. Campos and A. Tarancón, *Phys. Rev. E* **50**,91 (1994).

[6] S. Mukherji and S. M. Bhattacharjee, *Phys. Rev. E* **48**, 3427 (1993).

[7] A. Sokal in *Quantum Fields on the Computer*, *World Scientific, Singapore*, (1992).

[8] D. Berteskas and R. Gallagher, *Data Networks*, *Prentice Hall, Englewood Cliffs*, (1987).

[9] F. Bonomi and K. W. Fendick, *IEEE Network* **9**, 25 (1995); H. T. Kung and R. Morris, *IEEE Network* **9**, 40 (1995); K. K. Ramakrishnan and P. Newman, *IEEE Network* **9**, 49, (1995).

[10] L. Kleinrock, *IEEE Communications Magazine* **30**, 36, (1992).

[11] S. Katz, J.L. Lebowitz and H. Spohn, *Phys. Rev. B* **28**, 1655 (1983).

[12] G. Parisi and F. Rapuano, *Phys. Lett. B* **157**, 301, (1985).

[13] L. M. Li and P. K. McKinley, *Computer*, **February**, 62, (1993).

[14] D. J. Pritchard and D. A. Nicole, *IEEE Trans. Parallel and Distributed Systems* **4** 111 (1993).

[15] A. Tanenbaum, *Modern Operating Systems*, *Prentice Hall, Englewood Cliffs*, (1992).

Conclusiones

Las conclusiones de esta memoria se han expuesto individualmente a lo largo de cada capítulo. A continuación pasamos a resumir y comentar los resultados más importantes que se han obtenido.

- **El Modelo O(4) Anti-ferromagnético**

  La introducción de un acoplo negativo a segundos vecinos en el modelo σ no lineal hace que aparezca frustración en los vacíos encontrados en el diagrama de fases. La consecuencia de la frustración en este modelo es la aparición de antiferromagnetismo en distintas dimensionalidades. La forma que hemos encontrado más simple para introducir antiferromagnetismo en $4d$ es trabajar en una red F_4 con acoplos negativos. La transición del vacío desordenado paramagnético al vacío AF a planos es la más interesante puesto que los datos numéricos son compatibles con segundo orden y los exponentes críticos no son los de campo medio.

  Se han expuesto las explicaciones alternativas, razonables dentro de la evidencia numérica, que pueden dar cuenta de los resultados numéricos. Probablemente la explicación menos plausible es la posibilidad de tener trivialidad logarítmica puesto que la dimensión anómala del campo que hemos encontrado es demasiado distinta de cero, y este tipo de correcciones dan cuenta de pequeñas desviaciones a las predicciones de campo medio.

  Como se ha señalado, a la vista de los resultados obtenidos en O(2) y O(3) es muy difícil mantener esperanzas de que la transición en O(4) pueda ser de segundo orden. El escenario de primer orden débil parece ser el más plausible.

- **La transición de fase en el modelo SU(2)-Higgs**

  Esta transición de fase de nuevo es un ejemplo del problema que se encuentra en $d = 4$ a la hora de discernir entre transiciones de primer orden muy débiles y transiciones continuas.

Hemos visto que en SU(2)-Higgs la prueba más directa que demuestra el caracter de primer orden de la transición, a saber la medición del calor latente, no es accesible a un tiempo de cálculo razonable. Se ha estudiado el problema en un espacio de parámetros extendido, lo cual ha ayudado a tener una visión global del mecanismo de debilitamiento de la transición de fase. La observación de la tendencia de los exponentes críticos efectivos hacia los valores de primer orden constituye una evidencia del caracter de primer orden de la transición.

- **U(1) compacto con topologías toroidal y esférica**

  Este es un problema podríamos decir que clásico en el estudio de TCC en la red. Las cuestiones abiertas son dos: el orden de la transición de fase y los mecanismos que la producen. En concreto se ha venido conjeturando sobre una posible influencia de las condiciones de contorno en el orden de la transición de fase.

  En esta memoria se ha expuesto el estudio de la transición de fase desconfinante en U(1) puro gauge en redes con topología toroidal y esférica (homotópica a S^4). Se han estudiado los efectos de tamaño finito asociados a ambas topologías encontrando que en la red esférica hay más efectos de tamaño finito incontrolados que en la toroidal debido a las inhomogeneidades.

  En cuanto al orden de la transición de fase, se ha chequeado la existencia de gap de energía para redes suficientemente grandes en ambas topologías, lo cual caracteriza a la transición como de primer orden. Así mismo se ha dado una estimación del calor latente en el límite de volumen infinito.

- **Modelos bidimensionales de flujo de partículas**

  Se ha formulado un modelo para describir, en general, sistemas que envuelven un flujo de información.

  Se ha encontrado que se pueden obtener mejoras en el flujo permitiendo a las partículas fluctuar alrededor de la trayectoria de mínima distancia. La introducción del parámetro κ permite al sistema evitar regiones altamente congestionadas.

  La combinación apropiada de flexibilidad en la direccionalidad del movimiento de las partículas hacia su destino, es decir fluctuaciones térmicas, y posibilidad de evitar zonas congestionadas, es decir el parḿetro κ, es lo que permite un flujo óptimo de partículas en la red.

Relación de publicaciones

1. *"The Confining Higgs phase transition in U(1)-Higgs Lattice Gauge Theory "*
   Colaboración RTN (J.L. Alonso et al.)
   Phys. Lett. **B296** (1992) p 154

2. *"The U(1)-Higgs model:critical behavior in the confining Higgs region "*
   Colaboración RTN (J.L. Alonso et al.)
   Nuc. Phys. **B405** (1993) p 574

3. *"The U(1)-Higgs model: study of the confining Higgs transition "*
   Colaboración RTN (J.L. Alonso et al.)
   Nuc. Phys. **B30** (Proc. Suppl.) (1993) p 701

4. *"Instanton like contribution to the dynamics of the Yang-Mills fields on the twisted torus "*
   Colaboración RTN (J.L. Alonso et al.)
   Phys. Lett. **B305** (1993) p 366

5. *"Critical behavior of Random Walks"*
   I. Campos y A. Tarancón,
   Phys. Rev. **E50** (1994) p 91

6. *"Thermal and repulsive traffic flow"*
I. Campos, F. Clerot, L.A. Fernández y A. Tarancón,
Phys. Rev. **E52** (1995) p 5946

7. *"Anti-ferromagnetic 4D O(4) model"*
I. Campos, L.A. Fernández y A. Tarancón
Phys. Rev. **D55** (1997) p 2965

8. *"Anti-ferromagnetism in four dimensions: the search for non triviality"*
J.L. Alonso et al.
Nuc. Phys. **B53** (Proc. Suppl.) (1997) p 680

9. *"On the SU(2)-Higgs phase transition"*
I. Campos
Nuc. Phys. **B514** (1998) p 336

10. *"The order of the SU(2)-Higgs phase transition"*
I. Campos
Nuc. Phys. **B63** (Proc. Suppl.) (1998) p 676

11. *"First order signatures in the 4D pure compact U(1) gauge theory with toroidal and spherical topologies"*
I. Campos, A. Cruz y A. Tarancón
Phys. Lett. **B424** (1998) p 328

12. *"A study of the phase transition in 4D pure compact U(1) LGT on toroidal and spherical lattices"*
I. Campos, A. Cruz y A. Tarancón
Aceptado en Nuc. Phys. B

EPILOGO

En efecto, rematado ya su juicio, vino a dar en el más extraño pensamiento que jamás dió loco en el mundo, y fue que le pareció convenible y necesario, así para el aumento de su honra como para el servicio de su república, hacerse caballero andante e irse por todo el mundo con sus armas y su caballo a buscar aventuras y a ejercitarse en todo el aquello que él había leído que los caballeros andantes se ejercitaban, desfaciendo todo género de agravio, y poniéndose en ocasiones y peligros, donde, acabándolos, cobrase eterno nombre y fama.

Capítulo primero: Que trata de la condición y ejercicio del famoso hidalgo Don Quijote de la Mancha
"El Ingenioso hidalgo Don Quijote de la Mancha"
(Miguel de Cervantes Saavedra)